

MAGNETIC CIRCULAR DICHROISM STUDIES OF THE NEUTRAL AND ANIONIC  
FORMS OF A SERIES OF PORPHYRINS, CHLORINS, AND BACTERIOCHLORINS

A THESIS

Presented to

The Faculty of the Division of Graduate Studies

by

Gilbert F. Kuipers

In Partial Fulfillment

of the Requirements for the Degree

Doctor of Philosophy


in the School of Chemistry


Georgia Institute of Technology


August, 1978

MAGNETIC CIRCULAR DICHROISM STUDIES OF THE NEUTRAL AND ANIONIC  
FORMS OF A SERIES OF PORPHYRINS, CHLORINS, AND BACTERIOCHLORINS

Approved:

  
\_\_\_\_\_  
Ronald H. Felton, Chairman

  
\_\_\_\_\_  
Donald J. Royer

  
\_\_\_\_\_  
Donald C. O'Shea

Date approved by Chairman: Aug 25, 1978

## ACKNOWLEDGMENTS

The author is grateful to Dr. Ronald H. Felton for initiating this project and for his guidance and suggestions. The author also wishes to thank Dr. Donald J. Royer, Dr. Donald C. O'Shea and Dr. Roger Wartel for their reading of this thesis and their suggestions. Special thanks is extended to Dr. Ichiro Fujita for constructing the MCD spectrometer and for his help in understanding the MCD of porphyrins. The author is extremely grateful to Dr. Len Spaulding's suggestions on the preparation of the anions. Dr. Hideo Sambe and Dr. Duncan Cheung are also to be thanked for their help.

Especially, the author is indebted to his parents, family, and friends for their support and encouragement throughout this period of study.

## TABLE OF CONTENTS

	Page
ACKNOWLEDGMENTS . . . . .	ii
LIST OF TABLES . . . . .	v
LIST OF ILLUSTRATIONS . . . . .	vii
SUMMARY . . . . .	x
Chapter	
I. INTRODUCTION . . . . .	1
II. THEORY . . . . .	5
Origin of A, B, C, and D Terms	
Pi-Electron Calculation of Porphyrin Molecular	
Orbital Wavefunctions	
Zero Field Splitting of an Orbitally Degenerate	
Ground State and its Effect Upon the MCD	
Spectrum	
III. EXPERIMENTAL . . . . .	55
Materials	
Preparation of Porphyrin Anions	
MCD Spectrometer (Designed and Constructed by	
Dr. Ichiro Fujita)	
Results and Discussion	
Introduction	
Molecular Orbital Model	
Neutral Porphyrins and Related Systems	
Electronic Configurations of Monoanions	
Zero Field Splitting of Metalloporphyrin	
Monoanion	
Assignments of Bands II, III, IV, and V in	
Porphyrin Monoanion	
Chlorin and Bacteriochlorin Anion Assign-	
ment	
Porphyrin Dianion	
IV. CONCLUSIONS . . . . .	172
APPENDIX A . . . . .	174
APPENDIX B . . . . .	178

	Page
BIBLIOGRAPHY . . . . .	187
VITA . . . . .	192

## LIST OF TABLES

Table		Page
1.	Summary of the Relationship Between the Theoretical a, b, and c Terms and the Experimental A, B, and C Terms . . . . .	24
2.	Doublet State Configurations and Energies . .	27
3.	Singlet State Configurations and Energies . .	28
4.	Neutral Porphyrin Molecular Orbital Coefficients . . . . .	73
5.	Neutral Porphyrin Molecular Orbitals . . . . .	75
6.	States After Configuration Interaction for Neutral Compounds . . . . .	91
7.	Electric and Magnetic Dipoles Between Orbitals of Neutral Compounds . . . . .	93
8.	Electric and Magnetic Dipoles Between States of Neutral Compounds . . . . .	94
9.	Neutral Porphyrin and Chlorin Spectra . . . . .	95
10.	Neutral Bacteriochlorin Spectra . . . . .	100
11.	Monoanion Configurations . . . . .	102
12.	Porphyrin Monoanion States . . . . .	136
13.	Prophyrin Anion Electric and Magnetic Dipoles.	137
14.	Metalloporphyrin Monoanion Absorption and MCD Spectra . . . . .	138
15.	Experimental Metal-Free Porphyrin Monoanion Spectra . . . . .	140
16.	Metallochlorin and Metallobacteriochlorin Anion States . . . . .	152
17.	Chlorin Monoanion Spectra . . . . .	153
18.	Bacteriochlorin Monoanion Spectra . . . . .	154

Table		Page
19.	Electric and Magnetic Dipoles Between Chlorin Monoanion States . . . . .	156
20.	Electric and Magnetic Dipoles Between Bacteriochlorin Monoanion States . . . . .	157
21.	Porphyrin Dianion States and Spectra-Calculations and Data . . . . .	169

## LIST OF ILLUSTRATIONS

Figure		Page
1.	Structures and Names of Metal Derivatives of the Compounds Studied . . . . .	3
2.	Decomposition of the Electric Field Vector for Plane Polarized Light into Two Equal Circular Components . . . . .	6
3.	Decomposition of the Electric Field Vector for Plane Polarized Radiation into Two Circular Components of Equal Intensity but Unequal Pitch . . . . .	7
4.	Decomposition of the Electric Field Vector for Plane Polarized Light into Circular Components of Different Magnitudes . . . . .	9
5.	MCD <u>a</u> Term Due to a Degenerate Excited State. .	12
6.	MCD <u>a</u> and <u>c</u> Terms Due to a Degenerate Ground State . . . . .	16
7.	MCD <u>b</u> Term Due to Mixing of the States by the Magnetic Field . . . . .	19
8.	Energy Levels for a Nearly Degenerate Ground State . . . . .	37
9.	The Ratio of the Integrated Area of the MCD Spectrum to the Integrated Area of the Absorption Spectrum Versus the Reciprocal of the Temperature as Calculated from Eqs. (165) and (166) . . . . .	53
10.	The Ratio of the Integrated Area of the MCD Spectrum to the Integrated Area of the Absorption Spectrum Versus the Reciprocal of the Temperature as Calculated from Eqs. (165) and (166) . . . . .	54
11.	Three Electrode Electrolysis Apparatus . . . . .	60
12.	Two Electrode Electrolysis Apparatus . . . . .	61
13.	Apparatus for Metal Reductions . . . . .	64

Figure	Page
14. MCD Spectrometer . . . . .	67
15. Highest Filled and Virtual SCF Molecular Orbital Energies of Metallocomplexes . . . . .	75
16. CuTPP Neutral in 50% Dimethylformamide and 50% Tetrahydrofuran . . . . .	79
17. CuTPC Neutral in 50% Dimethylformamide and 50% Tetrahydrofuran . . . . .	80
18. ZnTPC Neutral in Dimethylformamide . . . . .	81
19. H <sub>2</sub> TPBc Neutral . . . . .	82
20. ZnTPBc Neutral . . . . .	83
21. MCD and Absorption Spectra of CuTPP Monoanion in Dimethylformamide at Room Temperature . . .	106
22. MCD Parameters Vs. 1/T for the Three State Model with No Zero Field Splitting . . . . .	109
23. MCD and Absorption Spectra of TBA <sup>+</sup> ZnTPP in 2MTHF . . . . .	111
24. Integrated Spectra of TBA <sup>+</sup> ZnTPP <sup>-</sup> in 2MTHF . .	112
25. MCD Parameters Vs. 1/kT for the Three State Model with a 100 cm <sup>-1</sup> Zero Field Splitting . .	114
26. MCD Parameters Vs. 1/kT for the Three State Model with a 200 cm <sup>-1</sup> Zero Field Splitting . .	115
27. MCD Parameters Vs. 1/kT for the Three State Model with a 300 cm <sup>-1</sup> Zero Field Splitting . .	116
28. Calculated MCD and Absorption Spectra for the Three State Model . . . . .	120
29. ZnEtio Monoanion at 200°K . . . . .	121
30. ZnEtio Monoanion at 100°K . . . . .	122
31. H <sub>2</sub> Etio Monoanion . . . . .	123
32. H <sub>2</sub> TPP Monoanion . . . . .	124
33. ZnEtio Monoanion at 200 °K . . . . .	128

Figure	Page
34. ZnEtio Monoanion Soret at 100°K . . . . .	129
35. ZnTPP Monoanion Soret at Room Temperature . . .	130
36. ZnTPP Monoanion Soret at 100°K . . . . .	131
37. H <sub>2</sub> Etio Monoanion Soret at Room Temperature . .	132
38. H <sub>2</sub> TPP Monoanion Soret at Room Temperature . . .	133
39. ZnTPC Monoanion . . . . .	145
40. CuTPC Monoanion . . . . .	146
41. H <sub>2</sub> TPC Monoanion . . . . .	147
42. ZnTPBc Monoanion . . . . .	148
43. H <sub>2</sub> TPBc Monoanion . . . . .	149
44. Disodium ZnTPP Dianion . . . . .	161
45. Disodium ZnEtio Dianion . . . . .	162
46. Bis-tetrapropylammonium H <sub>2</sub> TPP Dianion . . . . .	163
47. Six Orbital Model of Porphyrin Dianion States .	166

## SUMMARY

The magnetic circular dichroism spectra have been obtained for neutral and anionic forms of a series of porphyrins, chlorins, and bacteriochlorins. The analysis of these spectra not only aid in assigning the electronic transitions, but also allow an estimation of the distortions on the inner 16-atom pi system that characterizes these porphyrinic species. The signs of the MCD terms require an analysis of the nature of the distortion and symmetry and relative energies of the various excited states.

Analysis of the  $1E_g$  to  $1B_{1u}$  band of the metalloporphyrin monoanion spectra shows that the ground state is orbitally nondegenerate. The action of the crystal field is to remove the degeneracy of the  $^2E_g$  ground state, leaving a  $100\text{-}200\text{ cm}^{-1}$  energy separation between the energies of the two states. The orbital angular momentum is not significantly reduced, but is close to the self-consistent-field molecular orbital (SCF-MO) value of  $2.2 \hbar$ . Knowledge of this ground state splitting allows the interpretation of much of the porphyrin anion spectra (both metal free and metalloporphyrins). The crystal splitting of the dianions is greater than that of the monoanions.

In a reinvestigation of the theory of neutral chlorin and bacteriochlorin MCD spectra, we find that calculated MCD spectra of these compounds should be inverted for both Q and

B bands, respectively, when compared to MCD spectra of neutral metalloporphyrin. This result is found experimentally.

## CHAPTER I

## INTRODUCTION

Although observations and theories of magnetic circular dichroism (MCD) spectra date back to the early days of this century, only recently has there been a surge of interest in exploiting this powerful method for elucidating problems of electronic structure.<sup>1-11</sup> This resurgence has been stimulated largely by the availability of sensitive MCD spectrometers and by their application to molecules of biological importance. Indeed, since the 1960's there has been a growing interest in applying this technique to porphyrins and related compounds.

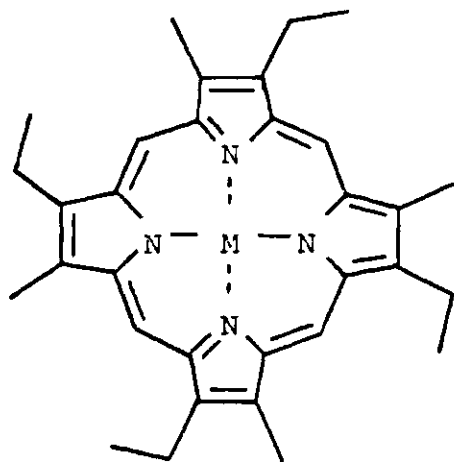
The occurrence of porphyrins or their derivatives (chlorophyll, bacteriochlorophyll) in biological electron transport chains provides a powerful rationale for the examination of the physical properties of reduced or oxidized forms of these compounds. For example, primary photosynthetic events in bacterial reaction center preparations are now interpreted to proceed by way of photooxidation of  $P_{870}$ , a bacteriochlorophyll dimer, to yield  $P_{870}^{+\cdot}$  and the anion radical of bacteriopheophytin, the magnesium-free analog of bacteriochlorophyll.<sup>12-14</sup> Similarly an enzymatically active form of peroxidase, called Compound I, has been tentatively

identified as a pi-cation radical of an iron porphyrin.<sup>15</sup> Some other porphyrins or related structures include hemoglobin, vitamin B<sub>12</sub>, bile pigments, and myoglobin.<sup>16,17</sup>

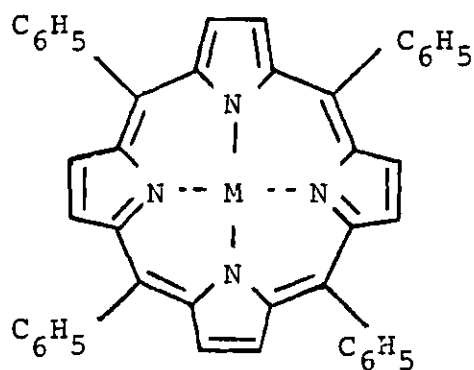
The structures and abbreviations for the compounds studied in this thesis are given in Figure 1. All have the basic 24 atom porphyrin ring structure. (For chlorins and bacteriochlorins, reduction of pyrrole rings remove respectively two and four atomic orbitals from the  $\pi$  system.) This porphyrinic core is a source of strong  $\pi-\pi^*$  absorption in the visible and near UV regions. Assignments of electronic transitions with the aid of MCD spectra have been successful for neutral porphyrins,<sup>18-20</sup> chlorins,<sup>21-25</sup> and phthalocyanine,<sup>26,27</sup> several neutral and anionic polynuclear aromatic hydrocarbons,<sup>28-34</sup> and other compounds.

As will be discussed later, the MCD spectrum for a transition may be characterized by three parameters (a, b, and c).<sup>1,5,6,8,10,19,35,36</sup> The b term is shaped like the absorption and is due to magnetic field induced mixing of electronic states. The a term resembles the first derivative of the absorption and is due to a degenerate ground or excited state. The third MCD parameter, the c term, resembles the absorption and arises from a Boltzmann distribution over the components of a degenerate ground state. Following Serber,<sup>36</sup> these parameters are combined into the observable quantities A, B, and C.

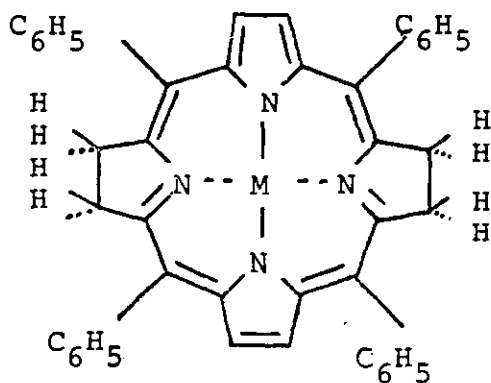
Molecular orbital calculations of symmetrical porphyrin



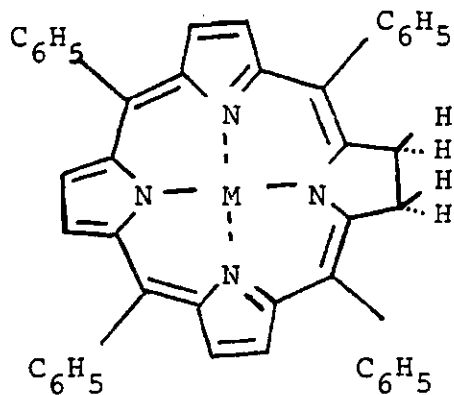
Etioporphyrin I;  
Etio



5,10,15,20-tetraphenylporphyrin  
TPP



2,3,12,13-tetrahydro-t,10,15,20-  
tetraphenylporphyrin;  
TPBc



2,3-dihydro-5,10,15,20-  
tetraphenylporphyrin;  
TPC

Figure 1. Structures and Names of Metal Derivatives  
of the Compounds Studied.

monoanions suggest that these ionic species are characterized by a  ${}^2E_g$  ( $D_{4h}$  point group) ground state. As such, the porphyrin anions share with coronene and phthalocyanine anions the feature of an orbitally degenerate ground state. The MCD spectra of these species have been interpreted as displaying g-terms, expected for electronically degenerate ground states.<sup>26,28,37</sup> Not considered, in these earlier studies, is the removal of orbital degeneracy by zero field splitting.<sup>38,39</sup> This neglect seems unwarranted since, recently, Maslov has found evidence of zero field splitting in the zinc etioporphyrin anion from linear dichroism measurements in a frozen glass.<sup>40</sup>

As will be shown, the MCD spectra of porphyrinic anions provide a much more demanding test for assignments of electronic transitions than do the absorption spectra. Temperature dependence of the MCD spectra yields information on zero field splitting in metalloporphyrin anions. The spectra of the chlorins and bacteriochlorins will be related to a different type of reduction in symmetry.

## CHAPTER II

### THEORY

#### Origin of A, B, C, and D Terms

Magnetic as well as neutral optical circular dichroism reflects the different interactions of right and left circularly polarized light with a medium.<sup>36, 41-48</sup>

Three different types of polarizations will be described: plane, circular, and elliptical. For circularly polarized light, the extremity of the electric vector as a function of the distance which the beam has travelled through the medium forms a helix. The helix pitch is the wavelength and the radius of the helix is proportional to the amplitude of the electric vector. By superimposing equal amplitudes of coherent beams comprised of left and right circularly polarized light, plane polarized light is produced (Figure 2). The definition of right-handed polarization corresponds to the helix being right-handed. As such it agrees with Stephens'<sup>5</sup> definition, but is opposite to the chemist's customary convention. If the beam traverses a medium which has different refractive indices for the two circular components, the two components are propagated at different velocities causing a rotation of the plane of linear polarization (optical rotatory dispersion) (Figure 3). Likewise, should the beam traverse a medium in which the

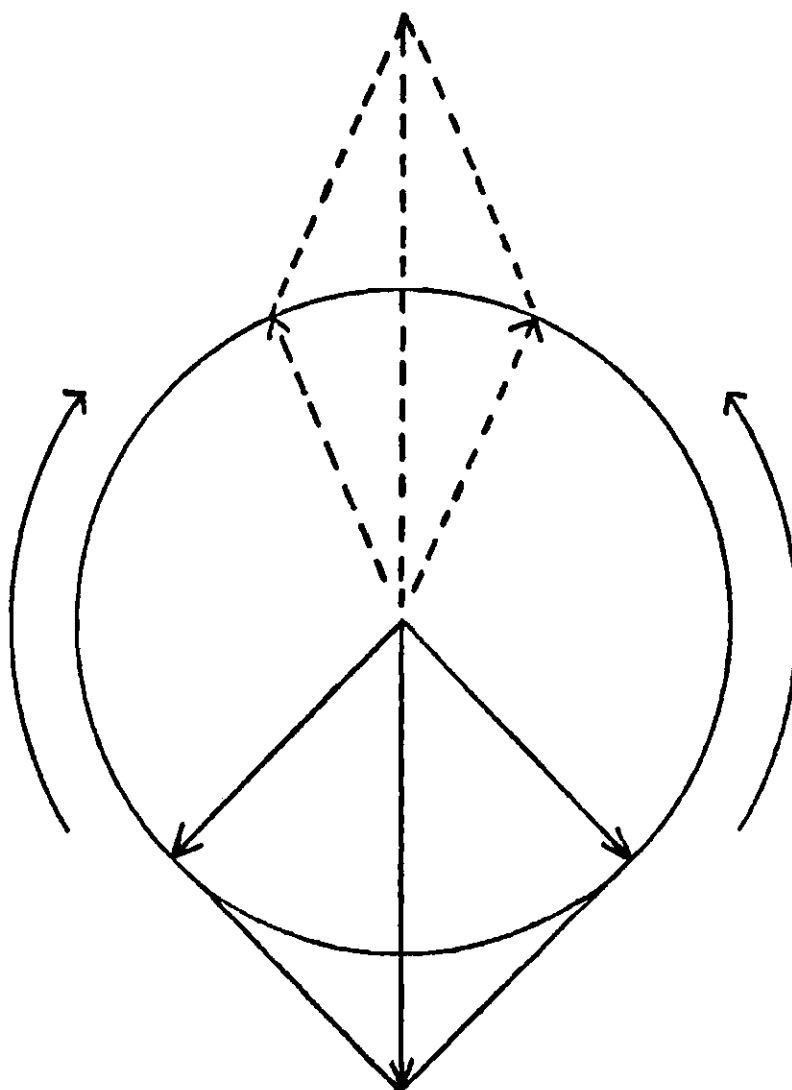


Figure 2. Decomposition of the Electric Field Vector for Plane Polarized Light into Two Equal Circular Components. The direction of propagation of the beam is out of the plane of the page and is such that the tip of the electric vector of the incident left circularly polarized light traverses a left-handed helix. The dotted lines represent the positions at a later time.

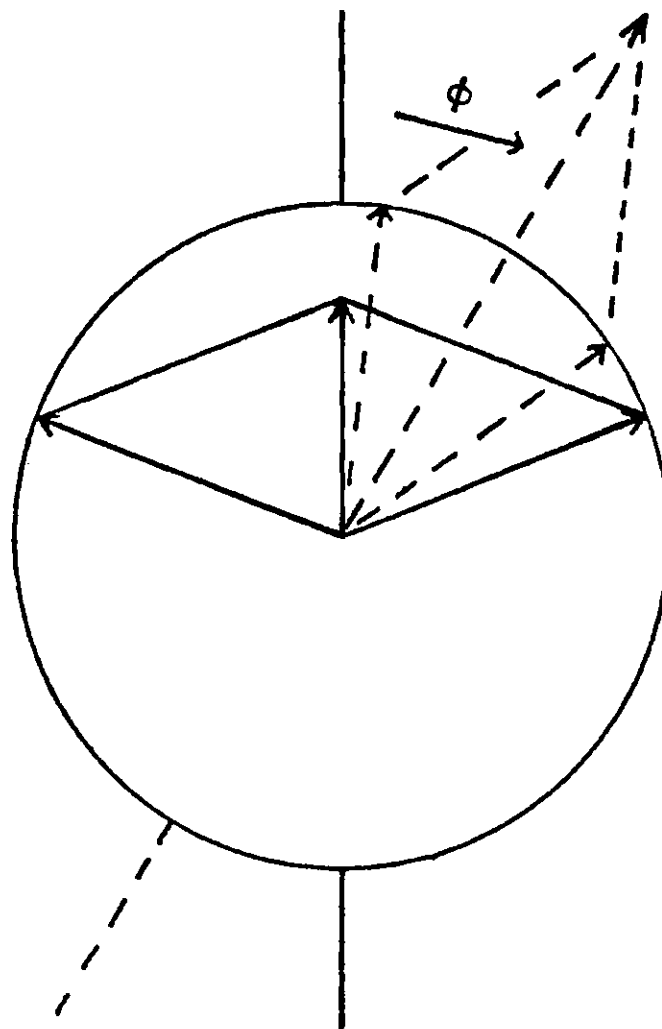


Figure 3. Decomposition of the Electric Field Vector for Plane Polarized Radiation into Two Circular Components of Equal Intensity but Unequal Pitch.  $\phi$  is the angle of rotation in radians per unit path length.

absorption of the components are different, then the resultant beam will become elliptically polarized (Figure 4). The component irradiances of the electromagnetic wave are given by the usual Poynting vector ( $\bar{S} = \frac{1}{c} \bar{E} \times \bar{H}$ ) for these components. If  $I_0$  is the incident irradiance averaged over one cycle, then the component intensities are

$$I_{L,R} = \frac{I_0}{2} 10^{-A_{L,R}} \quad (1)$$

where

$$A_{L,R} = \epsilon_{L,R} \ell c \quad (2)$$

$A_{L,R}$  are the absorbances and  $\epsilon_{L,R}$  are the extinction coefficients of left and right circularly polarized radiation respectively. The path length is  $\ell$  and  $c$  is the molar concentration of the absorbing species.

The tangent of the ellipticity,  $\theta$ , is the ratio of the difference of the intensities to their sum, namely,

$$\tan \theta = \frac{I_L - I_R}{I_L + I_R} = \tanh \left( \frac{A_L - A_R}{4 \log e} \right) \quad (3)$$

for  $\theta \ll 1$ , the ellipticity becomes,

$$\theta = \frac{A_L - A_R}{4 \log e} \quad (4)$$

The molar ellipticity,  $[\theta]_M$ , is defined analogously to an extinction coefficient, so that

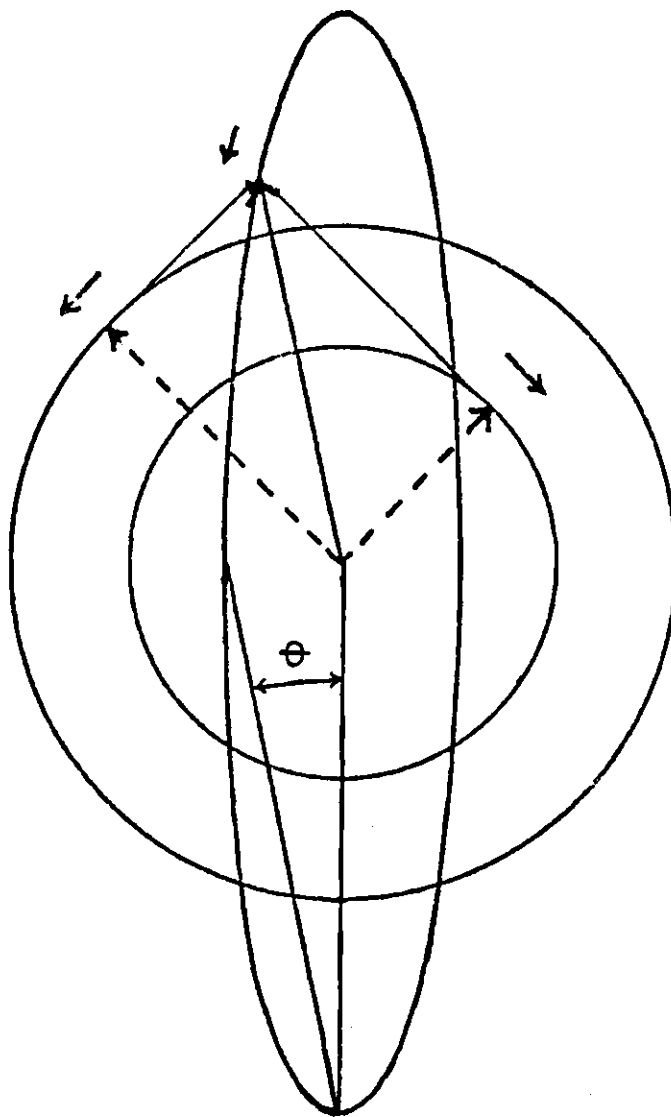


Figure 4. Decomposition of the Electric Field Vector for Plane Polarized Light into Circular Components of Different Magnitudes.  $\theta$  is the circular dichroism.

$$[\theta]_M = \theta / \ell c \quad (5)$$

where  $\ell$  is the path length in cm and  $c$  is the concentration of the absorbing species. It is customary to express  $[\theta]_M$  in units of degree ml/cm decimole, in which case

$$\begin{aligned} [\theta]_M &= \frac{1}{4 \log e} \frac{180}{\pi} (100) (A_L - A_R) / \ell c \\ &\approx 3300 (\epsilon_L - \epsilon_R) \end{aligned} \quad (6)$$

For magnetic optical activity, the molar ellipticity is normalized with respect to the magnetic field intensity (in gauss)

$$[\theta]_M = 3300 \frac{(\epsilon_L - \epsilon_R)}{H} \quad (7)$$

If  $\theta \ll 1$ , then the total absorbance is the average of the component absorbances. The extinction coefficient is

$$\epsilon = \frac{\epsilon_L + \epsilon_R}{2} \quad (8)$$

Considering only electric dipole allowed transitions, the pertinent extinction coefficients for a transition from state  $|a\rangle$  to state  $|j\rangle$  of a molecule, atom, or color center are given by

$$\epsilon_{L,R}(a \rightarrow j) = |\langle j | \bar{m}_{L,R} | a \rangle|^2 f(\nu, \nu_0) \quad (9)$$

with

$$\bar{m}_{L,R} = \bar{m}_x \mp i\bar{m}_y \quad (10)$$

Here,  $\bar{m}_x$  and  $\bar{m}_y$  are the electric dipole operators and  $f(\nu, \nu_0)$  is a line shape function centered about the transition energy,  $\nu_0$ . The direction of propagation of the radiation and the magnetic field lie along the +Z direction.

Three factors will affect the difference,  $\epsilon_L - \epsilon_R$ . These are: (a) the Zeeman splitting of the energies of states  $|a\rangle$  or  $|j\rangle$  caused by interaction between an orbital magnetic moment associated with the states and the external magnetic field, (b) the mixing of  $|a\rangle$  and  $|j\rangle$  with other electronic, vibrational, rotational, or spin states due to the magnetic field, and (c) a population distribution over the components of the ground state,  $|a\rangle$ , should it be orbitally degenerate in the absence of a magnetic field.<sup>27,48</sup>

As an illustrative example, consider an isolated atom with a  $^1S$  ground state and a  $^1P$  excited state. In the presence of a magnetic field, the previously three-fold degenerate  $^1P$  levels are now separated from each other by  $\beta H$  ( $\beta$  = Bohr magneton) (Figure 5). The extinction coefficients are

$$\epsilon_L = |\langle j | \bar{m}_L | a \rangle|^2 f(\nu, \nu_0 + \beta H) \quad (11)$$

$$\epsilon_R = |\langle j | \bar{m}_R | a \rangle|^2 f(\nu, \nu_0 - \beta H) \quad (12)$$

with

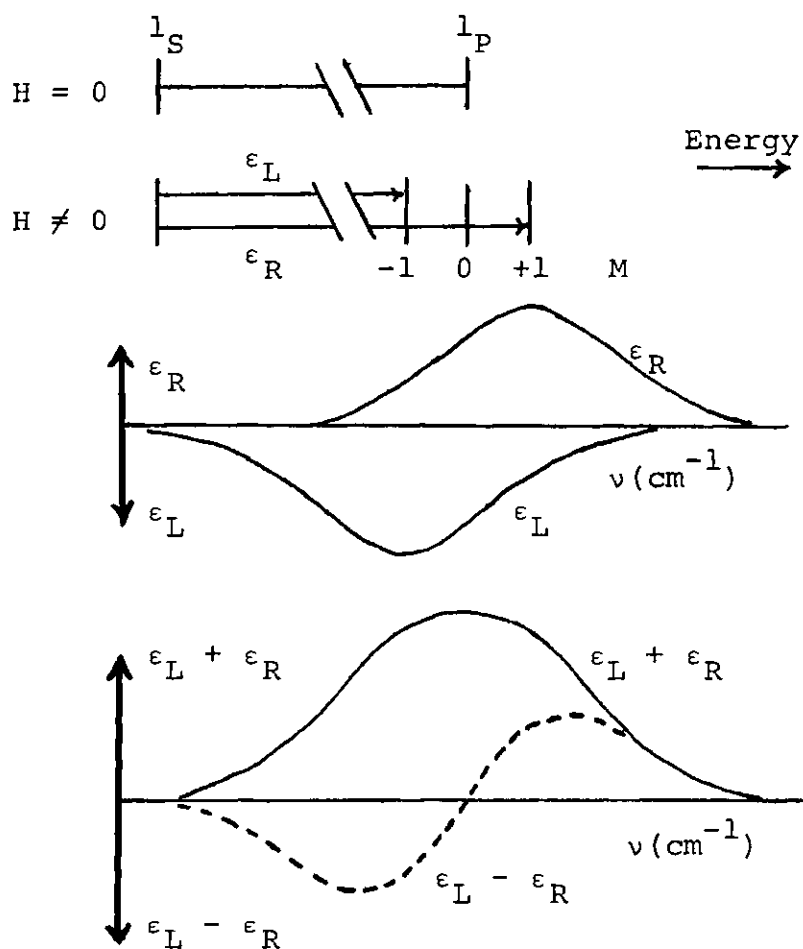


Figure 5. MCD a Term Due to a Degenerate Excited State. The difference (---) in the circularly polarized components gives rise to a derivative shaped MCD spectrum. The solid line is the absorption spectrum.

$$|\langle j | \bar{m}_L | a \rangle|^2 = |\langle j | \bar{m}_R | a \rangle|^2. \quad (13)$$

When the Zeeman splitting is small compared to the band width, a Taylor series expansion of the lineshape function can be used,

$$f(\nu, \nu_0 \pm \beta H) = f(\nu, \nu_0) \pm \beta H f'(\nu, \nu_0), \quad (14)$$

where  $f'(\nu, \nu_0)$  is the first derivative of the lineshape function and satisfies

$$\int_{\text{band}} f'(\nu, \nu_0) \nu d\nu = -1 \quad (15)$$

The difference,

$$\epsilon_L - \epsilon_R = -2\beta H |\langle j | \bar{m} | a \rangle|^2 f'(\nu, \nu_0) \quad (16)$$

gives rise to the MCD a term, while the sum,

$$\epsilon = \frac{\epsilon_L + \epsilon_R}{2} = |\langle j | \bar{m} | a \rangle|^2 f(\nu, \nu_0) \quad (17)$$

yields the absorption spectrum.

There is an alternative way of analyzing this system which does not assume any particular lineshape function. This is the well-known method of statistics called moment analysis. The  $n$ th central moment of  $x$  about  $\nu_0$  is defined by<sup>49,50</sup>

$$\langle x \rangle_n = \frac{1}{k} \sum_{i=1}^k x_i (\nu_i - \nu_0)^n \quad (18)$$

$x$  is a function of  $\nu_i$ . The average value of  $x$  is found at  $\nu_0$ .

(For a continuous function, the summation is replaced by an integral.) For each value of  $\epsilon_L$  at  $\nu_i + \beta H$ , the same value of  $\epsilon_R$  is found at  $\nu_i - \beta H$ , therefore only two arbitrary points on the lineshape function need to be considered. The summation over all  $i$  will cause the term,  $(\nu_i - \nu_0)$ , to vanish. Assuming that the lineshape functions are normalized, then the MCD moments will be

$$\begin{aligned} \langle (\epsilon_L - \epsilon_R) \rangle_n &= |\langle j | \bar{m} | a \rangle|^2 \{ [(\nu_i + \beta H) - \nu_0]^n \\ &\quad - [(\nu_i - \beta H) - \nu_0]^n \} \end{aligned} \quad (19)$$

$$= |\langle j | \bar{m} | a \rangle|^2 [(\beta H)^n - (-\beta H)^n]$$

$$\langle (\epsilon_L - \epsilon_R) \rangle_0 = 0 \quad (20)$$

$$\langle (\epsilon_L - \epsilon_R) \rangle_1 = 2 |\langle j | \bar{m} | a \rangle|^2 \beta H \quad (21)$$

The moments of absorption will be

$$\langle \epsilon \rangle_n = \langle (\epsilon_L + \epsilon_R) / 2 \rangle = |\langle j | \bar{m} | a \rangle|^2 [(\beta H)^n + (-\beta H)^n] \quad (22)$$

$$\langle \epsilon \rangle_0 = |\langle j | \bar{m} | a \rangle|^2 \quad (23)$$

$$\langle \epsilon \rangle_1 = 0$$

Thus, the zeroth moment of absorption is the dipole strength, while the first moment of the MCD spectrum gives the  $\underline{a}$  term.

Next consider an atom with  $^1P$  ground state and a  $^1S$

excited state (Figure 6). This case is the reverse of the preceding example. In this instance, application of a magnetic field will lead to a Boltzmann population distribution over the occupied three sublevels of the lower state. If the relative populations of these sublevels are  $N_{-1}$ ,  $N_0$ , and  $N_1$ , where the subscripts denote the  $M_L$  values, then,

$$\epsilon_L = |\langle a | \bar{m} | j \rangle|^2 N_{-1} f(v, v_0 - \beta H) \quad (25)$$

$$\epsilon_R = |\langle a | \bar{m} | j \rangle|^2 N_1 f(v, v_0 + \beta H) \quad (26)$$

$$N_{-1} + N_0 + N_1 = 1 \quad (27)$$

$$\begin{aligned} \epsilon_L - \epsilon_R &= 2 |\langle a | \bar{m} | j \rangle|^2 [N_{-1} - N_1] f(v, v_0) \\ &\quad - \beta H (N_{-1} + N_1) f'(v, v_0) \end{aligned} \quad (28)$$

$$\begin{aligned} \epsilon &= \frac{\epsilon_L + \epsilon_R}{2} = |\langle a | \bar{m} | j \rangle|^2 N_{-1+N_1} f(v, v_0) \\ &\quad + \beta H (N_1 - N_{-1}) f'(v, v_0) 2. \end{aligned} \quad (29)$$

For small magnetic fields or high temperatures  $\beta H \ll kT$ , (28) and (29) may be simplified since,

$$N_{-1} - N_1 = \frac{1}{3} [e^{-(-\beta H/kT)} - e^{-\beta H/kT}] = \frac{2}{3} \frac{\beta H}{kT} \quad (30)$$

and

$$N_1 + N_{-1} = \frac{2}{3}, \quad (31)$$

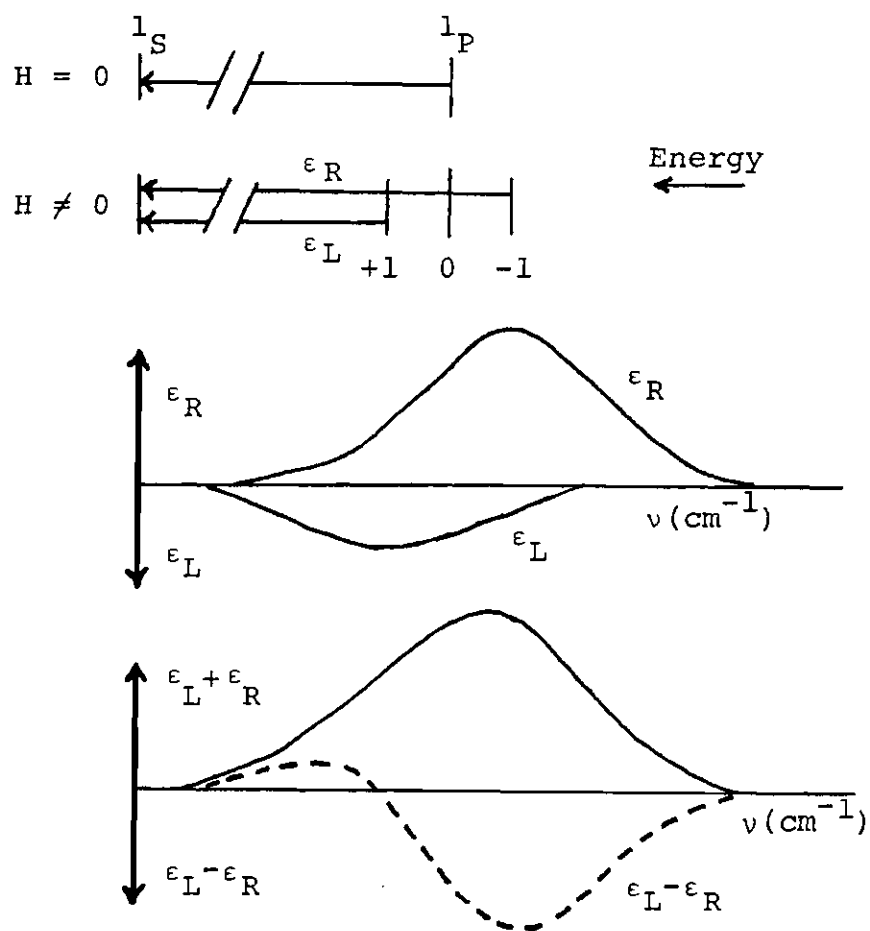


Figure 6. MCD a and c Terms Due to a Degenerate Ground State. The MCD spectrum (---) is temperature dependent. As  $T \rightarrow 0$ , the MCD spectrum approaches that of the absorption spectrum. As  $T \rightarrow \infty$ , the MCD spectrum approaches the derivative of the absorption spectrum.

then

$$\epsilon_L - \epsilon_R = |\langle a | \bar{m} | j \rangle|^2 \left[ \frac{2\beta H f(\nu, \nu_0)}{3kT} - \frac{2\beta H}{3} f'(\nu, \nu_0) \right] \quad (32)$$

and

$$\epsilon = \frac{\epsilon_L + \epsilon_R}{2} = |\langle a | \bar{m} | j \rangle|^2 \left[ \frac{1}{3} f(\nu, \nu_0) + \frac{1}{3} \frac{\beta^2 H^2}{kT} f''(\nu, \nu_0) \right] \quad (33)$$

The influence of the magnetic field on the absorption spectrum is at second order. The MCD spectrum will contain both a and c term contributions.

In terms of moments, as before,

$$\langle (\epsilon_L - \epsilon_R) \rangle_n = |\langle j | \bar{m} | a \rangle|^2 [N_{-1}(\beta H)^n - N_1(-\beta H)^n] \quad (34)$$

$$\langle (\epsilon_L - \epsilon_R) \rangle_0 = |\langle j | \bar{m} | a \rangle|^2 \left( \frac{2\beta H}{3kT} \right) \quad (35)$$

$$\langle (\epsilon_L - \epsilon_R) \rangle_1 = |\langle j | \bar{m} | a \rangle|^2 \left( \frac{2}{3}\beta H \right) \quad (36)$$

$$\langle \epsilon \rangle_0 = |\langle j | \bar{m} | a \rangle|^2 \left( \frac{1}{3} \right) \quad (37)$$

$$\langle \epsilon \rangle_1 = \frac{1}{2} |\langle j | \bar{m} | a \rangle|^2 \left( \frac{2\beta^2 H^2}{3kT} \right) \approx 0 \quad (38)$$

The neglect of  $\langle \epsilon \rangle_1$  is justified since  $\beta H \ll kT$ .

The temperature dependent part of the MCD spectrum, Eq. (32) or Eq. (35), is denoted as the c term, and the derivative shaped contribution, Eq. (32) or Eq. (36), is an accompanying a term due to the degenerate ground state. Once again, the absorption spectrum, given by Eq. (33), depends

upon neither the temperature nor the magnetic field as long as  $\beta H < kT$ .

Consider now a molecule with three nondegenerate states,  $|a\rangle$ ,  $|j\rangle$ , and  $|k\rangle$  (Figure 7). The energy differences between these states will be assumed to be large compared to the Zeeman splitting. A homogenous external magnetic field applied along the z axis mixes the original states to form three new states,  $a'$ ,  $j'$ , and  $k'$  with zeroeth order energies of  $E_{a'}$ ,  $E_{j'}$ , and  $E_{k'}$ . The states to first order in the perturbation,  $-\bar{\mu} \cdot \bar{H}$ , are

$$|a'\rangle = |a\rangle + \frac{\langle k | \bar{\mu}_z | a \rangle |k\rangle H_z}{E_k - E_a} + \frac{\langle j | \bar{\mu}_z | a \rangle |j\rangle H_z}{E_j - E_a} \quad (39)$$

and

$$|j'\rangle = |j\rangle + \frac{\langle a | \bar{\mu}_z | j \rangle |a\rangle H_z}{E_a - E_j} + \frac{\langle k | \bar{\mu}_z | j \rangle |k\rangle H_z}{E_k - E_j} \quad (40)$$

where  $\mu_z = \frac{e\hbar}{2mc} L_z$  is the magnetic moment operator along the field direction. Using Equations (39) and (40), the transition dipoles between the perturbed states are now

$$\begin{aligned} |\langle a' | \bar{m}_{L,R} | j' \rangle|^2 &= |\langle a | \bar{m}_{L,R} | j \rangle|^2 \pm 2iH_z \left[ \frac{\langle j | \bar{\mu}_z | k \rangle}{E_k - E_j} \right. \\ &\quad \cdot (\langle a | \bar{m}_y | j \rangle \langle a | \bar{m}_x | k \rangle - \langle a | \bar{m}_x | j \rangle \langle a | \bar{m}_y | k \rangle) \\ &\quad \left. + \frac{\langle k | \bar{\mu}_z | a \rangle}{E_k - E_a} (\langle a | \bar{m}_y | j \rangle \langle j | \bar{m}_x | k \rangle - \langle a | \bar{m}_x | j \rangle \langle j | \bar{m}_y | k \rangle) \right] \end{aligned} \quad (41)$$

This equation is in the form

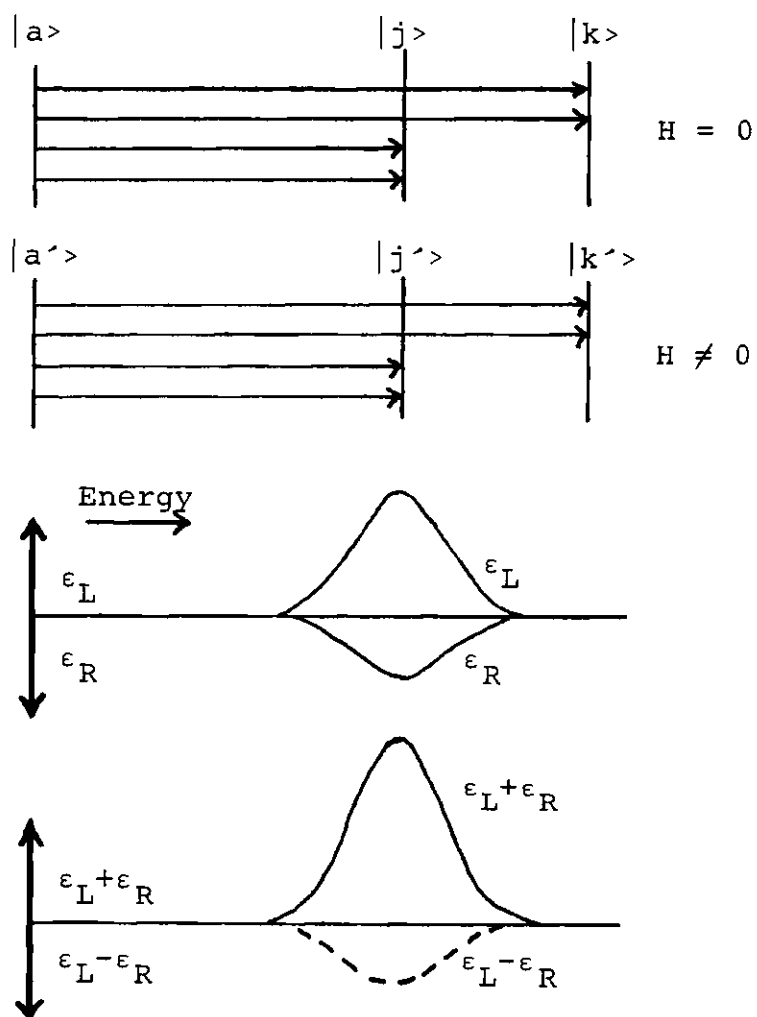


Figure 7. MCD b Term Due to Mixing of the States by the Magnetic Field. At zero field strength  $\epsilon_L = \epsilon_R$ .

$$X_{L,R} = Y_{L,R} \pm ZH_z \quad (42)$$

The extinction coefficient for this transition is proportional to the sum

$$X_L + X_R = Y_L + ZH_z + Y_R - ZH_z = Y_L + Y_R. \quad (43)$$

The difference of extinction coefficients is given by

$$\epsilon_L - \epsilon_R = Y_L - X_R = Y_L + ZH_z - Y_R + ZH_z = 2ZH_z. \quad (44)$$

Thus the first term of Eq. (41) is just the unperturbed dipole strength and contributes to the absorption spectrum, while the second term denoted as the b term contributes to the MCD. The appearance of magnetic field induced mixing of electronic state is explicit in the b term. If the transition  $|a\rangle$  to  $|j\rangle$  is isolated and  $|a\rangle$  is the only populated state, then the only apparent effect of the magnetic field will be to change the amplitude of  $\epsilon_L - \epsilon_R$ . Neither the total absorption nor the transition energy is affected.

Suppose now that  $E_k - E_j$  is smaller than the linewidth, then both transitions  $|a\rangle$  to  $|j\rangle$  and  $|a\rangle$  to  $|k\rangle$  must be considered. If these transitions are both polarized in the same direction, then the absorption spectrum will be the sum of the two transitions, but the MCD spectrum will cancel. On the other hand, suppose the transitions to be polarized perpendicular to each other. Assume that state  $|j\rangle$  is x dipole allowed

and  $|k\rangle$  is y dipole allowed, then

$$\epsilon_L(a \rightarrow j) - \epsilon_R(a \rightarrow j) = - \frac{4iH_z \langle a | \bar{m}_x | j \rangle \langle a | \bar{m}_y | k \rangle \langle j | \bar{\mu}_z | k \rangle f(\nu, E_j)}{E_k - E_j} \quad (45)$$

and

$$\epsilon_L(a \rightarrow k) - \epsilon_R(a \rightarrow k) = + \frac{4iH_z \langle a | \bar{m}_x | j \rangle \langle a | \bar{m}_y | k \rangle \langle j | \bar{\mu}_z | k \rangle f(\nu, E_k)}{E_k - E_j} \quad (46)$$

These lineshape functions may be expanded about a common point,  $\nu_0$ , by means of a Taylor series.

$$\nu_0 = \frac{E_k + E_j}{2}, \quad E_k > E_j \quad (47)$$

$$\epsilon_L - \epsilon_R = 4iH_z \langle a | \bar{m}_x | j \rangle \langle a | \bar{m}_y | k \rangle \langle j | \bar{\mu}_z | k \rangle f'(\nu, \nu_0) \quad (48)$$

$$\epsilon = [|\langle a | \bar{m}_x | j \rangle|^2 + |\langle a | \bar{m}_y | k \rangle|^2] f(\nu, \nu_0) \quad (49)$$

Note that this difference term is identical in form with the a term. A combination of magnetic field induced splitting and zero field splitting of approximately degenerate excited levels gives rise to the MCD A term. A more rigorous analysis of this case has been carried out by Sutherland, et. al.<sup>48,57</sup>

Finally consider the case where  $E_k - E_a$  is smaller than the linewidth and  $E_k - E_a \ll kT$ . This example corresponds to a ground state which suffers zero field splitting. The zero field splitting is much greater than any splitting caused by

the magnetic field. Dipole intensities of both  $|a\rangle$  to  $|j\rangle$  and  $|k\rangle$  to  $|j\rangle$  transitions must be calculated. Should the two transitions be polarized in the same direction, then the MCD spectrum vanishes. Assuming that  $|a\rangle$  to  $|j\rangle$  is x dipole allowed and  $|k\rangle$  to  $|j\rangle$  is y dipole allowed as is the case in the porphyrin anions, then

$$\epsilon_L(a \rightarrow j) - \epsilon_R(a \rightarrow j) = - \frac{4iH_z \langle k | \bar{\mu}_z | a \rangle \langle a | \bar{m}_x | j \rangle \langle j | \bar{m}_y | k \rangle f(\nu, E_j - E_a) N_a}{E_k - E_a} \quad (50)$$

$$\epsilon_L(k \rightarrow j) - \epsilon_R(k \rightarrow j) = + \frac{4iH_z \langle k | \bar{\mu}_z | a \rangle \langle a | \bar{m}_x | j \rangle \langle j | \bar{m}_y | k \rangle f(\nu, E_j - E_k) N_k}{E_k - E_a} \quad (51)$$

$$\epsilon_L - \epsilon_R = 4iH_z [f'(\nu, \nu_0) - \frac{f(\nu, \nu_0)}{kT}] [\langle k | \bar{\mu}_z | a \rangle \langle a | \bar{m}_x | j \rangle \langle j | \bar{m}_y | k \rangle] \quad (52)$$

$N_a$  is the population of state  $|a\rangle$  and  $N_k$  is the population of state  $|k\rangle$ .

$$N_a + N_k = 1 \quad (53)$$

Note that this combination of b terms is identical to the previously discussed, Eq. (32), c and a terms for a degenerate state. This case, which is applicable to the porphyrin mono-anions, will be treated in a more precise manner elsewhere.

In summary the observed MCD spectra will consist of transitions between groups of states. Each group contains vibrational, spin, and electronic levels. The a terms arise from the Zeeman splitting of the degenerate levels, the c terms come from a population distribution over Zeeman split

levels in the ground electronic state, and the b terms arise from magnetic field induced mixing of the zero field states. The observed a and c terms will be enriched at the expense of the b terms. Following Serber,<sup>36</sup> these observable quantities are called A, B, and C terms. The MCD A term resembles the first derivative of the absorption, while both B and C terms resemble the absorption spectrum, but are distinguished from one another by the temperature dependence of the C terms. This relationship between the individual a, b, and c terms and the observable A, B, and C terms is given in Table 1. Note that although the presence of a or c terms requires the molecule to possess at least three fold symmetry, the presence of observable A or C terms implies only approximate degeneracy. Therefore, it is possible to use nondegenerate molecular orbital calculations for almost degenerate molecules to calculate the A, B, and C terms and compare the results to these quantities derived from analysis of the MCD experimental spectra.

#### Pi-Electron Calculation of Porphyrin Molecular Orbital Wavefunctions

The  $\pi$  molecular orbitals are generated by a self-consistent-field molecular orbital (SCF-MO) computer program<sup>51</sup> using the methods of Pariser and Parr<sup>52</sup> and of Pople<sup>53</sup> for the closed-shell molecules, and that of Roothaan<sup>54,55</sup> for open-shell doublets. The mathematical treatment assumes that the sigma electron system can be combined with the

Table 1. Summary of the Relationship Between the Theoretical  
a, b, and c Terms and the Experimental A, B, and C Terms.

THEORY	EXPERIMENTAL
DEGENERATE STATE PRESENT	
1 Zeeman split excited states (a term)	A The MCD spectrum resembles the first derivative of the absorption spectrum.
2 Boltzmann distribution over Zeeman split ground state (a and c terms)	B The MCD spectrum has the same shape as the absorption spectrum.
NON-DEGENERATE STATES (b terms)	
3 State separations are greater than bandwidths. (In principle this term contributes in varying amounts to all MCD spectra.)	C The MCD spectrum has the same shape as the absorption spectrum, but has a $1/T$ dependence. There is also an A term present.
4 The separation between excited states is less than the bandwidth and the transition dipoles to these states are perpendicular.	
5 The separation between the ground state and at least one excited state is $\leq kT$ .	

nuclear attraction to form a one-electron core potential for the  $\pi$  electrons. Differential overlap between orbitals on different centers is set to zero. The semiempirical parameters are those of Weiss:<sup>56</sup> for carbon atoms, core charge ( $Z$ ) is +1, ionization potential ( $\alpha_C$ ) is -11.24 eV and repulsion integral ( $\gamma_{CC}$ ) is 9.4915 eV; for nitrogens in metallo-complexes,  $z$  is 1.5,  $\alpha_N$  is -20.59 eV, and  $\gamma_{NN}$  is 12.120 eV; for nitrogens in free bases either  $Z$  is 1 and  $\alpha_N$  is -14.54 (N-H) or  $Z$  is 2 and  $\alpha_N$  is -26.64 eV. The resonance integrals are given by

$$\beta_{ij} = -2.371S(R_{ij})\text{eV}/S(1.39\text{\AA}). \quad (54)$$

$S(R_{ij})$  is the overlap of the two Slater  $p_z$  orbitals separated by distance,  $R_{ij}$ , and with the Slater orbital exponents

$$\xi = 3.24. \quad (55)$$

Restricted Hartree-Fock theory gives the Fock operators<sup>51,52</sup>

$$F_C = H + 2J_T - K_T \quad (56)$$

and<sup>54,55</sup>

$$F_O = H + 2J_T - K_T + 2(M_T - K_O) \quad (57)$$

for the pseudo-eigenvalue problem

$$F\phi_i = \epsilon_i\phi_i. \quad (58)$$

Here  $F_C$  and  $F_O$  are the closed and open shell Fock operators, respectively;  $H$  is the one electron operator;  $J_T$  and  $K_T$  are the total Coulomb and exchange operators, respectively;  $M_T$  is the exchange coupling operator;  $K_O$  is the exchange operator for the half filled shell;  $\phi_i$ 's are the molecular orbitals; and  $\epsilon_i$ 's are the orbital energies. Application of these orbitally non-degenerate calculations to the porphyrin ions is not unreasonable, since (as it will be shown later) there is experimental evidence that the orbital degeneracy is removed in solution.

After the molecular orbitals are obtained, the configuration interaction matrix elements can be calculated among the lowest energy singly excited states, lowest energy doubly excited states and the ground state. The program used allows the inclusion of sixty configurations. Whenever possible, all configurations  $\leq 5.0$  eV were included. In all cases, all states were used which had at least a 10% contribution to either the ground state or optically accessible excited states. For closed shell spectra of the neutral compounds, double excitations were not necessary to explain the spectra. However, for the dianions three types of doubly excited configurations are necessary ( $^1\chi_2$ ,  $^1\chi_3$ , and  $^1\chi_4$ ). For the open shell molecules only one type of doubly excited configuration ( $^2\chi_5$ ) corresponding to  $k, m \rightarrow 2n$  is necessary. These configurations along with their excitation energies are given in Tables 2 and 3.

Table 2. Doublet State Configurations and Energies.  
 1, 2, ..., k are filled orbitals, m is the unique half filled orbital, and n, o, ..., z are virtual orbitals.  
 ${}^2\chi_0$  is the ground state. J and K are the Coulomb and exchange integrals, respectively.

### Configurations

$${}^2\chi_0 = |\phi_1 \bar{\phi}_1 \cdots \phi_k \bar{\phi}_n \phi_m|$$

$${}^2\chi_1 = |\phi_1 \bar{\phi}_1 \cdots \phi_k \phi_m \bar{\phi}_n|$$

$${}^2\chi_2 = |\phi_1 \bar{\phi}_1 \cdots \phi_k \bar{\phi}_k \phi_n|$$

$${}^2\chi_3 = \frac{1}{\sqrt{2}} \{ |\phi_1 \bar{\phi}_1 \cdots \phi_k \phi_m \bar{\phi}_n| - |\phi_1 \bar{\phi}_1 \cdots \bar{\phi}_k \phi_m \phi_n| \}$$

$${}^2\chi_4 = \frac{1}{\sqrt{6}} (2|\phi_1 \bar{\phi}_1 \cdots \phi_k \bar{\phi}_m \phi_n| - |\phi_1 \bar{\phi}_1 \cdots \phi_k \phi_m \bar{\phi}_n| - |\phi_1 \bar{\phi}_1 \cdots \phi_k \phi_m \phi_n|)$$

### Excitation Energies

$${}^2\chi_1 : \epsilon_m - \epsilon_k + 1/2J_{mm} + 3/2K_{km} - J_{km}$$

$${}^2\chi_2 : \epsilon_n - \epsilon_m + 1/2J_{mm} + 3/2K_{km} - J_{mn}$$

$${}^2\chi_3 : \epsilon_n - \epsilon_k + K_{mn} + K_{mk} + 2K_{kn} - J_{kn}$$

$${}^2\chi_4 : \epsilon_n - \epsilon_k + 2K_{mn} + 2K_{mk} - J_{kn}$$

$${}^2\chi_5 : 2\epsilon_n - \epsilon_k - \epsilon_m - 2J_{kn} + K_{kn} + J_{nn} - 2J_{mn} + 3K_{mn} + J_{km} + 1/2K_{km} + 1/2J_{mm}$$

Table 3. Singlet State Configurations and Energies.  
 1, 2, ...k are filled orbitals and n, o, ...z  
 are virtual orbitals.  $^1\chi_0$  is the ground state.  
 J and K are the Coulomb and exchange integrals,  
 respectively.

### Configurations

$$^1\chi_0 = |\phi_1\bar{\phi}_1 \cdots \phi_j\bar{\phi}_j\phi_k\bar{\phi}_k|$$

$$^1\chi_1 = \frac{1}{\sqrt{2}} (|\phi_1\bar{\phi}_1 \cdots \phi_j\bar{\phi}_j\phi_k\bar{\phi}_n| - |\phi_1\phi_1 \cdots \phi_j\bar{\phi}_j\bar{\phi}_k\phi_n|)$$

$$^1\chi_2 = |\phi_1\bar{\phi}_1 \cdots \phi_j\bar{\phi}_j\phi_n\bar{\phi}_n|$$

$$^1\chi_3 = \frac{1}{\sqrt{2}} (|\phi_1\bar{\phi}_1 \cdots \phi_j\bar{\phi}_j\phi_k\bar{\phi}_n| - |\phi_1\bar{\phi}_1 \cdots \bar{\phi}_j\phi_k\phi_n\bar{\phi}_n|)$$

$$^1\chi_4 = \frac{1}{\sqrt{2}} (|\phi_1\bar{\phi}_1 \cdots \phi_j\bar{\phi}_j\phi_n\bar{\phi}_o| - |\phi_1\bar{\phi}_1 \cdots \phi_j\bar{\phi}_j\bar{\phi}_n\phi_o|)$$

### Excitation Energies

$$\chi_1: \epsilon_n - \epsilon_k - J_{kn} + 2K_{kn}$$

$$\chi_2: 2\epsilon_n - 2\epsilon_k - 2(2J_{kn} - K_{kn}) + J_{nn} + J_{kk}$$

$$\chi_3: 2\epsilon_n - \epsilon_j - \epsilon_k - (2J_{kn} - K_{kn}) - (2J_{jn} - K_{jn}) + J_{kj} + J_{nn} + K_{jk}$$

The next step in calculating an MCD spectrum is to obtain the angular momenta and transition dipoles among the orbitals.<sup>12,52,57</sup> Then the matrix elements among the various configurations are calculated in terms of the previous quantities. Finally, the matrix elements of  $\bar{M}_z$  and  $e\bar{r}$  among the configurations are combined with the configuration interaction expansion coefficients to obtain values for the angular momenta<sup>19</sup> and electric dipoles<sup>52</sup> among the states. At this point we have the state energies and matrix elements of angular momentum and x and y components of the electric dipole operator among the states. The  $\underline{b}$  terms for a transition from state  $|a\rangle$  to state  $|j\rangle$  are given by

$$\begin{aligned}
 b(a \rightarrow j) = & i \left\{ \sum_{k \neq j} [\langle j | \bar{\mu}_z | k \rangle (\langle a | \bar{m}_y | j \rangle \langle a | \bar{m}_x | k \rangle \right. \\
 & \left. - \langle a | \bar{m}_x | j \rangle \langle a | \bar{m}_y | k \rangle) / (E_k - E_j) \right\} \\
 & + \sum_{k \neq a} [\langle k | \bar{\mu}_z | a \rangle (\langle a | \bar{m}_y | j \rangle \langle j | \bar{m}_x | k \rangle \\
 & - \langle a | \bar{m}_x | j \rangle \langle j | \bar{m}_y | k \rangle) / (E_k - E_a) ] \}
 \end{aligned} \tag{59}$$

with the dipole strength appearing as

$$D(a \rightarrow j) = |\langle a | \bar{m}_x | j \rangle|^2 + |\langle a | \bar{m}_y | j \rangle|^2. \tag{60}$$

Equations (59) and (60) are valid for orbitally non-degenerate states. The A and C terms are calculated from the  $\underline{b}$  terms whenever  $E_k - E_j$  or  $E_k - E_a$  approach the linewidth of the transition.<sup>8,36</sup>

$$A(a \rightarrow j) = \frac{i}{a, j} \sum [\langle a | \bar{\mu}_z | a \rangle - \langle j | \bar{\mu}_z | j \rangle] [\langle a | \bar{m}_x | j \rangle \langle j | \bar{m}_y | a \rangle] \quad (61)$$

$$C(a \rightarrow j) = \frac{i}{a, j} \sum \langle a | \bar{\mu}_z | a \rangle \langle a | \bar{m}_x | j \rangle \langle j | \bar{m}_y | a \rangle$$

$$B(a \rightarrow j) = \sum_{a, j} \left\{ i \sum_{k \neq a} \frac{\langle k | \bar{\mu}_z | a \rangle}{E_k - E_a} [\langle a | \bar{m}_x | j \rangle \langle j | \bar{m}_y | k \rangle - \langle a | \bar{m}_y | j \rangle \langle j | \bar{m}_x | k \rangle] \right. \\ \left. + \sum_{k \neq j} \frac{\langle j | \bar{\mu}_z | k \rangle}{E_k - E_j} [\langle a | \bar{m}_x | j \rangle \langle k | \bar{m}_y | a \rangle - \langle a | \bar{m}_y | j \rangle \langle k | \bar{m}_x | a \rangle] \right\} \quad (62)$$

The final step is to compare these parameters with the experimental data. For a single transition at an energy,  $\nu_0$ , the absorption spectrum has a line shape which is given by  $f(\nu, \nu_0)$  (see Eq. 9) and magnitude which is given by the D term. The MCD spectrum due to the A term resembles the first derivative of the absorption spectrum, while for both B and C terms the contribution resembles the absorption spectrum, but can be distinguished from one another by the temperature dependence of the C term contribution. (At this point we should note that while the D term is always positive, the A, B, and C terms can be of either sign.) The observed spectra will be due to the summation of the spectral contributions of all electronic transitions. If the units are  $[\theta]_M$ ,  $\text{deg cm}^2 \text{ gauss}^{-1} \text{ dmole}^{-1}$ ;  $\epsilon$ ,  $\text{liter cm}^{-1} \text{ mole}^{-1}$ ;  $\nu$ ,  $\text{cm}^{-1}$ ; B,  $\text{Debye}^2 \text{ Bohr magneton cm}^{-1}$ ; A and C,  $\text{Debye}^2 \text{ Bohr magneton}$ ; and  $kT$ ,  $\text{cm}^{-1}$ ; then the experimental spectrum (in terms of normalized line

shape functions) is given by<sup>6,8</sup>

$$\frac{[\theta]_M}{\nu} = -33.53 \sum_i \left[ \left( B_i + \frac{C_i}{kT} \right) f_i + A_i f_i' \right] \quad (63)$$

and the absorption spectrum by<sup>6,8</sup>

$$\frac{\epsilon}{\nu} = 108.9 \sum_i D_i f_i \quad (64)$$

The summation is over all transitions.  $f_i$  and  $f_i'$  are line-shape functions with  $f_i'$  being the first derivative of  $f_i$ .

$$\int_{\text{band}} f_i d\nu = 1 \quad (65)$$

$$\int_{\text{band}} f_i' d\nu = 0 \quad (66)$$

and

$$\int_{\text{band}} f_i' \nu d\nu = -1 \quad (67)$$

#### Zero Field Splitting of an Orbitally Degenerate Ground State and its Effect Upon the MCD Spectrum

In the preceding discussion, the theoretical a, b, and c terms were introduced to explain the A, B, and C terms of MCD spectra.<sup>36</sup> The terms were derived by assuming that the wave-functions can be expanded accurately to first order in the magnetic field. For a and c terms, choice of complex zeroeth order states for which  $H_{\text{pert}} = -\vec{\mu} \cdot \vec{H}$  is diagonal avoids the problem of a prior diagonalization. The b terms due to nearly degenerate states can mimic the a and c terms if the

zero field splitting is much greater than the magnetic field perturbation, but less than the linewidth. Under these conditions, the calculations for a, b, and c terms are fairly straightforward. However, if the zero field splitting and the magnetic field splitting are of the same magnitude, then both perturbations must be considered simultaneously. Although the resulting spectra may still be interpreted as A, B, and C terms, the origin of these terms will be more complex than the a, b, and c terms.<sup>36</sup>

Since the chlorins, bacteriochlorins, and metal free porphyrins have no higher than 2-fold symmetry, they will not normally have doubly degenerate states.<sup>70,71</sup> If the zero field splittings are much greater than the magnetic field splittings, the spectra of these compounds may be interpreted from b terms. However, since the metalloporphyrins have  $D_{4h}$  symmetry, then it is possible to have doubly degenerate  $E_u$  or  $E_g$  states for the metalloporphyrins. Transitions involving these states would give rise to a or c terms. However, there is mounting evidence that porphyrins in solution are subjected to an external potential which lowers the symmetry of these species and thus removes orbital degeneracy.<sup>58</sup> Without prior knowledge of the nature of this perturbation, it is impossible to know whether or not this zero field perturbation is of the same order of magnitude as the magnetic field splitting. Since the methods of Serber<sup>36</sup> and Stephens<sup>8</sup> apply these two perturbations

separately and thus imply that one of the two perturbations is much more important than the other; a different approach must be used applying both perturbations simultaneously. At the same time it is advantageous to see if other effects such as spin might influence the MCD spectrum.

The ground state of the metalloporphyrin monoanion in  $D_{4h}$  symmetry is  ${}^2E_g$ . The allowed transitions will be from  ${}^2E_g$  to  ${}^2A_{1u}$ ,  ${}^2A_{2u}$ ,  ${}^2B_{1u}$ , and  ${}^2B_{2u}$ . A three state model which encompasses the ground state and one of these excited states can be used to explain the MCD spectra. The model used in this derivation consists of two orthonormal real states,  $|x\rangle$  and  $|y\rangle$ , which are components of the  ${}^2E_g$  level and a third state representing one of the nondegenerate, optically accessible states,  $|j\rangle$ .  $|j\rangle$  will be chosen as a  $B_{1u}$  state in order to compare these calculations with the lowest excited state of the metalloporphyrin anion spectra.

The treatment employed follows a three state model used by Sutherland, et. al.,<sup>48,57</sup> in their discussion of the zero-field splitting of the excited  ${}^1E_u$  state of neutral porphyrins. The Hamiltonian in the presence of an external magnetic field,  $H$ , applied along the  $+z$  direction of a space fixed axis is

$$H = H_0 + \frac{\beta}{\hbar} L_z H_z + g\beta S_z H_z + \frac{\lambda L_z S_z}{\hbar} + H_{ZF} \quad (68)$$

$H_0$  is the molecular Hamiltonian which is an eigenoperator of  $|x\rangle$ ,  $|y\rangle$ , and  $|j\rangle$  with eigenvalues  $E_0$ ,  $E_0$ , and  $E_j$ . The second

and third terms are respectively the interactions of orbital and spin angular momentum with the external magnetic field. The fourth term represents the spin-orbit interaction of the ring angular momentum,  $L_z$ , with the unpaired spin angular momentum,  $S_z$ . Finally,  $H_{zF}$  is the zero field interaction induced by the solvent molecules or counter ions remove the degeneracy of  $|x\rangle$  and  $|y\rangle$ .

Limiting the effective interactions to a single one along the N-N axes of the porphyrin leads to

$$(H_O + H_{zF})|x\rangle = E_x|x\rangle \quad (69)$$

and

$$(H_O + H_{zF})|y\rangle = E_y|y\rangle \quad (70)$$

The possibility of a range of different interaction values<sup>59</sup> or of a rotation of the zero field interaction are both ignored.<sup>60</sup> The objective of this derivation is to provide a qualitative picture of the influence of the crystal field splitting on MCD splitting.

Since  $[H, S_z] = 0$ ,  $S_z$  is a good quantum number. Transitions take place between states with the same eigenvalues of  $S_z$ .

The states  $|x\rangle$  and  $|y\rangle$  satisfy the following relations, which define the phase convention,

$$L_z|x\rangle = iM_z\hbar|y\rangle \quad (71)$$

and

$$L_z |y\rangle = -iM_z \hbar |x\rangle \quad (72)$$

Thus, for  $M_z > 0$ , the states  $|x\rangle$  and  $|y\rangle$  transform like the  $x$  and  $y$  coordinates.

A matrix representation of  $H$  breaks up into a pair of  $2 \times 2$  submatrices with the elements ( $\pm 1/2$  represent the  $S_z$  value)

$$\langle x, \pm \frac{1}{2} | \bar{H} - E\bar{I} | x, \pm \frac{1}{2} \rangle = E_x \pm \frac{g\beta H_z}{2} - E \quad (73)$$

$$\langle y, \pm \frac{1}{2} | \bar{H} - E\bar{I} | y, \pm \frac{1}{2} \rangle = E_y \pm \frac{g\beta H_z}{2} - E \quad (74)$$

$$\langle x, \pm \frac{1}{2} | \bar{H} - E\bar{I} | y, \pm \frac{1}{2} \rangle = -iM_z (H_z \beta \pm \lambda/2) \quad (75)$$

$$\langle y, \pm \frac{1}{2} | \bar{H} - E\bar{I} | x, \pm \frac{1}{2} \rangle = iM_z (H_z \beta \pm \lambda/2) \quad (76)$$

The resulting eigenvalues may be simplified by using

$$E_o = (E_x + E_y)/2, \quad (77)$$

$$\Delta E_N = (E_y - E_x)/2, \quad (78)$$

and

$$\Delta E_T^{\pm} = [(\Delta E_N)^2 + M_z^2 (\beta H_z \pm \lambda/2)^2]^{1/2}. \quad (79)$$

Diagonalization of  $H$  yields eigenvalues, labelled by  $S_z = \pm 1/2$ , viz.,

$$E_1^{\pm} = E_0 \pm \frac{g\beta H_z}{2} - \Delta E_T^{\pm} \quad (80)$$

and

$$E_2^{\pm} = E_0 \pm \frac{g\beta H_z}{2} + \Delta E_T^{\pm} \quad (81)$$

The associated eigenvectors are

$$|1^{\pm}\rangle = \alpha^{\pm}|x\rangle - i\gamma^{\pm}|y\rangle \quad (82)$$

and

$$|2^{\pm}\rangle = \gamma^{\pm}|x\rangle + i\alpha^{\pm}|y\rangle \quad (83)$$

with

$$\alpha^{\pm} = \frac{\Delta E_N + \Delta E_T}{\sqrt{M_z^2 [\beta H_z \pm \lambda/2]^2 + [\Delta E_N + \Delta E_T^{\pm}]^2}} \quad (84)$$

and

$$\lambda^{\pm} = \frac{M_z (\beta H_z \pm \lambda/2)}{\sqrt{M_z^2 [\beta H_z \pm \lambda/2]^2 + [\Delta E_N + \Delta E_T^{\pm}]^2}} \quad (85)$$

To obtain the absorption and magnetic circular dichroism spectra, the dipole strengths must be calculated for transitions from the four occupied levels to the final state  $|j\rangle$  (see Figure 8).

The transition dipoles for  $|j\rangle$  and  $|i\rangle$  are

$$e\langle j|\vec{r}|i^{\pm}\rangle = \hat{x}eC_i^{\pm}x\langle j|\vec{x}|x\rangle \pm \hat{y}eC_i^{\pm}x\langle j|\vec{y}|y\rangle \quad (86)$$

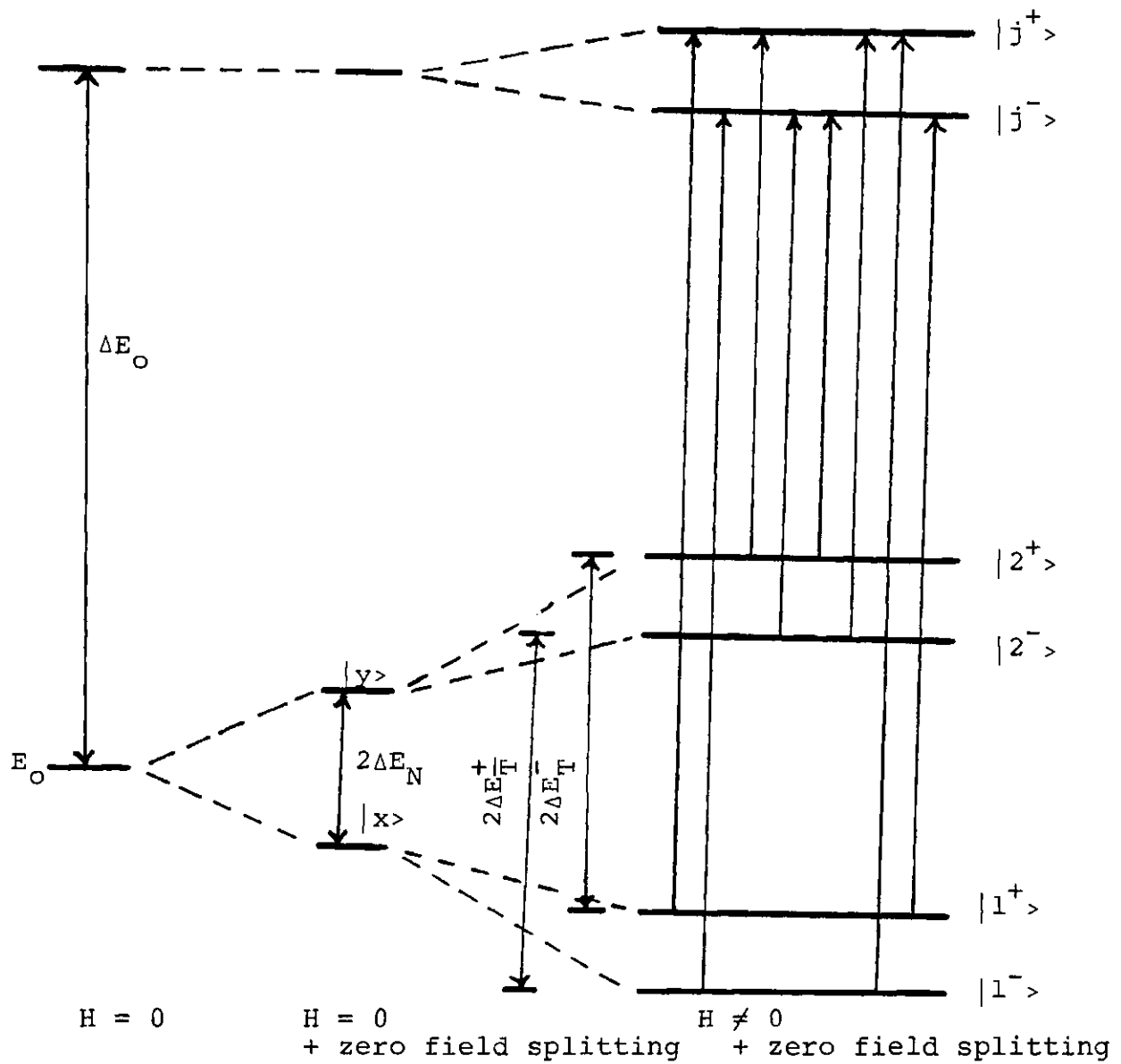


Figure 8. Energy Levels for a Nearly Degenerate Ground State. The energies are given in Equa. (77-79) and are not shown to scale. The eigenvectors are given by Eqs. (82) and (83). The eight extinction coefficients are given by Eqs. (147-150).

and

$$e\langle j|\bar{r}|i\rangle = \hat{x}eC_{1x}^{\pm}\langle j|\bar{x}|x\rangle \pm \hat{y}eC_{1y}^{\pm}\langle j|\bar{y}|y\rangle \quad (87)$$

Here  $e$  is the electron charge,  $\bar{r}$  is the radius vector in the molecule's coordinate system,  $\bar{r} = x\hat{x} + y\hat{y}$ ,  $C_{1x}^{\pm} = \alpha^{\pm}$ ,  $C_{1y}^{\pm} = i\gamma^{\pm}$ ,  $C_{2x}^{\pm} = \gamma^{\pm}$ , and  $C_{2y}^{\pm} = i\alpha^{\pm}$ . The sign convention depends on the initial definition of the phase convention for  $L_z$ .

For  $B_{1u}$  and  $B_{2u}$  states the sign is negative. For  $A_{1u}$  and  $A_{2u}$  states the sign is positive.

The probabilities of absorption of left and right circularly polarized light are obtained from

$$\langle j| \left( \frac{\hat{x} \pm i\hat{y}}{\sqrt{2}} \right) \cdot \bar{e}r | i \rangle, \quad (88)$$

where  $\frac{\hat{x} \pm i\hat{y}}{\sqrt{2}}$  are the unit vectors for the two components of the light. However,

$$\langle j| \left( \frac{\hat{x} \pm i\hat{y}}{\sqrt{2}} \right) \cdot \bar{e}r | i \rangle \neq \langle i| \left( \frac{\hat{x} \pm i\hat{y}}{\sqrt{2}} \right) \cdot \bar{e}r | j \rangle \quad (89)$$

Thus, care must be taken in choosing the combination which represent the right circularly polarized light (RCPL) and the left circularly polarized light (LCPL). It will be assumed for the present that the light beam is traveling along the  $z$  direction. An incorrect choice here will have the effect of reversing the direction of the light beam. This would invert the calculated spectrum.

Following Riehl and Richardson,<sup>61</sup> we will consider

$$\hat{e}_R = \frac{1}{\sqrt{2}} (\hat{x} - i\hat{y}) \quad (90)$$

and

$$\hat{e}_L = \frac{1}{\sqrt{2}} (\hat{x} + i\hat{y}) \quad (91)$$

where  $\hat{e}_R$  and  $\hat{e}_L$  represent the RCPL and LCPL respectively. This convention corresponds to left circularly polarized radiation tracing out a right handed helix as the radiation propagates along the +z space fixed axis (chemist's convention). The interaction Hamiltonian coupling the radiation field and the matter Hamiltonian is written in terms of complex field operators

$$H_{int} = - \frac{1}{2} \tilde{d}^+ \cdot \tilde{f} - \frac{1}{2} \tilde{d} \cdot \tilde{f}^+ \quad (92)$$

with

$$\tilde{f} = i \sum_{\ell} \left( \frac{2\hbar\omega_{\ell}}{\epsilon_0 V} \right)^{1/2} \{ \hat{e}_L a_{\ell L} e^{i\tilde{k}_{\ell} \cdot \tilde{r}} - \hat{e}_L a_{\ell}^+ e^{-i\tilde{k}_{\ell} \cdot \tilde{r}} \} \quad (93)$$

$$\tilde{f}^+ = i \sum_{\ell} \left( \frac{2\hbar\omega_{\ell}}{\epsilon_0 V} \right)^{1/2} \{ \hat{e}_R a_{\ell R} e^{i\tilde{k}_{\ell} \cdot \tilde{r}} - \hat{e}_R a_{\ell L}^+ e^{-i\tilde{k}_{\ell} \cdot \tilde{r}} \} \quad (94)$$

being the complex field operators. The summation is over the  $\ell$  modes of the field in the quantization volume  $V$ . The annihilation and creation operators for the photon field are

$$a_{\ell L} = \frac{1}{\sqrt{2}}(a_{\ell x} - ia_{\ell y}) \quad (95)$$

$$a_{\ell R} = \frac{1}{\sqrt{2}}(a_{\ell x} + ia_{\ell y}) \quad ]- \text{annihilation} \quad (96)$$

$$a_{\ell L}^+ = (a_{\ell L})^+ \quad (97)$$

$$a_{\ell R}^+ = (a_{\ell R})^+ \quad ]- \text{creation} \quad (98)$$

The operators  $\tilde{d}$  and  $\tilde{d}^+$  are complex polarization operators formed from molecular sources of current and charge density. These are

$$\tilde{d} = \tilde{p} + i \tilde{m}; \quad (99)$$

$$\tilde{d}^+ = \tilde{p} - i \tilde{m} \quad (100)$$

with

$$p_i = r_{i\alpha} \delta(r - R_\alpha) \quad (101)$$

$$m_i = m'_{i\alpha} \delta(r - R_\alpha) \quad (102)$$

Here  $r_{i\alpha}$  and  $m'_{i\alpha}$  are the  $i$ th ( $x, y, z$ ) components of the electric and magnetic moments.

The amplitude for absorption of a LCPL photon from the field is found from the dipole matrix element

$$R_{L,i} = \langle n_\ell - 1 | \langle j | -1/2 \tilde{d}^+ \cdot \tilde{f} | i \rangle | n_\ell \rangle \quad (103)$$

$$\approx \langle n_{\ell}-1 | \langle j | \hat{e}_L \cdot \hat{d}^+ a_{\ell L} | i \rangle | n_{\ell} \rangle \quad (104)$$

$$\approx \frac{1}{\sqrt{2}} \langle j | (\hat{x} + i\hat{y}) \cdot e\vec{r} | i \rangle \quad (105)$$

where only the electric dipole component of  $\hat{d}$  is employed. For a dipole allowed transition, the magnetic component will be small. The probability of absorption is proportional to

$$R_{L,i;R,i}^{2\pm} = \frac{1}{2} |\langle j | (\hat{x} \pm i\hat{y}) \cdot e\vec{r} | i^{\pm} \rangle|^2 \quad (106)$$

$$R_{L,i;R,i}^{2\pm} = \frac{1}{2} |C_{ix}^{\pm} R_x^{\pm} + iC_{iy}^{\pm} R_y^{\pm}|^2 \quad (107)$$

where L and R refer, respectively, to  $x + iy$  and  $x - iy$ , and

$$R_x = e \langle j | x | x \rangle; \quad (108)$$

$$R_y = e \langle j | y | y \rangle; \quad (109)$$

In terms of the coefficients,  $\alpha^{\pm}$  and  $\gamma^{\pm}$ , we may write

$$R_{L,1}^{\pm 2} = \frac{1}{2} (\alpha^{\pm} R_x)^2 + \frac{1}{2} (\gamma^{\pm} R_y)^2 - \alpha^{\pm} \gamma^{\pm} R_x R_y \quad (110)$$

$$R_{R,1}^{\pm 2} = \frac{1}{2} (\alpha^{\pm} R_x)^2 + \frac{1}{2} (\gamma^{\pm} R_y)^2 + \alpha^{\pm} \gamma^{\pm} R_x R_y \quad (111)$$

$$R_{L,2}^{\pm 2} = \frac{1}{2} (\gamma^{\pm} R_x)^2 + \frac{1}{2} (\alpha^{\pm} R_y)^2 + \alpha^{\pm} \gamma^{\pm} R_x R_y \quad (112)$$

$$R_{R,2}^{\pm 2} = \frac{1}{2} (\gamma^{\pm} R_x)^2 + \frac{1}{2} (\alpha^{\pm} R_y)^2 - \alpha^{\pm} \gamma^{\pm} R_x R_y \quad (113)$$

The relative populations of the four levels of this approximately degenerate state are

$$N_1^+ = e^{-g\beta H/kT} e^{+\Delta E_T^+/kT} / Z \quad (114)$$

$$N_2^+ = e^{-g\beta H/kT} e^{-\Delta E_T^+/kT} / Z \quad (115)$$

$$N_1^- = e^{\Delta E_T^-/kT} / Z \quad (116)$$

$$N_2^- = e^{-\Delta E_T^-/kT} / Z \quad (117)$$

$$Z = e^{\Delta E_T^-/kT} + e^{-\Delta E_T^-/kT} + e^{-g\beta H/kT} [e^{\Delta E_T^+/kT} + e^{-\Delta E_T^+/kT}] \quad (118)$$

$$Z = 2\cosh(\Delta E_T^-/kT) + 2e^{-g\beta H/kT} [\cosh(\Delta E_T^+/kT)] \quad (119)$$

where

$$E_0 = 0. \quad (120)$$

The total absorption intensity is the sum of the individual eight contributions weighted by the occupancy of each level.

$$\begin{aligned} R^2 = & N_1^+ [(R_{L,1}^+)^2 + (R_{R,1}^+)^2] + N_2^+ [(R_{L,2}^+)^2 + (R_{R,2}^+)^2] \\ & + N_1^- [(R_{L,1}^-)^2 + (R_{R,1}^-)^2] + N_2^- [(R_{L,2}^-)^2 + (R_{R,2}^-)^2] \end{aligned} \quad (121)$$

$$R^2 = \frac{1}{2}(R_x^2 + R_y^2) \quad (122)$$

The MCD spectrum is due to the difference between the absorption of LCPL and RCPL. Consider the case of a large zero field splitting at relatively low temperatures.

$$E_T^{\pm} \approx E_N \gg kT \quad (123)$$

The temperature is high enough so that both spin states are equally populated. Spin orbit coupling will be ignored. The populations of the two  $s_z' = 1/2$  levels with energy,  $E_1$  are

$$N_1^{+} = N_1^{-} = 1/2. \quad (124)$$

The difference in the absorption intensity of LCPL and RCPL is

$$\delta R^2 = N_1^{+} [(R_{L,1}^{+})^2 - (R_{R,1}^{+})^2] \quad (125)$$

$$+ N_1^{-} [(R_{L,1}^{-})^2 - (R_{R,1}^{-})^2]$$

$$= -2\alpha^{\pm}\gamma^{\pm}R_xR_y. \quad (126)$$

Since

$$\alpha^{\pm}\gamma^{\pm} = M_z [\beta H_x \pm \lambda/2] / 2\Delta E_T^{\pm}, \quad (127)$$

then

$$\delta R^2 = - \frac{\beta M_z R_x R_y H_z}{\Delta E_N} \quad (128)$$

The MCD signal will be negative for a transition from a split

$\underline{{}^2E_g}$  to either  $\underline{B_{1u}}$  or  $\underline{B_{2u}}$  excited states. If the phase convention for  $L_z$  had been reversed, then the choice of transition dipoles in this derivation would have been for  $A_{1u}$  and  $A_{2u}$ . Since this phase convention determines the sign of  $M_z$ , the MCD for transitions from a split  $\underline{{}^2E_g}$  to either  $A_{1u}$  or  $A_{2u}$  excited states should be positive. As should be expected, this expression is simply a single B term. Thus, if the separation between excited states is much greater than the zero field splitting which in turn is greater than  $kT$ , a crude estimate of the MCD can be obtained from this one term.

The full treatment of this system requires the incorporation of the temperature dependent occupation of the four levels, accounting for the random orientation of the molecules in the fluid, and an allowance for the finite bandwidth of the transitions. The coordinate system  $x, y, z$  of a molecule is specified by Euler angles in a space fixed XYZ system.<sup>62</sup> Probabilities of absorption of LCPL and RCPL are given by projecting the molecular transition moment onto the XY plane.

The probabilities of absorption are

$$(R_{L,1}^{\pm})^2 = |\langle j | [\frac{\bar{x}+i\bar{y}}{\sqrt{2}}] \cdot \bar{e}r | 1^{\pm} \rangle|^2 = A_1^{\pm} - A_2^{\pm} \quad (129)$$

$$(R_{L,2}^{\pm})^2 = |\langle j | [\frac{\bar{x}+i\bar{y}}{\sqrt{2}}] \cdot \bar{e}r | 2^{\pm} \rangle|^2 = A_3^{\pm} + A_2^{\pm} \quad (130)$$

$$(R_{R1}^{\pm})^2 = |\langle j | [\frac{\bar{x}-i\bar{y}}{\sqrt{2}}] \cdot \bar{e}r | 1^{\pm} \rangle|^2 = A_1^{\pm} + A_2^{\pm} \quad (131)$$

$$(R_{R2}^{\pm})^2 = |\langle j | [\frac{\bar{x}-i\bar{y}}{\sqrt{2}}] \cdot e\bar{r} | 2^{\pm} \rangle|^2 = A_3^{\pm} - A_2^{\pm} \quad (132)$$

where

$$A_1^{\pm} = (B_{11}^2 + B_{21}^2) (\alpha^{\pm})^2 (R_x^{\pm})^2 + (B_{22}^2 + B_{12}^2) (\gamma^{\pm} R_y^{\pm})^2 \quad (133)$$

$$A_2^{\pm} = (2\alpha^{\pm} \gamma^{\pm}) (R_x^{\pm} R_y^{\pm}) (B_{11} B_{22} - B_{12} B_{21}) \quad (134)$$

$$A_3^{\pm} = (B_{11}^2 + B_{21}^2) (\gamma^{\pm} R_x^{\pm})^2 + (B_{22}^2 + B_{12}^2) (\alpha^{\pm} R_y^{\pm})^2 \quad (135)$$

$$B_{11} = \overline{Xx} = \cos \psi \cos \phi - \cos \theta \sin \psi \sin \theta \quad (136)$$

$$B_{12} = \overline{Xy} = -\sin \psi \cos \phi - \cos \theta \cos \psi \sin \phi \quad (137)$$

$$B_{21} = \overline{Yx} = \cos \psi \sin \phi + \cos \theta \sin \psi \cos \phi \quad (138)$$

$$B_{22} = \overline{Yy} = \sin \psi \cos \phi + \cos \theta \cos \psi \cos \phi \quad (139)$$

$$R_x = e \langle j | \bar{x} | x \rangle \quad (140)$$

$$R_y = e \langle j | \bar{y} | y \rangle \quad (141)$$

Next we account for the spectral broadening which occurs at various orientations. If this broadening is of a random nature, then a normalized Gaussian shape function

$$f(\nu, \nu_1) = \frac{1}{\Delta \sqrt{\pi}} \exp [-(\nu - \nu_i(\theta))/\Delta]^2 \quad (142)$$

can be used.  $\Delta$  is the bandwidth,  $\nu$  is the energy ( $\text{cm}^{-1}$ ) of the incident radiation,  $\nu_i(\theta)$  being the center of the absorp-

tion band.

The molar extinction coefficients are related to the absorption probabilities by<sup>48</sup>

$$\frac{\epsilon(\nu)}{\nu} = \frac{16\pi^2 e^2 N R^2}{3n\lambda^3 \ln 10} \quad (143)$$

where  $N$  is Avogadro's number and  $n$  is the index of refraction of the medium.

The molar extinction coefficients can now be calculated by averaging over all values of  $\theta$ ,  $\phi$ , and  $\psi$ , assuming random orientations. The volume element is  $\sin\theta d\theta d\phi d\psi/8\pi^2$ .

Integration over  $\phi$  and  $\psi$  involve integrals of the form

$$\int_0^{2\pi} \sin^2 x dx = \int_0^{2\pi} \cos^2 x dx = \pi \quad (144)$$

and

$$\int_0^{2\pi} \sin x \cos x dx = 0. \quad (145)$$

By grouping all of the constants into one term,

$$S = \frac{2e^2 N \pi^2}{3n\lambda^3 \ln 10} \quad (146)$$

the eight extinction coefficients become

$$\begin{aligned} \frac{\epsilon_{L1}^{\pm}}{\nu} = & \int_0^{\pi} N_1^{\pm} \sin\theta [(1+\cos^2\theta)(\alpha^{\pm 2} R_x^{\pm 2} + \gamma^{\pm 2} R_y^{\pm 2}) \\ & - 4\alpha^{\pm} \gamma^{\pm} R_x^{\pm} R_y^{\pm} \cos\theta] (d\theta) (f(\nu, \nu_1^{\pm})) \end{aligned} \quad (147)$$

$$\begin{aligned} \frac{\epsilon_{R1}^{\pm}}{\nu} = & \int_0^{\pi} N_1^{\pm} \sin\theta [(1+\cos^2\theta)(\alpha^{\pm 2} R_x^{\pm 2} + \gamma^{\pm 2} R_y^{\pm 2}) \\ & + 4\alpha^{\pm} \gamma^{\pm} R_x^{\pm} R_y^{\pm} \cos\theta] d\theta (f(\nu, \nu_1^{\pm})) \end{aligned} \quad (148)$$

$$\begin{aligned} \frac{\epsilon_{L2}^{\pm}}{\nu} = & \int_0^{\pi} N_2^{\pm} \sin\theta [(1+\cos^2\theta)(\alpha^{\pm 2} R_y^{\pm 2} + \gamma^{\pm 2} R_x^{\pm 2}) \\ & + 4\alpha^{\pm} \gamma^{\pm} R_x^{\pm} R_y^{\pm} \cos\theta] d\theta (f(\nu, \nu_2^{\pm})) \end{aligned} \quad (149)$$

$$\begin{aligned} \frac{\epsilon_{R2}^{\pm}}{\nu} = & \int_0^{\pi} N_2^{\pm} \sin\theta [1+\cos^2\theta)(\alpha^{\pm 2} R_y^{\pm 2} + \gamma^{\pm 2} R_x^{\pm 2}) \\ & - 4\alpha^{\pm} \gamma^{\pm} R_x^{\pm} R_y^{\pm} \cos\theta] d\theta (f(\nu, \nu_2^{\pm})) \end{aligned} \quad (150)$$

The absorption and MCD spectra are given by

$$\frac{\epsilon}{\nu} = \frac{\epsilon_L + \epsilon_R}{2\nu} = \int_0^{\pi} (2\sin\theta) (1+\cos^2\theta) (d\theta) \quad (151)$$

$$\begin{aligned} & \{N_1^{+} (\alpha^{+2} R_x^{+2} + \gamma^{+2} R_y^{+2}) f(\nu, \nu_1^{+}) + N_1^{-} (\alpha^{-2} R_x^{-2} + \gamma^{-2} R_y^{-2}) f(\nu, \nu_1^{-}) \\ & + N_2^{+} (\alpha^{+2} R_y^{+2} + \gamma^{+2} R_x^{+2}) f(\nu, \nu_2^{+}) + N_2^{-} (\alpha^{-2} R_y^{-2} + \gamma^{-2} R_x^{-2}) f(\nu, \nu_2^{-}) \} \end{aligned}$$

and

$$\frac{\Delta \epsilon}{\nu} = \frac{\epsilon_L - \epsilon_R}{\nu} = -S \int_0^\pi (8 \sin \theta \cos \theta d\theta) \{ [(\alpha^+ \gamma^+ R_x^+ R_y^+) (N_1^+ f(\nu, \nu_1^+) - N_2^+ f(\nu, \nu_2^+))] + (\alpha^- \gamma^- R_x^- R_y^-) [N_1^- f(\nu, \nu_1^-) - N_2^- f(\nu, \nu_2^-)] \} \quad (152)$$

We will consider first the absorption spectrum. For this discussion it will be assumed that  $R = R_x^+ = R_x^- = R_y^+ = R_y^-$  and  $H = 0$  (zero magnetic field). The line shape functions can be expanded about a common frequency,  $\nu_0$ , the average transition energy,

$$f(\nu, \nu_2^\pm) = f(\nu, \nu_0) + \Delta E_T \frac{df(\nu, \nu_0)}{d\nu} + \dots \quad (153)$$

$$f(\nu, \nu_1^\pm) = f(\nu, \nu_0) - \Delta E_T \frac{df(\nu, \nu_0)}{d\nu} + \dots \quad (154)$$

The absorption spectrum can be written as a term in  $f(\nu, \nu_0)$  which is independent of all the various splittings (not too surprising since all transition dipoles have been assumed to be equal) and a term in  $df(\nu, \nu_0)/d\nu$ . This second term is directly proportional to

$$(\sqrt{\Delta E_N^2 + M_z^2 \lambda^2 / 4}) \tanh \left( \frac{\sqrt{\Delta E_N^2 + M_z^2 \lambda^2 / 4}}{kT} \right)$$

As  $kT \rightarrow 0$ , the tanh function  $\rightarrow 1$ . Reasonable estimates for the various parameters are  $\Delta E_N = 100 \text{ cm}^{-1}$ ,  $M_z = 2 \text{ M}$ , and  $\lambda = 5 \text{ cm}^{-1}$ . At very low temperatures, the spin orbit coupling will contribute about 0.1% of the asymmetry of the band. The integrated intensity will be independent of both crystal field and spin

orbit effects. Therefore, we may ignore the effect of spin orbit coupling on the absorption band.

Since  $\alpha^\pm \gamma^\pm = M_z (\beta H \cos \theta \pm \lambda/2) / 2\Delta E_T^\pm$ , the MCD spectrum is given by

$$\begin{aligned} \frac{\Delta \epsilon}{\nu} = & \int_0^\pi (8M_z \beta H \sin \theta \cos^2 \theta d\theta) \left[ \frac{R_x^+ R_y^+ (N_2^+ f(\nu, \nu_2^+) - N_1^+ f(\nu, \nu_1^+))}{2\Delta E_T^+} \right. \\ & \left. + \frac{R_x^- R_y^- (N_2^- f(\nu, \nu_2^-) - N_1^- f(\nu, \nu_1^-))}{2\Delta E_T^-} \right] \\ & + \int_0^\pi (8 \sin \theta \cos \theta d\theta) \left( \frac{M_z \lambda}{2} \right) \left[ \frac{R_x^+ R_y^+}{2\Delta E_T^+} (N_2^+ f(\nu, \nu_2^+) \right. \\ & \left. - N_1^+ f(\nu, \nu_1^+)) - \frac{R_x^- R_y^-}{2\Delta E_T^-} ((N_2^- f(\nu, \nu_2^-) - N_1^- f(\nu, \nu_1^-))) \right] \end{aligned} \quad (155)$$

If the magnetic field shifts the lineshape functions rigidly, then the four lineshape functions can be again expanded as Taylor series. In order to evaluate the MCD, we will again assume that all of the transition dipoles are equal. If  $\Delta E_N$  is larger than  $\beta H_z$ , then the  $\theta$  dependence of  $\Delta E_T^\pm$  will be negligible

$$\Delta E_T^\pm = [(\Delta E_N)^2 + M_z^2 \lambda^2 / 4]^{1/2} = \Delta E_T^0 \quad (156)$$

$$\begin{aligned}
\frac{\Delta \epsilon}{v} = & \int_0^\pi \left( \frac{4sM_z R^2 \beta H \sin\theta \cos^2\theta d\theta}{\Delta E_T^0} \right) (N_2^+ - N_1^+ + N_2^- - N_1^-) [f(v, v_0)] \quad (157) \\
& + \int_0^\pi (4sM_z R^2 \beta H \sin\theta \cos^2\theta d\theta) (N_2^+ + N_1^+ + N_2^- + N_1^-) \left[ \frac{df(v, v_0)}{dv} \right] \\
& + \int_0^\pi (-2R^2 M_z s \lambda \sin\theta \cos\theta d\theta) (N_2^+ - N_2^- + N_1^+ - N_1^-) \left[ \frac{df(v, v_0)}{dv} \right] \\
& + \int_0^\pi \left( \frac{-2R^2 M_z s \lambda \sin\theta \cos\theta}{\Delta E_T^0} \right) (N_2^+ - N_2^- - N_1^+ + N_1^-) [f(v, v_0)]
\end{aligned}$$

The above assumptions also lead to

$$N_2^+ + N_1^+ + N_2^- + N_1^- = 1 \quad (158)$$

$$N_2^+ - N_1^+ + N_2^- - N_1^- = -\tanh \left( \frac{\Delta E_T^0}{kT} \right) \quad (159)$$

$$N_2^+ + N_1^+ - N_2^- - N_1^- = -2 \tanh \left( \frac{g\beta H \cos\theta}{2kT} \right) \quad (160)$$

$$N_2^+ - N_1^+ - N_2^- + N_1^- = \tanh \left( \frac{\Delta E_T^0}{kT} \right) \tanh \left( \frac{g\beta H \cos\theta}{2kT} \right) \quad (161)$$

Expanding  $\tanh (g\beta H \cos\theta / 2kT)$  and keeping only the first term,

$$\tanh \left( \frac{g\beta H \cos\theta}{2kT} \right) = \frac{g\beta H \cos\theta}{2kT} \quad (162)$$

$$\begin{aligned}
\frac{\Delta \epsilon}{v} = & \frac{4}{3} R^2 M_z s \beta H \left[ - \frac{(2 + g\lambda / 2kT) \tanh (\Delta E_T^0 / kT)}{\Delta E_T^0} f(v, v_0) \right. \\
& \left. + (2 + \frac{g\lambda}{kT}) \frac{df(v, v_0)}{dv} \right] \quad (163)
\end{aligned}$$

$$\frac{\epsilon}{\nu} = \frac{16S}{3} R^2 f(\nu, \nu_0) \quad (164)$$

For reasonable values of the parameters,  $g \sim 2$ ,  $\lambda \sim 5 \text{ cm}^{-1}$ , and  $kT \sim 78 \text{ cm}^{-1}$  (at  $-160^\circ\text{C}$ ), the factor  $g\lambda/kT$  equals 0.13. Therefore spin and spin orbit effects will amount to 3% of the integrated MCD intensity at the lowest temperature and will decrease as the temperature increases. Finally,

$$\frac{\Delta\epsilon}{\nu} = -\frac{8}{3} R^2 M_z S_{BH} \left[ \frac{\tanh(\Delta E_T^0/kT)}{\Delta E_T^0} f(\nu, \nu_0) + \frac{df(\nu, \nu_0)}{d\nu} \right], \quad (165)$$

and

$$\frac{\epsilon}{\nu} = \frac{16}{3} S R^2 f(\nu, \nu_0). \quad (166)$$

If  $\frac{\Delta E_T}{kT} < \frac{\pi}{2}$ , then

$$\frac{\Delta\epsilon}{\epsilon} = \frac{\beta M_z H}{2} \left\{ \frac{f'(\nu, \nu_0)}{f(\nu, \nu_0)} + \frac{1}{kT} \left[ 1 - \frac{1}{3} \left( \frac{\Delta E_T}{kT} \right)^2 + \frac{2}{15} \left( \frac{\Delta E_T}{kT} \right)^4 + \dots \right] \right\} \quad (167)$$

For high temperatures or small zero field splitting, this is just the normal A/D and C/D term. If  $\Delta E_T/kT \gg \pi/2$ , then

$$\frac{\Delta\epsilon}{\epsilon} = \frac{\beta M_z H}{2\Delta E_T} \quad (168)$$

which is the normal B/D term.

Thus, only in the cases where  $\Delta E_T \approx kT$  is it possible to use the temperature dependence of the MCD as an indication of the degeneracy. If the zero field splitting is small, then

the spectra will be independent of the splitting. If the zero field splitting is large, then contributions due to other states may have to be considered. This can be seen by plotting the ratio of the integrated area of the MCD to the integrated area of the absorption for various zero field splittings and temperatures using the simplified expressions of Eqs. (165) and (166) (Figures 9 and 10).

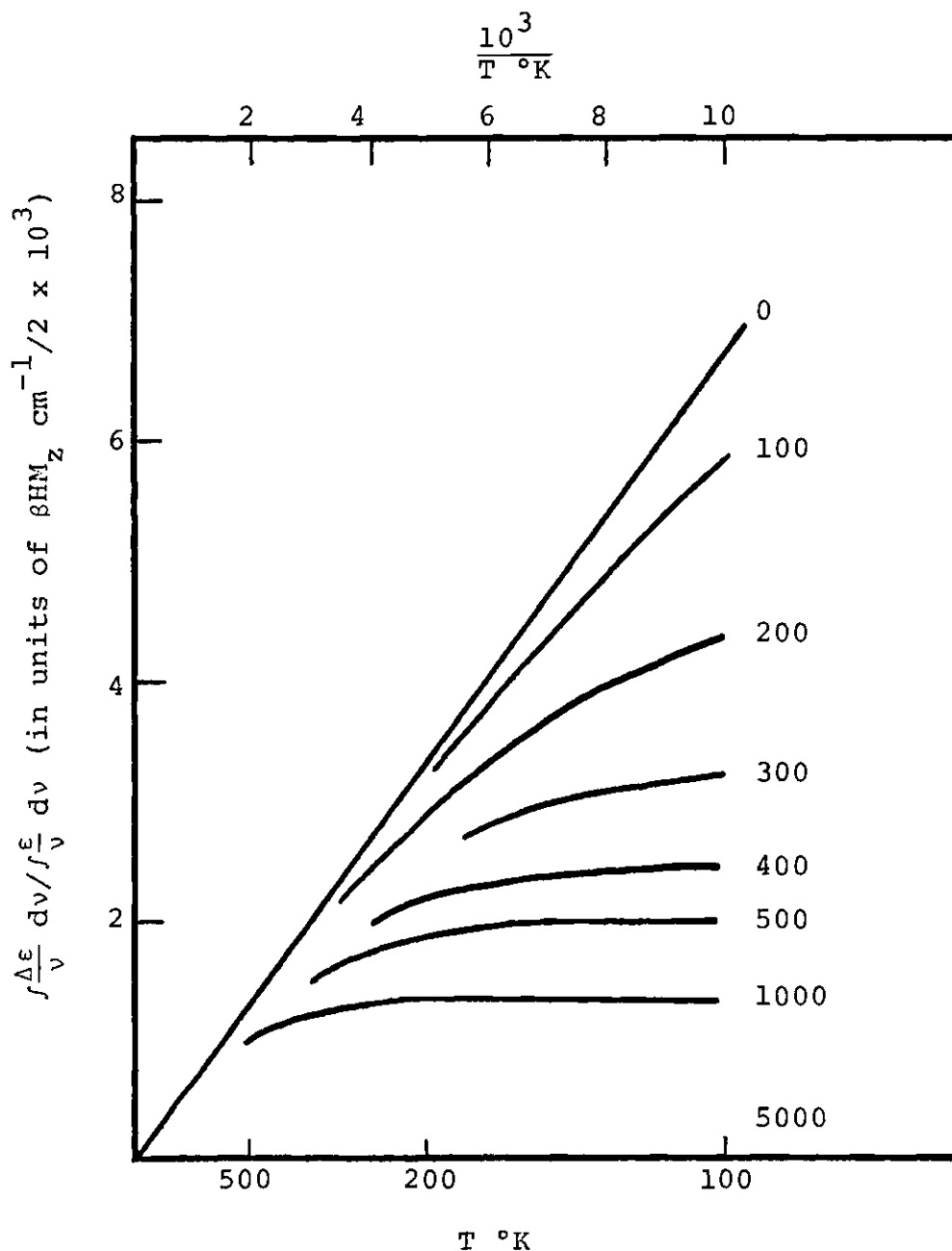


Figure 9. The Ratio of the Integrated Area of the MCD Spectrum to the Integrated Area of the Absorption Spectrum Versus the Reciprocal of the Temperature as Calculated from Eqs. (165) and (166). Note that in the experimental temperature region (about 300°K to 100°K), the curves for  $2\Delta E_T \lesssim 100 \text{ cm}^{-1}$  do not deviate significantly from that for exact degeneracy. As the zero field splitting increases, the temperature dependence of the MCD spectrum decreases.

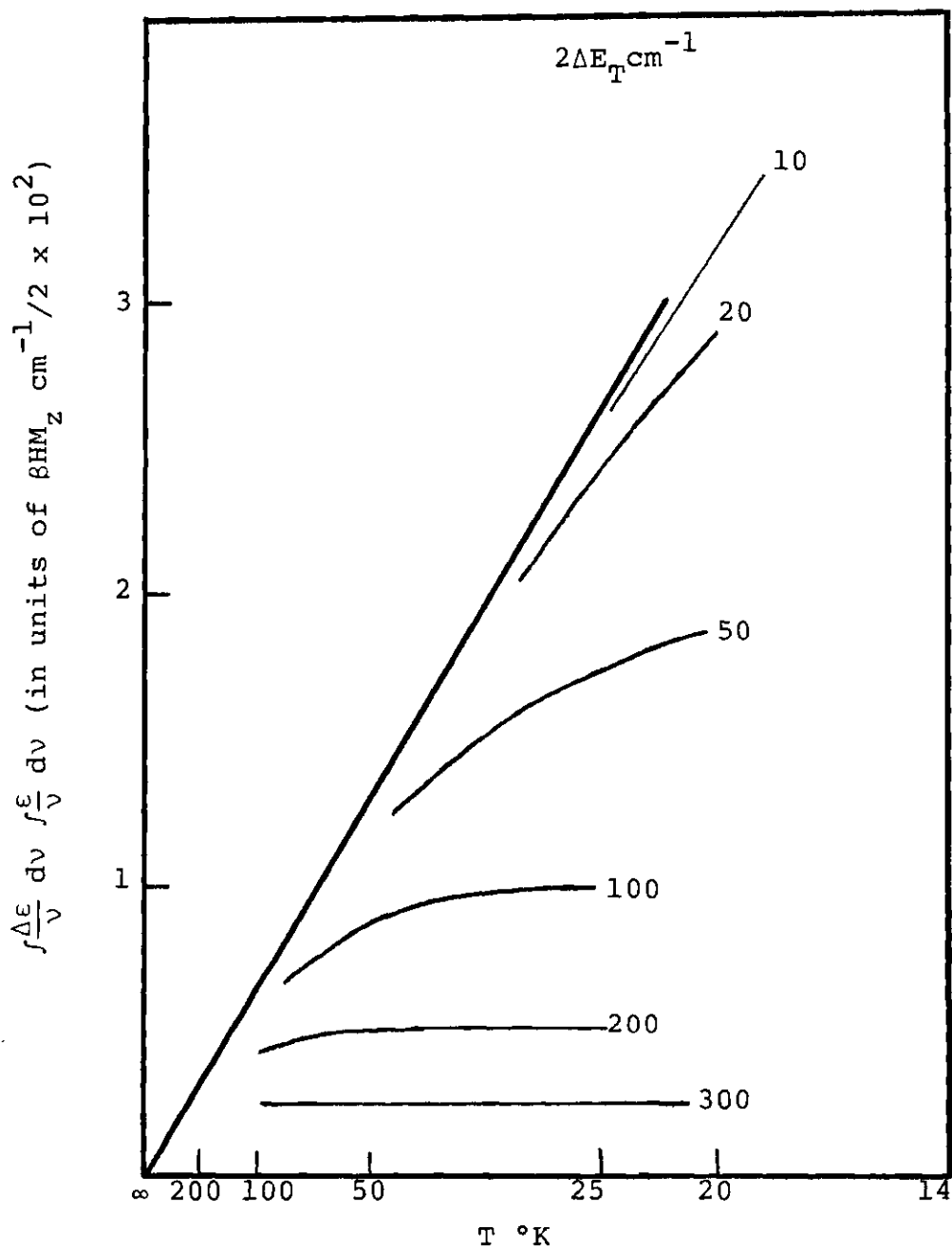


Figure 10. The Ratio of the Integrated Area of the MCD Spectrum to the Integrated Area of the Absorption Spectrum Versus the Reciprocal of the Temperature as Calculated from Eqs. (165) and (166). This is the low temperature portion of Figure 9. Note that smaller zero field splittings are detectable by lowering the temperature

## CHAPTER III

## EXPERIMENTAL

Materials

Metal free (free base) 5,10,15,20-tetraphenylporphyrin ( $H_2$ TPP) was prepared by condensing benzaldehyde and pyrrole in refluxing dimethylformamide (DMF).<sup>63</sup> Purification was afforded by column (5 x 30 cm) chromatography on Fisher A-540 neutral alumina using benzene as the elutant. Free base etioporphyrin-I was obtained from a sample prepared by Henry Kurtz.

The neutral free base porphyrins used for optical measurements were further purified by dissolving 10 mg of the free base in 100 ml of benzene. Extraction with 50 ml 68% (w/w) phosphoric acid was followed by neutralization of the acid layer with aqueous sodium hydroxide. The free base porphyrin was then dissolved in benzene and washed twice with a saturated aqueous sodium bicarbonate solution followed by two washings with water. The solvent was removed in a rotary evaporator and the porphyrin was dried under vacuum overnight.

Zinc and copper porphyrins were formed by metal insertion in refluxing DMF using the metal acetate.<sup>3,56</sup> Purification was accomplished by chromatography on Fisher A-540

alumina using benzene as elutant for the copper complex and a 50/50 (v/v) benzene-methylene chloride solution as elutant for zinc porphyrin.

Free base 2,3-dihydro-5,10,15,20-tetraphylporphyrin (tetraphenylchlorin,  $H_2TPC$ ) was made by diimide reduction.<sup>2,64</sup> 5 g  $H_2TPP$ , 10 g anhydrous potassium carbonate, and 473 ml of dry pyridine were heated with stirring to reflux under nitrogen in a 2 liter, 3 necked round bottom flask. Distilling out the water-pyridine azeotrope removes the trace of water. Every two hours between one and two grams toluenesulfonylhydrazine was added. The reduction could be stopped anytime and continued later by reducing the temperature and keeping the reaction mixture under nitrogen. Restarting the reaction is accomplished by raising the temperature and continuing to add the toluenesulfonylhydrazine. After 5 hours the optical spectrum was monitored. Upon completion of the reaction (usually 7 hours), the mixture was taken to near dryness on a rotary evaporator. Water and a small amount of benzene were added and the mixture again taken to near dryness. This sequence was repeated several times until the odor of pyridine was absent. The solid was filtered, washed with water, and dried under vacuum. The solid then could be purified by Whitlock's phosphoric acid-benzene extraction method when needed.<sup>2,64</sup>

The acid-benzene extraction method is based on relative basicities of the pigments. The diacid salt is more soluble

in a mineral acid than in benzene, while the neutral pigment is more soluble in benzene. As the pH of the inorganic layer is lowered, the porphyrin diacid salt is formed first, followed by sequential formation of chlorin and bacteriochlorin diacid salts. Sixty-eight percent (w/w) phosphoric acid will separate the porphyrin and chlorin mixture, while an 82% composition is needed for separation of chlorin-bacteriochlorin mixture. After the separation, the appropriate layer was washed with 5% sodium hydroxide solution (if the acid was saved, then benzene was added), saturated sodium bicarbonate, water, and dried over anhydrous sodium sulfate.

Zinc and copper 2,3-dihydro-5,10,15,20-tetraphenylporphyrin (ZnTPC and CuTPC) were made by metal insertion in refluxing DMF under nitrogen, using the metal acetate. Chromatography on neutral alumina was done under nitrogen and in the dark with benzene or a benzene-methylene chloride solution to remove the metalloporphyrin and free base porphyrin. The metal chlorin is eluted last. It was necessary to add ethanol to remove the zinc chlorin from the column.

Free base 2,3,12,13-tetrahydro-5,10,15,20-tetraphenylporphyrin ( $H_2$ TPBc, tetraphenylbacteriochlorin) was made by the same method as that used for the free base 2,3-dihydro-5,10,15,20-tetraphenylporphyrin except that the reaction was continued for a longer time (usually around 12 hours). Purification of the free bases by chromatography on neutral alumina under nitrogen and in the dark using benzene as the

elutant left a dark substance on the column. However, not much success was obtained in separating the free bases by chromatography. The reduction should be carried out until the produce of interest has reached a maximum (remembering that some of the peaks in the absorption spectra of the different compounds occur at the same wavelength).

Zinc 2,3,12,13-tetrahydro-5,10,15,20-tetraphenylporphyrin (ZnTPBc) was prepared by reacting the metal acetate with the free base tetraphenylbacteriochlorin in pyridine.<sup>65,66</sup> Znhydrous zinc acetate (made from heating the hydrous form at 140°C overnight) and H<sub>2</sub>TPBc were put in a Carius tube. Dry pyridine (deaerated with argon) was added. The tube was put on a vacuum line and through three freeze-thaw cycles (the solution was frozen, the system opened to a high vacuum ( $10^{-5}$  torr) for about 30 minutes, closed off, the solution was warmed to room temperature, and after about 30 minutes the procedure was repeated) and then sealed off. The tube was heated to just under 100°C overnight. The solution was cooled and then opened under argon. The reaction mixture was added to deaerated water and filtered. The solid material was dried under vacuum and used without further purification. Attempts to remove the trace (5%) of ZnTPC by chromatography only resulted in increasing the concentration of the ZnTPC. The absorption spectrum of the dried produce is slightly different from that of the freshly prepared product due to the removal of pyridine.

Dimethylformamide was distilled from calcium hydride through a 300 mm Widmer column at 20 torr and collected over 4 A molecular sieves. The DMF was poured into a storage bulb which then was attached to a vacuum line. After several freeze-thaw cycles the DMF was distilled over to a previously evacuated storage bulb that contained activated 4 A molecular sieves. The DMF was stored in this contained until needed.

2-methyltetrahydrofuran (2-MTHF), tetrahydrofuran (THF), and dimethoxyethane (DME) were fractionally distilled from  $\text{LiAlH}_4$ , collected, and poured into a storage bulb. This was attached to a vacuum line, put through several freeze-thaw cycles, and the solvent was distilled into a storage bulb containing sodium-potassium alloy. The solvent was freeze-thawed several times and stored until needed.

Tetrapropylammonium perchlorate (TPAP) and tetrabutylammonium perchlorate (TBAP) were prepared by reacting the tetraalkylammonium halide with perchloric acid in water and twice recrystallizing the precipitate from ethanol and water.

All the other chemicals used were commercially available reagent grade and used as received.

#### Preparation of Porphyrin Anions

Electrolysis was performed in the cells shown in Figures 11 and 12. The platinum-glass seals were made vacuum tight by the use of Torr Seal (Varian Associates). Typically, ca. 2 mg porphyrin (enough to get an absorbance of about 1 in the region of interest) and 2 grams of the carrier salt

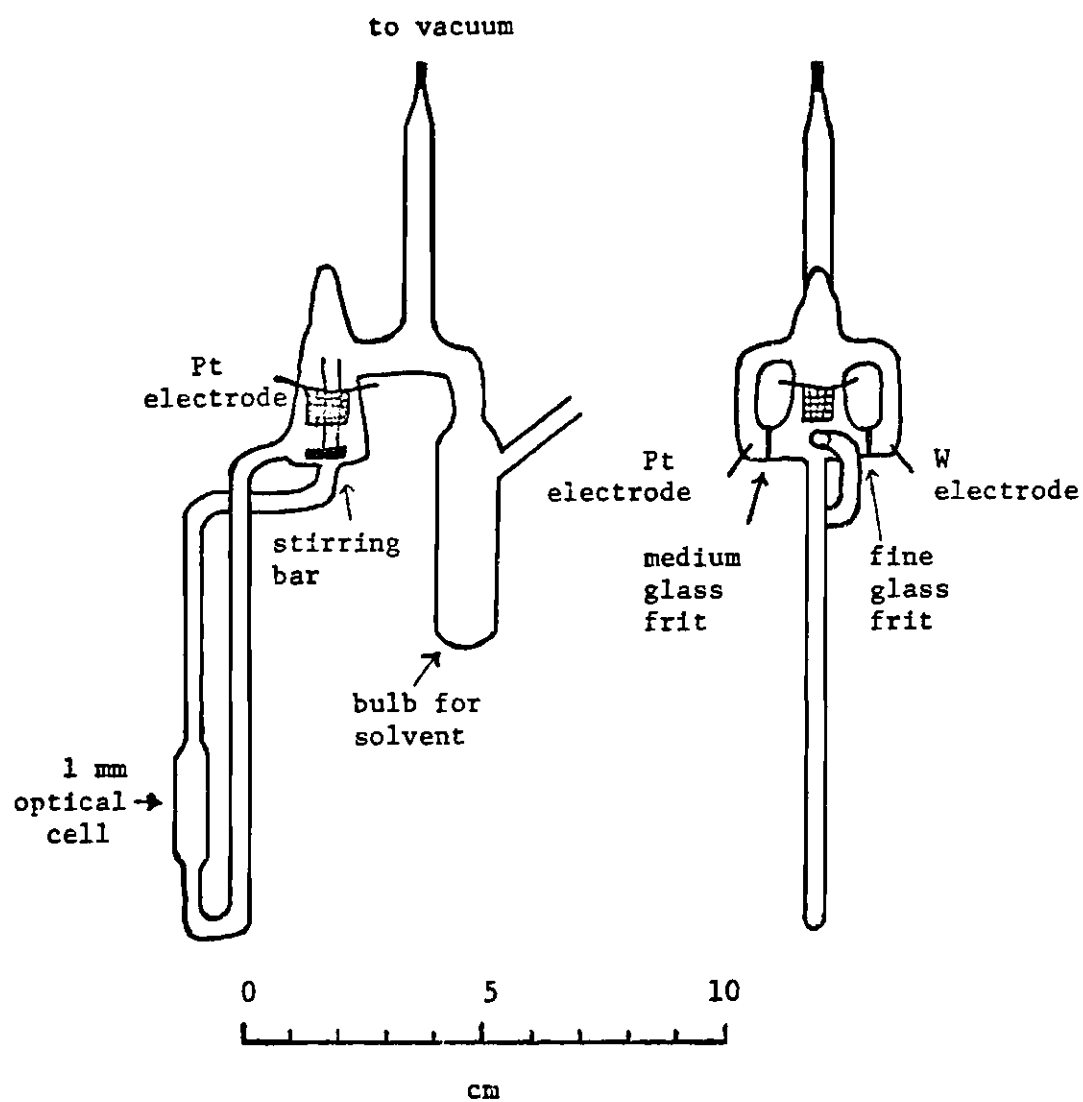


Figure 11. Three Electrode Electrolysis Apparatus.

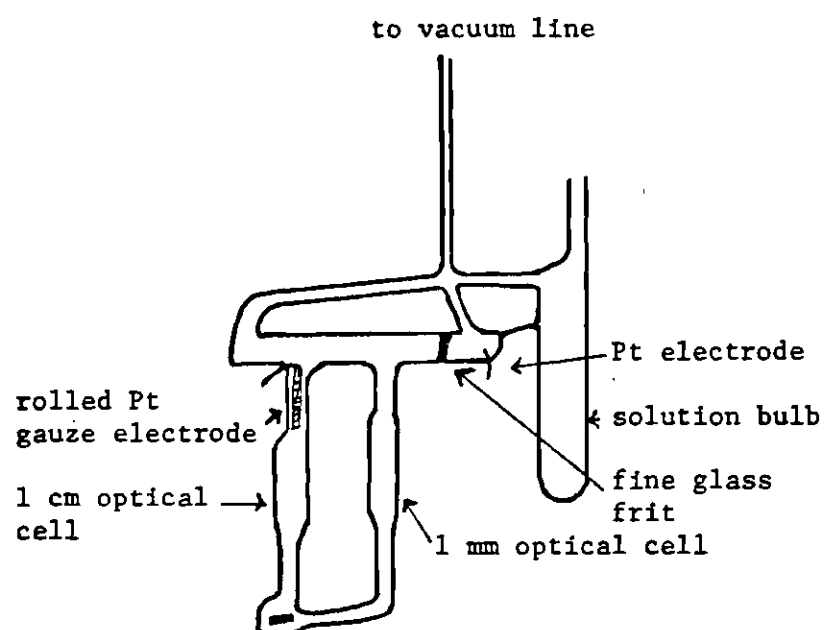


Figure 12. Two Electrode Electrolysis Apparatus.

were added through the side arm which was then sealed off. The device was evacuated, DMF distilled in the solution was freeze-thawed several times. The solution was frozen and the device sealed off. The concentration of the solution could be varied by pouring only part of the solution from the bulb and distilling the rest over. However, since a dilution of the porphyrin gives also a dilution of the electrolyte, extensive dilutions were avoided.

The electrolysis was carried out in a Cary 14R UV-VIS-IR recording spectrometer so that the reduction could be monitored regularly without changing the position of the cell. The presence of isosbetic points and comparison with previously published spectra were used to check the purity of the products. In case of doubt as to what species were formed (as occurred when trying to make the dianions of the free base tetraphenylchlorin and etioporphyrin) the products were oxidized to see if the original absorption could be recovered.

After obtaining the ion of the interest the apparatus was removed from the Cary and positioned rigidly in the MCD spectrometer. After this the absorption spectrum was taken with the Cary spectrometer to check that no decomposition had taken place.

Anions with a metal counterion were formed by reacting the porphyrin with naphthalene anion. Excess naphthalene and a premeasured amount of the porphyrin were placed into a bulb through an arm (Figure 13) which was then sealed off.

Sodium metal was introduced through a side arm which was then sealed off. The device was attached to a vacuum line. The bulb containing the porphyrin and naphthalene were cooled and the device evacuated. The sodium was distilled into the next segment and the original segment sealed off. The porphyrin and naphthalene were sublimed along the tube or into the other bulb. This bulb was cooled and the device evacuated to about  $10^{-5}$  torr, and the solvent was distilled in. The solvent dissolved the porphyrin, then was distilled around the container, and finally recondensed over the sodium mirror. This was repeated several times to remove traces of water. Solvent was returned to the collector and the sodium distilled up to the next segment and solvent distilled in. This process was repeated until finally the solvent was distilled in, freeze-thawed and the device sealed off.

Porphyrin anions were prepared by distilling solvent and subliming naphthalene into the arm containing the sodium. Upon contact with the sodium film, sodium naphthalenide was produced. The naphthalenide anion was poured through the frit and reacted with the porphyrin solution. For preparation of  $\text{ZnTPP}^{-1,-2}$  and  $\text{ZnEtio}^{-1,-2}$ , only a portion of the porphyrin was used. Thus, it was possible to back titrate if necessary to obtain the monoanion uncontaminated with the neutral or dianion species.

The  $\text{ZnTPP}$  monoanion with tetrabutyl ammonium counterion was made by electrolytic reduction in a dry box (HE-43-2

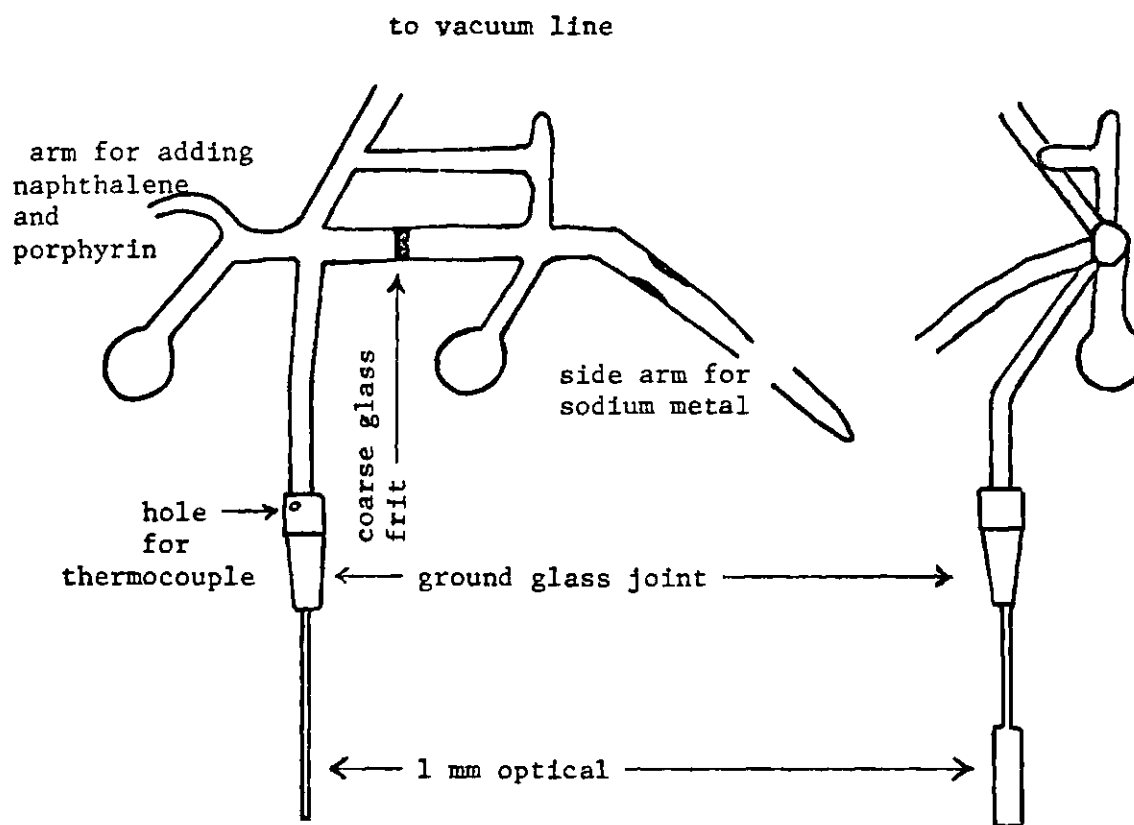


Figure 13. Apparatus for Metal Reductions.

Dri-Lab Glove Box, Vacuum/Atmospheres Company). Small samples were removed periodically during the reduction to check on the progress of the reaction. At completion, the solution was syringed into an apparatus containing a spherical bulb and an optical cell. A valve was added and the device was removed from the dry box. The sample was evacuated to dryness on a vacuum line and 2-MTHF solvent added. After two freeze-thaw cycles the device was sealed off.

For low temperature measurements a copper-constantan thermocouple was attached to the side of the optical cell. The apparatus was then placed in a dewar in the MCD device and the spectra taken at different temperatures.

The MCD spectra were calibrated by comparing the MCD spectra of the sample with the MCD spectra<sup>67</sup> of  $\text{Co}(\text{H}_2\text{O})_6^{2+}$  (20 kk band) in the visible region and  $\text{Ni}(\text{H}_2\text{O})_6^{2+}$  (15.5 kk band) in the near infrared region. The concentrations of these solutions were determined from their absorption spectra (on a Cary 14R). The temperature dependence of the absorption spectra was obtained by placing the dewar in a Cary 14R.

MCD Spectrometer (Designed and Constructed by  
Dr. Ichiro Fujita)

The basic design of the MCD spectrometer used here is similar to those of Velluz, et. al.,<sup>42</sup> Sutherland, et. al.,<sup>68</sup> Breeze and Ke,<sup>69</sup> and Linder.<sup>37</sup> The instrument is capable of measuring both natural and magnetic circular dichroism from about 1000 nm to 220 nm at temperatures from near liquid

nitrogen temperatures to room temperature. The data can be obtained in digital form, recorded directly or both. Manipulations of the data are performed by a computer and are discussed elsewhere.

A block diagram of the MCD is shown in Figure 14. Light from either a Sylvania tungsten halogen lamp (150 W, 10.5 V) (from near IR and VIS) or xenon arc (Osram XB0 450W) visible and near UV) is focused on the slit by a lens and mirror system and dispersed by a 0.5 m Jarrell Ash (Model 82-010 Ebert Scanning Spectrometer) monochromator (calibration  $\pm 2\text{\AA}$ ). Different blazed gratings were used depending on the regions of interest. The slit for the monochromator was controlled by a slit program. The slit system provides a coarse correction for the variations in lamp intensity and photomultiplier gain as the wavelength changes. In order to separate the extraordinary and the normal rays from the polarizer, the maximum slit width was restricted to 1.2 mm. Different slit programs were used for different lamps and different ranges.

The monochromatic beam is chopped with a Bulova sine wave tuning fork chopper set at 200 Hz. The light is collimated and the edges of the beam cut off with a field stop. The beam next passes through a Rochon polarizer and the emergent linearly polarized component is made alternately left and right circularly polarized by a piezo-optical modulator (Morvue Electronic Systems Model PEM-3) driven at 50

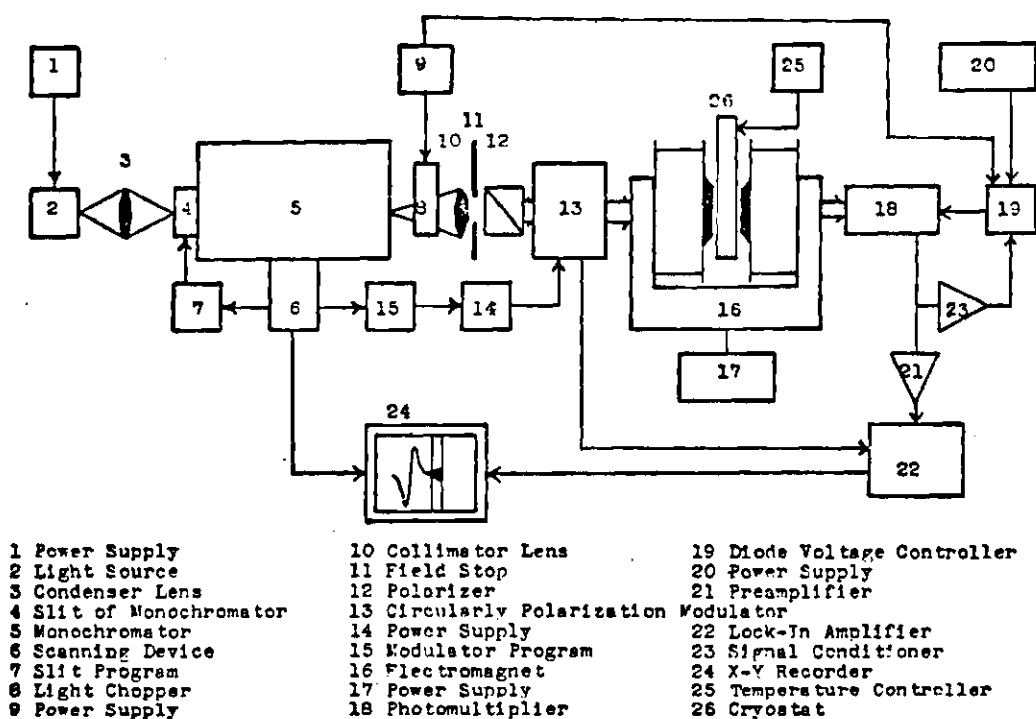


Figure 14. MCD Spectrometer.

kHz. The light beam passes through an 18 cm Walker/Magnion Model 1-75 B electromagnet bored axially with an 8 mm hole. Tapered pole pieces provide a 32 mm gap into which a Pyrex optical dewar could be placed. A 16 kilogauss magnetic field was used.

The photomultipliers were from Hamamatsu TV Company, LTD. A S-1, type R316 photocathode with a spectral response range of 400 to 1200 nm was used for the near IR range. A S-20, type 374, with a spectral response range of 185 to 850 nm was used for the visible and near UV range. A dynode voltage controller regulates the amplitude of the 200 Hz signal to maintain constant photocurrent. This controller provides corrections for amplitude errors resulting from sample absorption, lamp intensity variations, and errors in the slit program. Amplitude errors are corrected by changing the photomultiplier high voltage. The high voltage changes from -400 to -1200 volts as required to maintain the signal level constant to 0.2% of the 50 kHz component. The photomultiplier current is amplified and then detected by a Princeton Applied Research Model 121 Lock-In-Amplifier phase detector. The output of the phase-sensitive detector is directly proportional to the circular dichroism.

In order to see this consider the following.<sup>4,41,42</sup>  
If the piezooptical modulator is driven at some frequency  $\omega$ , the light will oscillate between the right and left circularly polarizations. The light may be considered to be composed

of two components

$$I_{\ell} = \frac{I_0}{2} [1 + \sin (\delta_0 \sin \omega t)] \quad (169)$$

$$I_r = \frac{I_0}{2} [1 - \sin (\delta_0 \sin \omega t)] \quad (170)$$

where  $I_0$  is the total intensity of the light,  $I_{\ell}$  is the intensity of the left circularly polarized component,  $I_r$  is the intensity of the right component,  $\delta$  is the relative phase lag, and  $t$  is the time.

The beam is chopped at frequency  $\omega_2$  with a tuning fork. After passage through the sample the two components become

$$I_{\ell} = \frac{I_0}{2} (\sin \omega_2 t) [1 + \sin (\delta_0 \sin \delta t)] 10^{-A_{\ell}} \quad (171)$$

$$I_r = \frac{I_0}{2} (\sin \omega_2 t) [1 - \sin (\delta_0 \sin \omega t)] 10^{-A_r} \quad (172)$$

where  $A_{\ell}$  is the absorption of the left circularly polarized light and  $A_r$  is that for the right. The light detected by the photomultiplier is

$$I = I_{\ell} + I_r = \frac{I_0}{2} (\sin \omega_2 t) \quad (173)$$

$$[(10^{-A_{\ell}} + 10^{-A_r}) + (10^{-A_{\ell}} - 10^{-A_r}) \sin (\delta_0 \sin \omega t)]$$

Thus the phase-detected output at  $\omega$  is directly proportional to the circular dichroism. The ratio of the second term to the first is proportional to

$$\frac{10^{-A_\ell} 10^{-A_r}}{10^{-A_\ell+10} 10^{-A_r}} = \tanh \left( \frac{A_\ell - A_r}{4 \log e} \right) \quad (174)$$

This is the same as Equation (3) in the theory section.

## Results and Discussion

### Introduction

In this section we will discuss the SCF-MO's which were used in these calculations. It will be shown that to a large extent, the spectra of the porphyrins, chlorins, and bacteriochlorins can be discussed in terms of the same orbitals. This will be shown in a manner analogous to a correlation diagram.

The spectra of the neutral porphyrinic compounds will be discussed in terms of a four orbital model. Contrary to previous calculations,<sup>19</sup> the signs of the MCD terms can be easily explained in terms of this simple model. Next, these spectra will be discussed in terms of more elaborate SCF-MO calculations using many configurations. It will be shown that the results of these more sophisticated calculations agree with those of the much simpler four orbital model.

The spectra of the monoanions will be shown to be much more complicated than their neutral spectral and require the use of at least six orbitals for their interpretation. The porphyrin monoanion presents a special problem in that the expected degenerate ground state is subject to a possible Jahn-Teller distortion and crystal field splittings. Analysis

of an isolated band in terms of a simple three state model will be used to show that the degeneracy of the metalloporphyrin monoanion ground state has been removed by a zero field splitting but the electronic angular momentum has not been significantly quenched. Knowledge of the ground state splitting then will be used to explain the rest of the spectra. The chlorin and bacteriochlorin monoanions have nondegenerate ground states and can be interpreted in terms of a seven orbital model.

Finally, further spectral evidence will show that the metalloporphyrin dianion is nondegenerate. The observed spectra will be described by means of nondegenerate calculations using a six orbital model with doubly excited configurations.

#### Molecular Orbital Model

Self consistent molecular orbital calculations on the porphyrins, chlorins, bacteriochlorins and their anions indicate that the basic features of these species can be accounted for by a seven orbital model derived from  $D_{4h}$  porphyrin molecular orbitals. The reason for this is the inner 16 atom, 18 electron ring is the main path of conjugation for all of these compounds. The four sets of outer carbons are ethylenic in nature. Thus the reduction of one or more of these outer rings can be regarded to first order as a perturbation of the 16 member inner ring. To the extent that the molecular orbitals do not depend on the contributions of these ethylenic

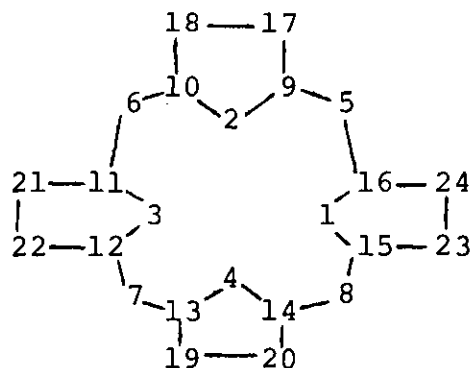
atomic orbitals, there will be a one to one correspondence between the molecular orbitals of the various species. The calculated neutral porphyrin molecular orbitals are given in Tables 4 and 5. The orbital energies are shown in Figure 15. The ones of interest are the occupied  $2b_{2u}$ ,  $1a_{1u}$ , and  $3a_{2u}$  and the unoccupied  $4e_g$ ,  $2b_{1u}$ , and  $3b_{2u}$  orbitals. In order to keep the same labels for these orbitals as the symmetry is lowered to  $C_{2v}$  or  $D_{2h}$ , these will be relabeled as  $a$ ,  $b_1$ ,  $b_2$ ,  $c_1$ ,  $c_2$ ,  $d_1$ , and  $d_2$ , respectively. In  $D_{4h}$  porphyrin the  $b_1$  and  $b_2$  orbitals are almost degenerate while the  $c_1$  and  $c_2$  are exactly degenerate. In addition to these, the  $3e_g$  and  $5e_g$  orbitals are involved in forbidden transitions in the near uv region, while the other orbitals are involved in transitions too high in energy to contribute significantly to the observed spectra. This model incorporates the four orbital model which Gouterman has used to explain the spectra of neutral porphyrins and related ring systems,<sup>70,71</sup> the five orbital model which Weiss used to explain the spectra of neutral chlorins and bacteriochlorins,<sup>21,22</sup> and the six orbital model which Maslov used to explain the spectra of the monoanions of these compounds.<sup>72</sup>

#### Neutral Porphyrins and Related Systems

The absorption and MCD spectra of neutral porphyrins have been subjected to numerous theoretical discussions.<sup>4,19,27,57,73,74</sup> These authors explain the essential features of porphyrin spectra in terms of Gouterman's four

Table 4. Neutral Porphyrin Molecular Orbital Coefficients.

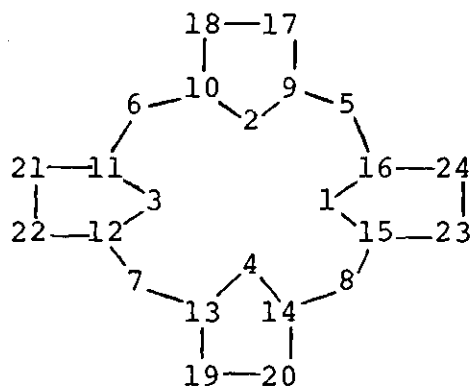
Atom	$2e_g$		$3e_g$		$4e_g$		$5e_g$	
1	.37	.00	.18	.00	.21	.00	.20	.00
2	.00	.37	.00	.18	.00	.21	.00	.20
3	-.37	.00	-.18	.00	-.21	.00	-.20	.00
4	.00	-.37	.00	-.18	.00	-.21	.00	-.20
5	-.25	-.25	.15	.15	-.27	-.27	-.10	.10
6	.25	-.25	-.15	.15	.27	-.27	-.10	-.10
7	.25	.25	-.15	-.15	.27	.27	.10	-.10
8	-.25	.25	.15	-.15	-.27	.27	.10	.10
9	-.28	-.02	.10	-.02	.23	-.16	.14	.28
10	.28	-.02	-.19	-.02	-.23	-.16	-.14	.28
11	.02	-.28	.02	.19	.16	.23	.28	-.14
12	.02	.28	.02	-.19	.16	-.23	.28	.14
13	.28	.02	-.19	.02	-.23	.16	-.14	-.28
14	-.28	.02	.19	.02	.23	.16	.14	-.28
15	-.02	.28	-.02	-.19	-.16	-.23	-.28	.14
16	-.02	-.28	-.02	.19	-.16	.23	-.28	-.14
17	-.11	-.16	.08	-.41	.24	.11	-.34	-.10
18	.11	-.16	-.08	-.41	-.24	.11	.34	-.10
19	.11	.16	-.08	.41	-.24	-.11	.34	.10
20	-.11	.16	.08	.41	.24	-.11	-.34	.10
21	.16	-.11	.41	.08	-.11	.24	-.10	.34
22	.16	.11	.41	-.08	-.11	-.24	-.10	-.34
23	-.16	.11	-.41	-.08	.11	-.24	.10	-.34
24	-.16	-.11	-.41	.08	.11	.24	.10	.34



numbering of atoms

Table 5. Neutral Porphyrin Molecular Orbitals.

Atom	Coordinate		$2a_{2u}$	$2b_{2u}$	$1a_{1u}$	$3a_{2u}$	$2b_{1u}$	$3b_{2u}$
	x	y						
1	2.082	0.000	-.28	.24	.00	.21	.00	-.24
2	0.000	2.082	-.28	-.24	.00	.21	.00	.24
3	-2.082	0.000	-.28	.24	.00	.21	.00	-.24
4	0.000	-.2082	-.28	-.24	.00	.21	.00	.24
5	2.421	2.421	.06	.00	.00	-.38	.31	.00
6	-2.421	2.421	.06	.00	.00	-.38	.31	.00
7	-2.421	-2.421	.06	.00	.00	-.38	-.31	.00
8	2.421	-2.421	.06	.00	.00	-.38	.31	.00
9	1.117	2.891	.03	.02	-.31	-.09	.11	-.29
10	-1.117	2.891	.03	.02	.31	-.09	-.11	-.29
11	-2.891	1.117	.03	-.02	-.31	-.09	-.11	.29
12	-2.891	-1.117	.03	-.02	.31	-.09	.11	.29
13	-1.117	-2.891	.03	.02	-.31	-.09	.11	-.29
14	1.117	-2.891	.03	.02	.31	-.09	-.11	-.29
15	2.891	-1.117	.03	-.02	-.31	-.09	-.11	.29
16	2.891	1.117	.03	-.02	.31	-.09	.11	.29
17	0.684	4.260	.29	.31	-.17	.15	.26	.11
18	-0.684	4.260	.29	.31	.17	.15	-.26	.11
19	-0.684	-4.260	.29	.31	-.17	.15	.26	.11
20	0.684	-4.260	.29	.31	.17	.15	-.26	.11
21	-4.260	0.684	.29	-.31	-.17	.15	-.26	-.11
22	-4.260	-0.684	.29	-.31	.17	.15	.26	-.11
23	4.260	-0.684	.29	-.31	-.17	.15	-.26	-.11
24	4.260	0.684	.29	-.31	.17	.15	.26	-.11



Numbering of atoms

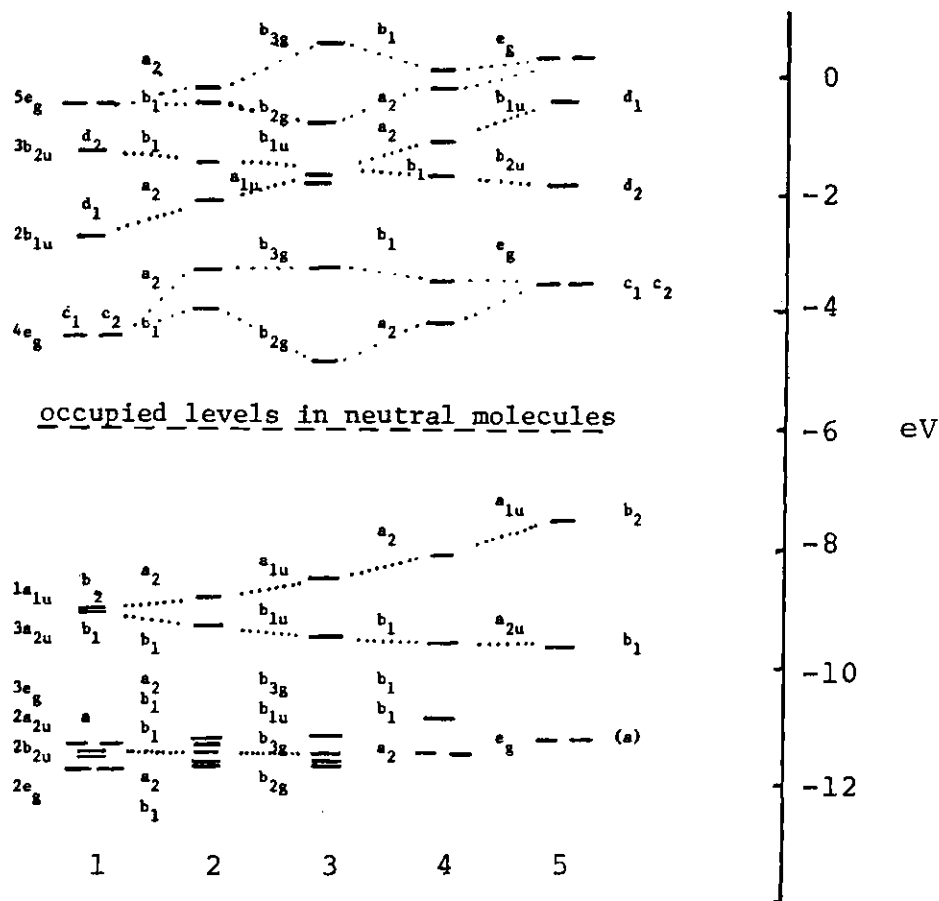


Figure 15. Highest Filled and Virtual SCF Molecular Orbital Energies of Metallocomplexes. 1) porphyrin, 2) chlorin, 3) opposite bacteriochlorin, 4) hexahydroporphyrin, and 5) octahydroporphyrin. Orbital a is 2b<sub>2u</sub>, b<sub>1</sub>, and b<sub>1u</sub> in complexes 1 to 3 respectively.

orbital model.<sup>70,71</sup> The two highest occupied orbitals are  $b_1$  and  $b_2$ , while  $c_1$  and  $c_2$  are the two lowest unoccupied orbitals (Figure 15). We will assume initially that  $b_1$  and  $b_2$  are degenerate and the  $c_1$  and  $c_2$  are degenerate. In  $D_{4h}$  porphyrins  $c_1$  and  $c_2$  will be degenerate. However, the  $b_1$  and  $b_2$  degeneracy is accidental. Four singly excited configurations can be formed by promotions from the  $b_1$  and  $b_2$  to the  $c_1$  and  $c_2$  orbitals. These may be represented as  $(b_1c_1)$ ,  $(b_1c_2)$ ,  $(b_2c_1)$ , and  $(b_2c_2)$ , where

$$(b_1c_1) \equiv \frac{1}{\sqrt{2}} \{ |b_1\bar{c}_1| - |\bar{b}_1c_1| \}. \quad (175)$$

Transition dipoles to the four electronic states are represented as  $R_{1y}$ ,  $R_{1x}$ ,  $R_{2x}$ , and  $R_{2y}$ , respectively. The magnetic dipoles between  $c_1$  and  $c_2$  and between  $b_1$  and  $b_2$  will be represented by  $m_c$  and  $m_b$ , respectively. At this point the model predicts that the porphyrin spectrum consists of two  $E_u$  states of the same energy. After configuration interaction there will be two new degenerate states,

$$B_x^\circ = \frac{1}{\sqrt{2}} [(b_1c_2) - (b_2c_1)] \quad (176)$$

$$B_y^\circ = \frac{1}{\sqrt{2}} [(b_1c_1) + (b_2c_2)] \quad (177)$$

and

$$Q_x^\circ = \frac{1}{\sqrt{2}} [(b_1c_2) + (b_2c_1)] \quad (178)$$

$$Q_Y^{\circ} = \frac{1}{\sqrt{2}} [(b_1 c_1) - (b_2 c_2)] \quad (179)$$

In the model  $R_{1y} = R_{2y} = R_{1x} = -R_{2x}$ , and therefore the transition to  $Q^{\circ}$  has zero intensity. All of the absorption spectrum intensity is contained in the  $B^{\circ}$  band. The angular momentum associated with the  $B^{\circ}$  band is  $-m_c + m_b$ , while that of the  $Q^{\circ}$  state is  $-m_c - m_b$ .

Before examining this situation further, it should be noted that the signs of orbitals, states, and transition dipoles are arbitrary. However, keeping track of the signs is crucial for both absorption and MCD calculations. Changing the sign of one of these terms changes the sign of at least one other term. In calculating the observable quantities (absorption and MCD spectra) these sign changes affect pairs of terms which are multiplied together. As required, the signs of physical observables are unique.

Consider now the situation where the degeneracies of the orbitals have been removed by a small perturbation. The absorption spectrum can still be divided into two bands,  $Q$  and  $B$ . The  $Q$  band will now have a nonzero intensity due to the mixing with the  $B$  band. The relative intensities of the two bands will thus depend on the nature of the perturbation. The MCD spectrum for each band should be a single  $A$  term, since each transition is from a nondegenerate ground state to a degenerate excited state. As the perturbation increases, each degenerate absorption band will split into two peaks with

oppositely signed B terms. The absorption and MCD spectra of a normal  $D_{4h}$  porphyrin, copper tetraphenylporphyrin, can be seen in Figure 16. The two A terms in the visible region are assigned to 0-0 and 0-1 vibrational components of Q. Figures 17 and 18 are for metallocomplexes of a dihydroporphyrin. The MCD spectrum of the chlorin exhibits oppositely signed components at the Q and B band upon comparison to the MCD spectrum of the porphyrin Q and B transitions (Figure 16). In Figures 19 and 20, the signs of the MCD spectrum found in the chlorins is maintained in the bacteriochlorin MCD spectra.

This sign reversal was first noted by Briat, et. al.,<sup>23</sup> and C. Houssier and K. Sauer<sup>24</sup> related this sign reversal to a lowering of the symmetry of these species. Unfortunately, this explanation predicts the wrong signs for the free bases of the symmetric porphyrins. The signs of the free bases for the porphyrins and for the reduced forms are observed to be identical to those of their respective metallated species.<sup>24</sup> McHugh, et. al.,<sup>9</sup> show that the perturbation from  $D_{4h}$  symmetry can be related to a parameter that determines the sign of the transition moments and thereby the MCD spectrum. In the rest of the discussion for the neutrals, we will show how the four orbital model predicts the signs of the MCD terms for the 0-0 vibrational components. The signs of the vibrational components will then be discussed. Finally, the four orbital model will be compared with the SCF-MO calculations.

Consider now the situation in the four orbital model

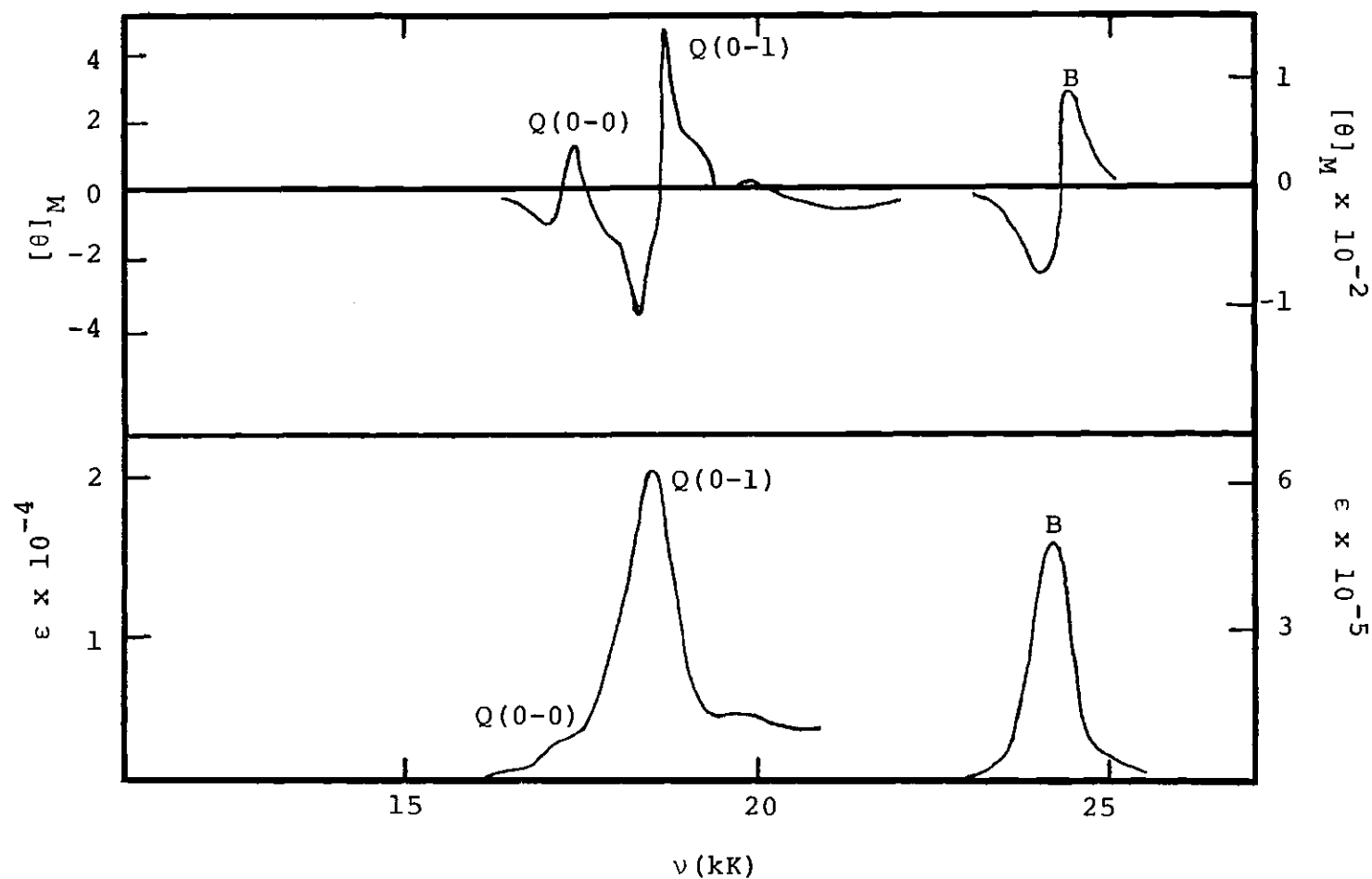


Figure 16. CuTPP Neutral in 50% Dimethylformamide and 50% Tetrahydrofuran (MCD Spectrum (Upper Figure); Absorption Spectrum (Lower Figure); Units are:  $[\theta]_M$ ,  $\text{deg cm}^2 \text{ gauss}^{-1} \text{ dmole}^{-1}$ ;  $\epsilon$ ,  $\text{liter cm}^{-1} \text{ mole}^{-1}$ ). The Soret band (25 kK) has a single A term, while in the visible region, two A terms are apparent. The spectra were taken at room temperature.

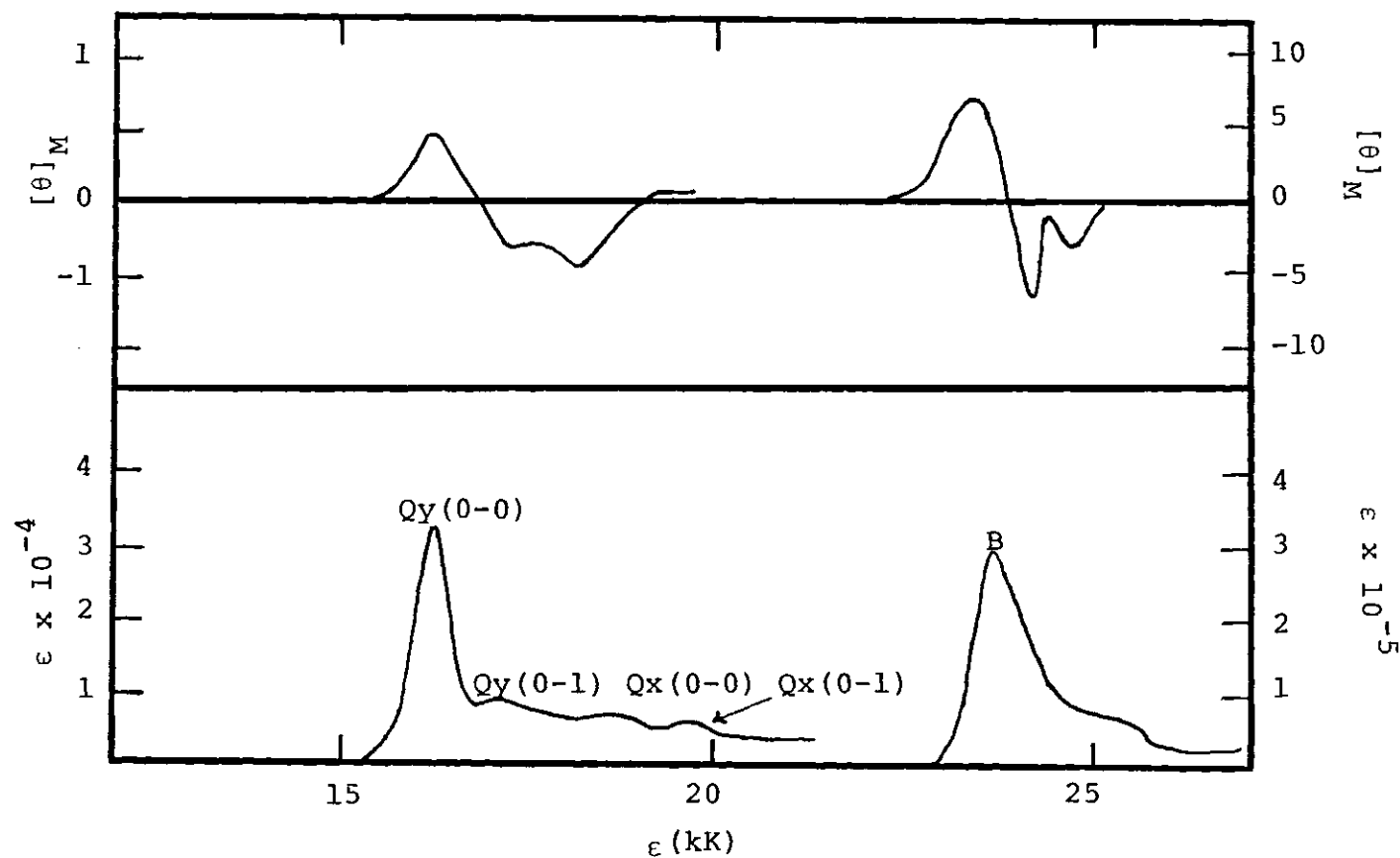


Figure 17. CuTPC Neutral in 50% Dimethylformamide and 50% Tetrahydrofuran. (MCD spectrum (upper figure); absorption spectrum (lower figure); units are:  $[\theta]_M$ ,  $\text{deg cm}^2 \text{ gauss}^{-1} \text{ dmole}^{-1}$ ;  $\epsilon$ ,  $\text{liter cm}^{-1} \text{ mole}^{-1}$ ). The spectra were taken at room temperature.

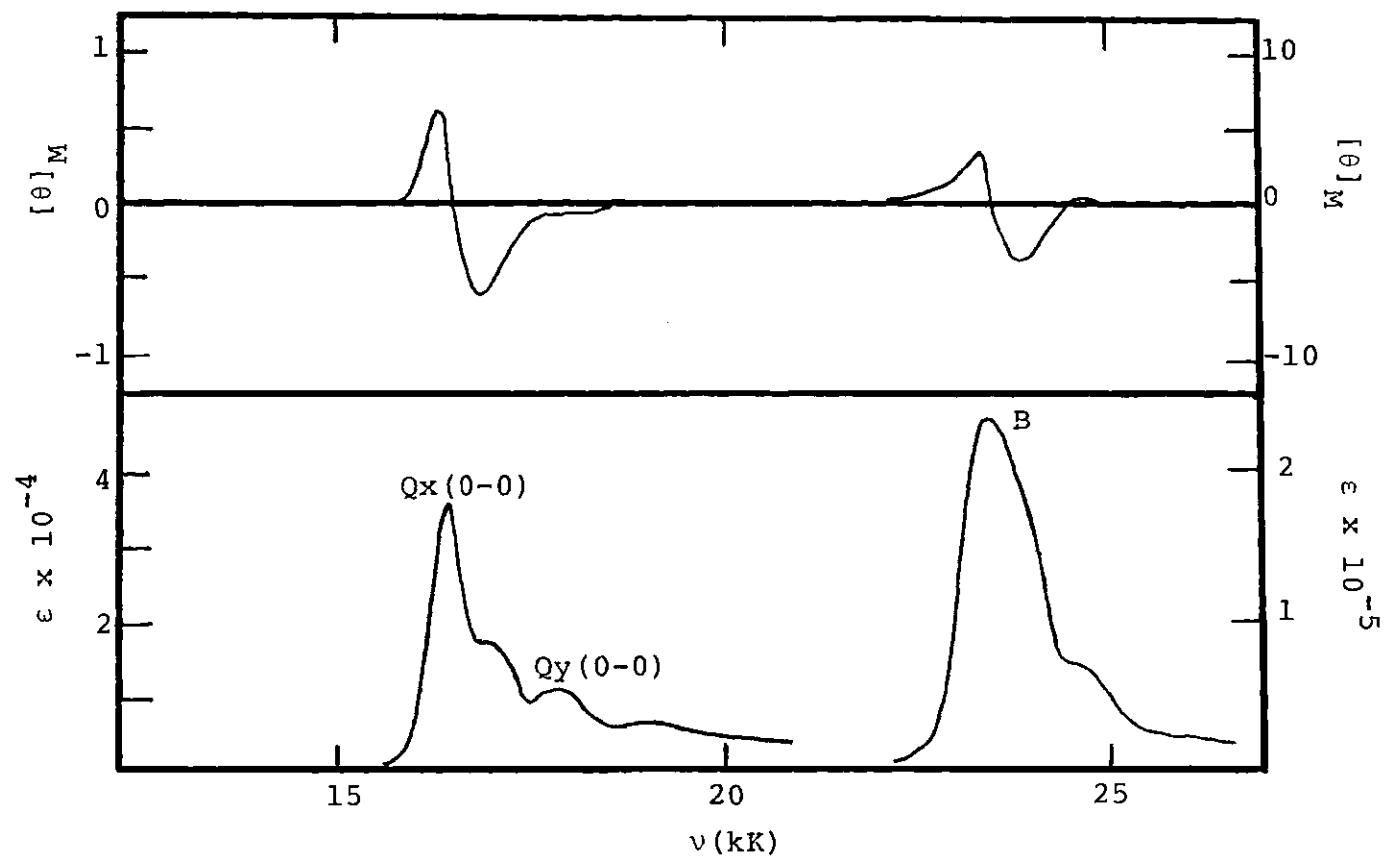


Figure 18. ZnTPC Neutral in Dimethylformamide (MCD Spectrum (Upper Figure); Absorption Spectrum (Lower Figure); Units are:  $[\theta]_M$ ,  $\text{deg cm}^2 \text{ gauss}^{-1} \text{ dmole}^{-1}$ ;  $\epsilon$ ,  $\text{liter cm}^{-1} \text{ mole}^{-1}$ ). The spectra were taken at room temperature.

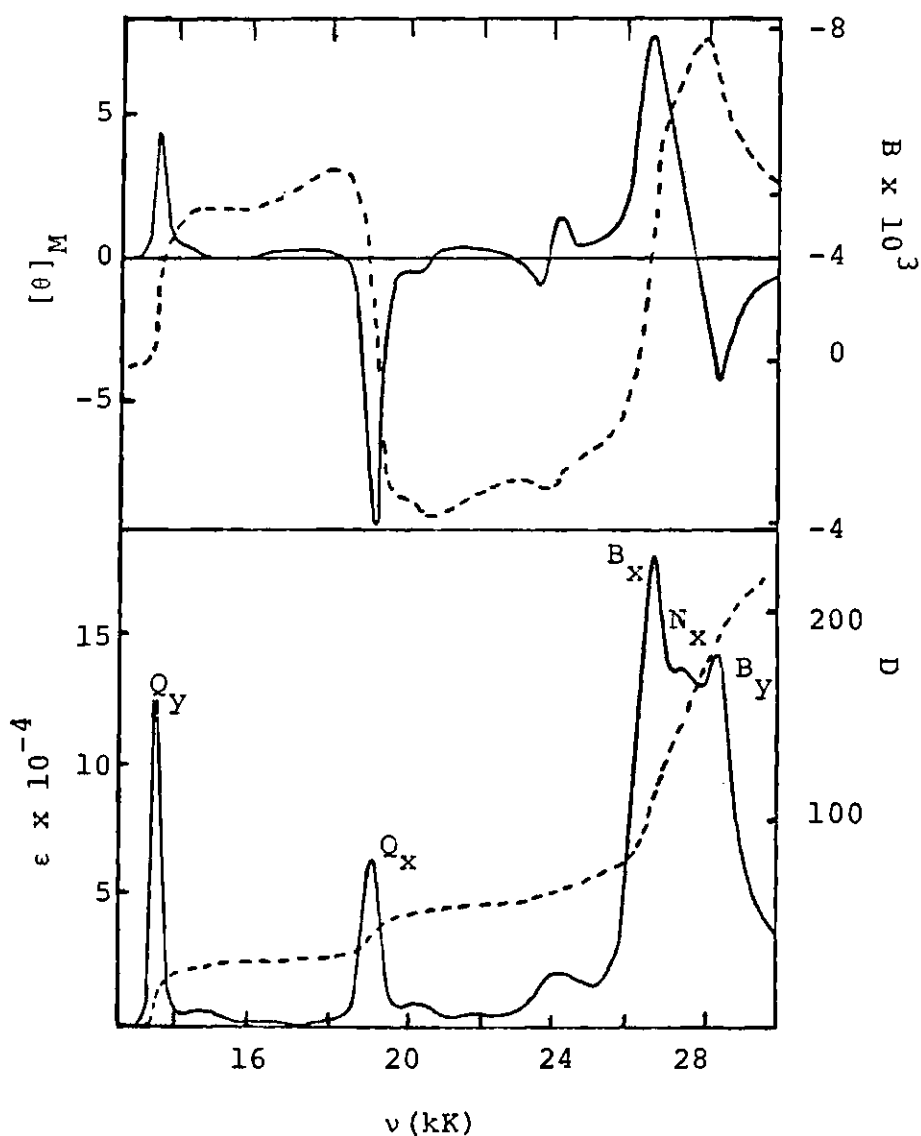


Figure 19.  $H_2TPBc$  Neutral. Upper figure is MCD spectrum; lower figure is absorption spectrum. The peak at 24 kK is an impurity. The dotted line represents the integrated B value or dipole intensity. The units are:  $[\theta]_M$ ,  $\text{deg cm}^2 \text{ gauss}^{-1} \text{ dmole}^{-1}$ ;  $\epsilon$ ,  $\text{liter cm}^{-1} \text{ mole}^{-1}$ ; D,  $\text{Debye}^2$ ; B,  $\text{Debye}^2 \text{ Bohr magneton cm}^{-1}$ . The spectra were taken at room temperature. The solvent is dimethylformamide.

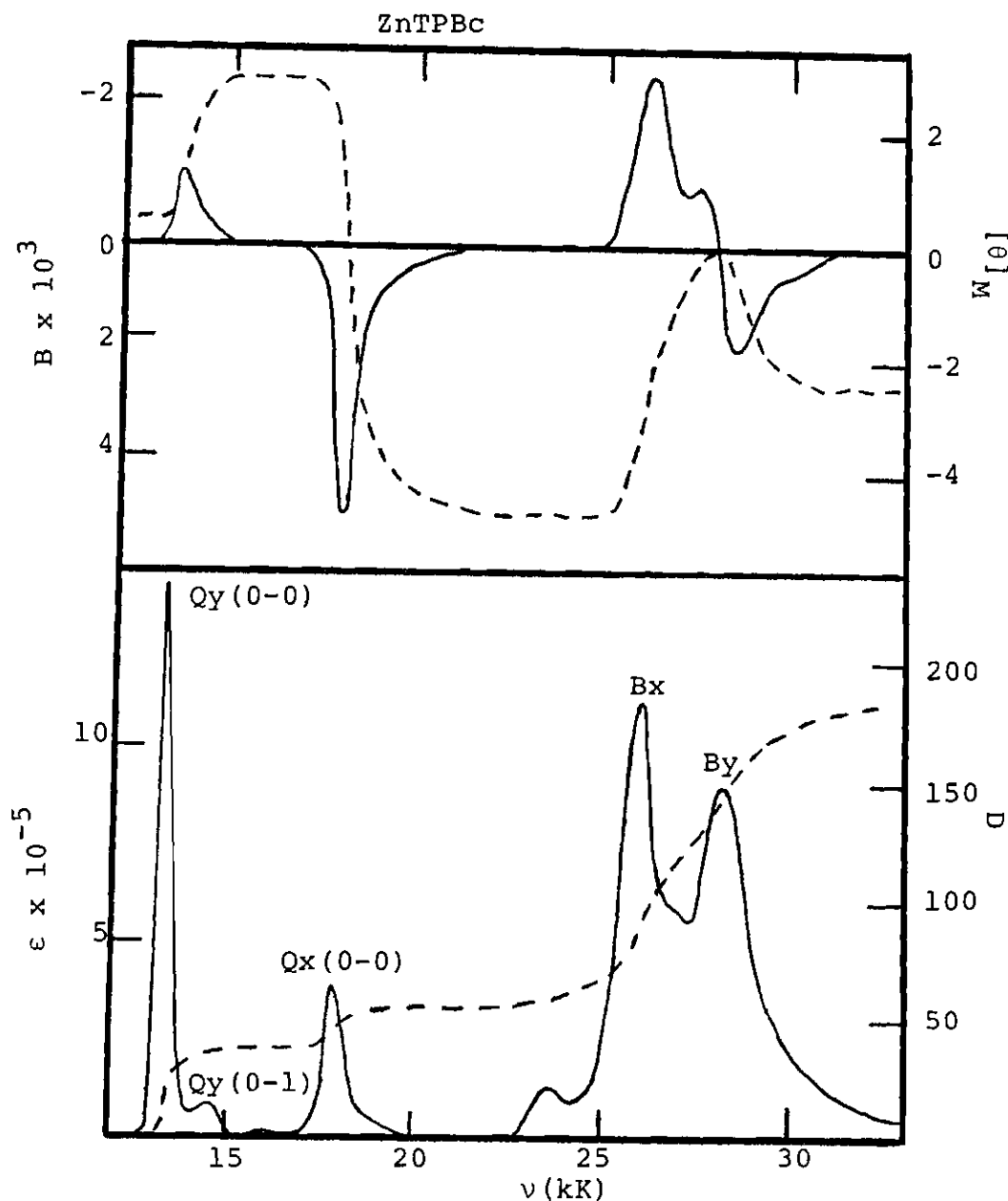


Figure 20. ZnTPBc Neutral. Upper figure is MCD spectrum; lower figure is absorption. The peak at 24 kK in the absorption spectrum is an impurity, and its contribution to the MCD spectrum has been removed. The dotted lines represent the integrated intensities. The units are  $[\theta]_M$ ,  $\text{deg cm}^2 \text{ gauss}^{-1} \text{ dmole}^{-1}$ ;  $\epsilon$ ,  $\text{liter cm}^{-1} \text{ mole}^{-1}$ ;  $D$ ,  $\text{Debye}^2$ ;  $B$ ,  $\text{Debye}^2 \text{ Bohr magneton cm}^{-1}$ . The spectra were taken at room temperature. The solvent is dimethylformamide.

where the degeneracies have been removed. First-order perturbation theory leads to the states,

$$Q_x = Q_x^{\circ} + \lambda_x B_x^{\circ} \quad (180)$$

$$Q_y = Q_y^{\circ} + \lambda_y B_y^{\circ} \quad (181)$$

$$\lambda_x = \{[\epsilon(c_2) - \epsilon(c_1)] + [\epsilon(b_2) - \epsilon(b_1)]\}/2\Delta \quad (182)$$

$$\lambda_y = \{[\epsilon(c_1) - \epsilon(c_2)] + [\epsilon(b_2) - \epsilon(b_1)]\}/2\Delta \quad (183)$$

where  $\epsilon(i)$  is the orbital energy of  $i$  and  $\Delta$  is the energy gap between the  $Q^{\circ}$  and  $B^{\circ}$  states before removing the degeneracies.<sup>70</sup>

(Actually we should multiply  $Q_x^{\circ}$  and  $Q_y^{\circ}$  by factors,  $\alpha_x$  and  $\alpha_y$ , such that  $\alpha_x^2 + \lambda_x^2 = 1$  and  $\alpha_y^2 + \lambda_y^2 = 1$ . These factors have been ignored since they will not affect the present argument.) The electric dipoles for these  $Q$  states will be proportional to  $\lambda_x$  and  $\lambda_y$ . The angular momentum of this state is given by  $-m_c - m_b + \lambda_x \lambda_y (-m_c + m_b) \approx -m_c - m_b \equiv \lambda_z$ .

Now consider the observable quantities. The absorption spectra intensity for the  $Q$  band will be given by the dipole strengths  $\lambda_x^2$  and  $\lambda_y^2$ , whose magnitudes depend on the relative orbital energies. For  $D_{4h}$  porphyrins  $c_1$  and  $c_2$  represent the  $e_g$  orbitals and thus  $\epsilon(c_2) - \epsilon(c_1) = 0$ . The transition dipoles for the  $x$  and  $y$  components are equal. The triple scalar product which determines the MCD A term is

$$\langle Q_x | \bar{L}_x | Q_y \rangle \cdot \{ \langle G | \bar{x} | Q_x \rangle \times \langle G | \bar{y} | Q_y \rangle \} = \alpha \lambda_z \lambda_y \lambda_x. \quad (184)$$

Note that although,

$$\langle G | \bar{x} | Q_x \rangle \langle G | \bar{y} | Q_y \rangle = - \langle G | \bar{y} | Q_y \rangle \langle G | \bar{x} | Q_x \rangle, \quad (185)$$

a change in the coordinate system will not change the calculated observable quantities since this change will also reverse the sign of  $\lambda_z$ . For the porphyrins, phthalocyanines, tetrabenzporphyrins, and tetrazaporphyrins,

$$|\epsilon(c_2) - \epsilon(c_1)| < |\epsilon(b_2) - \epsilon(b_1)|, \quad (186)$$

thus,  $\lambda_x \approx \lambda_y$ . For the chlorins, monoazaporphyrins, opposite diazaporphyrins, and opposite tetrahydroporphyrins the splitting of the  $c_1$  and  $c_2$  levels is greater than that of the  $b_1$  and  $b_2$  levels,<sup>75</sup> and  $\lambda_x \approx -\lambda_y$ . Note that the sign of this triple scalar product does not depend on the relative order of  $c_1$  and  $c_2$  or of  $b_1$  and  $b_2$ . This model predicts that the long wavelength band or Q band will be split into two components,  $Q_x$  and  $Q_y$ . (For the  $D_{4h}$  porphyrins these will have the same energy when the magnetic field intensity is zero.) For the first set of compounds the long wavelength component will have a negative MCD, while the other component will have positive MCD. For the second set of compounds, these signs will be reversed.

The components of the B band may be represented by

$$B_x = \alpha_x B_x^\circ - \lambda_x Q_x^\circ \quad (187)$$

$$B_y = \alpha_y B_y^\circ - \lambda_y Q_y^\circ \quad (188)$$

The magnitudes of the electric dipoles for the B band will be reduced by  $\lambda_x^2$  and  $\lambda_y^2$ . Splitting  $c_1$  and  $c_2$  or  $b_1$  and  $b_2$  will lower the intensity of this absorption band by an amount equal to that gained by the Q band. Since the signs of the electric dipoles are not changed by a small perturbation, any change in the signs of the MCD of the B band must be due to a change in the sign of the angular momentum. The angular momentum will be given by

$$\langle B_x | L_z | B_y \rangle = \alpha_x \alpha_y (-m_c + m_b) - \lambda_x \lambda_y (m_c + m_b) \quad (189)$$

The first problem in evaluating this is to determine  $m_c - m_b$ . According to the free electron model this is  $5 - 4 = 1$ . The Extended Huckel calculation using all two center integrals gives  $2.39 - 2.37 = 0.02$ .<sup>19</sup> The SCF calculations using only nearest neighbor  $1_z$  integrals gives  $2.228 - 2.369 = -0.141$ . The calculated values of  $m_c - m_b$  vary somewhat depending on the method of calculation and choice of parameters. (The error in calculating the SCF-MO value will be discussed in greater detail later.) In all of these calculations the value of  $m_c - m_b$  is found by the difference between two approximately equal numbers. Furthermore, as far as this four orbital model is correct, the value of this difference will

not change as the orbital energies are changed. Since the possible error in calculating this term is greater than its value, we will neglect  $-m_c + m_b$ . Therefore,

$$\langle B_x | \tilde{L}_z | B_y \rangle = -2m_c \lambda_x \lambda_y, \quad (190)$$

where  $m_c \approx m_b$  is assumed. For the B band of the porphyrin, the long wavelength component is predicted to be negative and the other component positive. These signs will be reversed for the chlorins and opposite tetrahydroporphyrins since  $\lambda_x \approx -\lambda_y$  (cf. Figures 17-20 vs. Figure 16). Thus the four orbital model is successful in showing the origin of the sign reversal in the MCD of the porphyrinic structures.

So far, we have ignored any additional effects due to vibrations. Throughout this thesis it is tacitly assumed that all of the vibrational components of an electronic transition have identical  $[\theta]_M/\epsilon$  values and that their lineshape functions are identical. Indeed, in interpreting the data, it is assumed that these vibronic components of a broad absorption band are arranged symmetrically about some central frequency. The validity of these assumptions is not obvious.

In order to examine these assumptions more carefully, it is necessary to treat each vibronic component separately. From Equation (41) it can be seen that the MCD spectrum for each vibronic component involves sums of terms in the form

$$\frac{\bar{m} \cdot \text{Im}(\bar{R}_1 \times \bar{R}_2)}{\Delta E} \quad (191)$$

while the absorption spectrum involves sums of terms in the form

$$\text{Re}(\bar{\mathbf{R}} \cdot \bar{\mathbf{R}}), \quad (192)$$

where  $\bar{\mathbf{m}}$  is the magnetic dipole moment;  $\bar{\mathbf{R}}$ ,  $\bar{\mathbf{R}}_1$ , and  $\bar{\mathbf{R}}_2$  are electric dipole moments;  $E$  is an energy difference;  $\text{Im}()$  and  $\text{Re}()$  denote the imaginary and real parts of the expression in parenthesis. Assuming the Born-Oppenheimer approximation is valid, then the wavefunction may be written as a product of an electronic wavefunction for fixed nuclear positions and a nuclear wavefunction which describes the vibrational motions in a potential field of the electrons. Assuming that the motion of the nuclei is small, then each dipole moment is in the form,

$$\langle Aa | \bar{\mathbf{O}} | Bb \rangle = \langle A | \bar{\mathbf{O}} | B \rangle \langle a | b \rangle \quad (193)$$

where  $|A\rangle$  and  $|B\rangle$  are the electronic wavefunctions,  $|a\rangle$  and  $|b\rangle$  are nuclear wavefunctions, and  $\bar{\mathbf{O}}$  is the appropriate dipole operator. For absorption we need to consider the square of the electric dipole moment between ground and excited vibrational states  $\langle Aa |$  is the ground state,  $|Bb\rangle$  is an excited state, and  $|\langle a | b \rangle|^2$  is the Frank-Condon factor. Within the Frank-Condon approximation the summation over all ground and excited levels for this transition will give  $|\langle A | \bar{\mathbf{O}} | B \rangle|^2$ , which is the calculated transition moment for fixed nuclei.

Unfortunately, it is not easy to perform this summation

for the MCD parameters since the individual components of this triple product cannot be calculated without knowing the overlap integrals among various states. It is even possible for the MCD terms for these various vibronic components to change signs. This sign reversal has been observed experimentally<sup>20</sup> in Q (0-1) transitions of metalloporphyrins and has been discussed in greater detail elsewhere.<sup>76</sup> Apparently, for allowed transitions of one vibrational mode, the theory<sup>19</sup> works quite successfully. The calculations in this section apply only to the 0-0 bands.

Next, let us see what the SCF-MO calculations predict for these compounds. The first part of this problem is to calculate the states using the self-consistent field molecular orbital Pariser-Parr-Pople configuration interaction method. In this calculation we obtain a set of molecular orbitals,  $|\phi_j\rangle$ ; configurations,  $|\chi_i\rangle$ ; and states  $|\psi_k\rangle$

$$|\phi_j\rangle = \sum_a k_{ja} |a\rangle \quad (194)$$

$$|\chi_i^{j \rightarrow k}\rangle = \frac{1}{\sqrt{2}} \{ |\phi_1 \bar{\phi}_1 \cdots \phi_j \bar{\phi}_k| - |\phi_1 \bar{\phi}_1 \cdots \bar{\phi}_j \phi_k| \} \quad (195)$$

$$|\psi_k\rangle = \sum_i c_{ik} |\chi_i^{j \rightarrow k}\rangle \quad (196)$$

Here,  $k_{ja}$ ,  $c_{ij}$ , and  $c_{ik}$  are the appropriate expansion coefficients, and  $|a\rangle$  is an atomic orbital centered on a carbon or nitrogen atom, in our case  $2p_z$  orbital. For these neutral compounds, configuration interaction over a large number of

configurations show that to account for the bacteriochlorin spectra, another orbital must be included. The three highest occupied orbitals are  $a$ ,  $b_1$ , and  $b_2$ , while  $c_1$  and  $c_2$  are degenerate. The configurations which will be used in these calculations are

$$1 : \text{Ground State} = |a^2 b_1^2 b_2^2| \quad (197)$$

$$2 : (ac_1) = \frac{1}{\sqrt{2}} \{ |ab_1^2 b_2^2 c_1| - |ab_1^2 b_2^2 c_1| \} \quad (198)$$

$$3 : (b_1 c_1) = \frac{1}{\sqrt{2}} \{ |a^2 b_1 b_2^2 c_1| - |a^2 b_1 b_2^2 c_1| \} \quad (199)$$

$$4 : (b_1 c_2) = \frac{1}{\sqrt{2}} \{ |a^2 b_1 b_2^2 c_2| - |a^2 b_1 b_2^2 c_2| \} \quad (200)$$

$$5 : (b_2 c_1) = \frac{1}{\sqrt{2}} \{ |a^2 b_1^2 b_2 c_1| - |a^2 b_1^2 b_2 c_1| \} \quad (201)$$

$$6 : (b_2 c_2) = \frac{1}{\sqrt{2}} \{ |a^2 b_1^2 b_2 c_2| - |a^2 b_1^2 b_2 c_2| \} \quad (202)$$

The resulting states are given in Table 6.

The second step is to calculate the various transition moment matrix elements between states. These matrix elements can be found by

$$\langle \psi_i | \bar{O} | \psi_j \rangle = \sum_{k, \ell} c_{ki} c_{\ell j} \langle \chi_k | \bar{O} | \chi_\ell \rangle \quad (203)$$

The matrix elements between configurations are reduced to matrix elements between molecular orbitals by<sup>77</sup>

$$\langle \chi(\text{ground state}) | \bar{O} | \chi(m \rightarrow n) \rangle = \sqrt{2} \langle \phi_m | \bar{O} | \phi_n \rangle \quad (204)$$

Table 6. States After Configuration Interaction for Neutral Compounds. Quantities in parenthesis are configurations displayed in Equations (197-202).

Metalloporphyrin States Energy (kK)	Configuration Interaction Coefficients
0	1.000 (1)
16.47	-0.7158(4) + 0.6983(5)
16.47	0.7158(3) + 0.6983(6)
28.14	0.6983(4) + 0.716 (5)
28.14	0.6983(3) - 0.716 (6)
Metallochlorin States	
0	1.000 (1)
15.64	-0.469 (4) - 0.871 (5)
17.90	0.747 (3) - 0.651 (6)
27.74	0.627 (3) + 0.743 (6)
28.53	0.870 (4) - 0.475 (5)
Metallobacteriochlorin States	
0	1.000 (1)
13.79	-0.342 (4) - 0.931 (5)
17.18	+0.070(2) + 0.810(3) - 0.571(6)
29.78	-0.390(2) - 0.507(3) - 0.764(6)
31.02	-0.908(2) + 0.282(3) + 0.286(6)
32.79	-0.930 (4) + 0.353 (5)

and

$$\langle \chi(m \rightarrow n) | \mathcal{O} | \chi(v \rightarrow \mu) \rangle = \delta_{mv} \langle \phi_n | \bar{\mathcal{O}} | \phi_\mu \rangle + \delta_{n\mu} \langle \phi_m | \bar{\mathcal{O}} | \phi_v \rangle. \quad (205)$$

These molecular orbital angular momentum matrix elements are in turn found from the atomic orbital angular matrix elements:

$$\langle \phi_n | \ell_z | \phi_m \rangle = \sum_k \sum_{kj} (k_{nk} k_{mj} - k_{nj} k_{mk}) \langle a_k | \ell_z | a_j \rangle \quad (206)$$

This integral can further be written as

$$\langle a_k | \ell_z | a_j \rangle = -i\hbar T(k,j) [\xi_k \eta_j - \eta_k \xi_j], \quad (207)$$

where  $(\xi_k, \eta_k)$  and  $(\xi_j, \eta_j)$  are the  $x, y$  coordinates of the two centers and  $T(k,j)$  has the form of an overlap integral.<sup>19</sup> Slater-type  $p_z$  orbitals are used for nitrogen and carbon atoms. Thus by combining the electric and magnetic dipoles between orbitals (Table 7) with the knowledge of the various states (Table 6), we can obtain Table 8, which is composed of the electric and magnetic dipoles between states of these neutral compounds. The final step in this calculation is to take the electric and magnetic dipoles between states of neutral compounds and the state energies to obtain the calculated spectra (Table 9).

Consider first the neutral metalloporphyrin. The lowest lying bands consist of a pair of degenerate transitions. Interpreted as an A term, the value, using the entries of Table 8, is given by Equation (61),

Table 7. Electric and Magnetic Dipoles Between Orbitals of Neutral Compounds. (The units are in Debye units and Bohr Magneton.)

Metalloporphyrin		Metallochlorin	
Orbitals	Dipole	Orbitals	Dipoles
$b_1b_2$	2.369 ( $M_z$ )	$b_1b_2$	3.594 (Y) 2.113 ( $M_z$ )
$b_1c_1$	20.882 (Y)	$b_1c_1$	-7.498 (X)
$b_1c_2$	20.882 (X)	$b_1c_2$	-2.425 (Y) 0.303 ( $M_z$ )
$b_2c_1$	20.226 (X)	$b_2c_1$	-8.423 (Y) -0.868 ( $M_z$ )
$b_2c_2$	-20.226 (Y)	$b_2c_2$	-7.477 (X)
$c_1c_2$	-2.228 ( $M_z$ )	$c_1c_2$	6.087 (Y) 1.904 ( $M_z$ )

Metallobacteriochlorin

Orbitals	Dipole
$ab_2$	-0.439 ( $M_z$ )
$ac_1$	0.488 (X)
$ac_2$	-1.367 (Y)
$b_1b_2$	2.099 ( $M_z$ )
$b_1c_1$	6.138 (Y)
$b_2c_1$	-10.215 (Y)
$b_2c_2$	-6.583 (X)

Table 8. Electric and Magnetic Dipoles Between States of Neutral Compounds (in Debye and Bohr Magneton units).

## Metalloporphyrin

1,2	-0.457X
1,3	0.457Y
1,4	16.170X
1,5	16.170Y
2,3	-4.596M <sub>Z</sub>
4,5	-0.140M <sub>Z</sub>

## Metallochlorin

1,2	5.955(Y)	1.531M <sub>Z</sub>
1,3	0.928X	
1,4	-14.187X	
1,5	12.868Y	-0.150M <sub>Z</sub>
2,3	2.697Y	3.884M <sub>Z</sub>
2,4	-3.586Y	-0.149M <sub>Z</sub>
3,5	8.507Y	1.150M <sub>Z</sub>
4,5	-0.257Y	-0.416M <sub>Z</sub>

## Metallobacteriochlorin

1,2	4.016Y
1,3	1.182X
1,4	4.689X
1,5	2.463X
1,6	5.159Y
2,3	3.673M <sub>Z</sub>
2,4	0.839M <sub>Z</sub>
2,5	0.362M <sub>Z</sub>
3,6	-1.693M <sub>Z</sub>
4,6	-0.256M <sub>Z</sub>
5,6	0.194M <sub>Z</sub>

Table 9. Neutral Porphyrin and Chlorin Spectra. (B has units of  $(\text{Debye})^2$  (Bohr magneton)  $(\text{cm}^{-1})$ ; A has units of  $(\text{Debye})^2$  (Bohr magneton); D has units of  $(\text{Debye})^2$ .)

Metalloporphyrin Calculated

	$\nu(\text{kK})$	D	Polarization	A	A/D
Q	16.5	0.21	X	-0.96	-4.70
	16.5	0.21	Y		
B	28.1	261.5	X	36.7	0.14
	28.1	261.5	Y		

Metalloporphyrin Experimental

	$\nu(\text{kK})$	D (0-0)	A (0-0)	A/D	
Q	17.34	2.93	-10.16	-3.47 <sup>a</sup>	
B	24.20	81.77	-22.77	-0.28 <sup>a</sup>	
Q	17.78			-1.73	(CuOEP) <sup>b</sup>
B	24.92			-0.19	
Q	17.54			-1.77	(ZnOEP) <sup>b</sup>
B	24.84			-0.15	
Q	17.91			-1.06	(AgOEP) <sup>b</sup>
B	24.46			-0.29	
Q	18.08			-0.93	(CoOEP) <sup>b</sup>
B	25.4			0.2	
Q	18.57	6.88	-19.08	-2.77	(PdOEP) <sup>c</sup>
Q	17.1	1.38	-1.96	-1.42	(MgOEP) <sup>c</sup>
		to 3.90	to -8.79	to -2.98	
Q	17.57	3.27	-5.01	-1.44	(ZnOEP) <sup>c</sup>
		to 6.42	to -0.65	to -2.06	

a) Zinc hematoporphyrin, ref. 18

b) Ref. 20

c) Ref. 27

Table 9. (Continued)  
Metallochlorin Calculated

	$\nu$ (kK)	D	Polarization	$B \times 10^3$	B/D
$Q_Y$	15.64	35.46	Y	-3.8	-0.11
$Q_X$	17.90	0.86	X	5.3	6.2
$B_X$	27.74	201.27	X	-3.2	-0.016
$B_Y$	28.53	165.59	Y	1.9	0.011

Experimental ZnTPC<sup>d</sup>

$Q_Y(0-0)$	16.4	11.5		-0.60	-0.052
$Q_Y(0-1)$	16.9	4.0		0.85	0.21
$Q_X(0-0)$	17.8	4.5		0.11	0.024
$Q_X(0-1)$	18.9	4.1		0.05	0.012
$B_X(0-0)$	23.3	51.5		-4.91	-0.095
$B_Y(0-0)$	23.9	56.0		4.15	0.074
N	24.7	14.6		-0.62	-0.042

Experimental CuTPC<sup>d</sup>

$Q_Y(0-0)$	16.2	11.8		-0.60	-0.051
$Q_Y(0-1)$	17.3	5.4		0.30	0.056
$Q_X(0-0)$	18.6	3.0		-0.50	0.17
$Q_X(0-1)$	19.7	1.9		-0.04	-0.02
$B_X(0-0)$	23.6	89.0		-7.31	-0.082
$B_Y(0-0)$	24.0	43.4		2.04	0.047
N	25.0	38.0		1.79	0.047

d) Assignment of CuTPC and ZnTPC transitions are discussed in text.

$$A_Q = - \frac{(-4.596)(-0.457)(0.457)}{(2.54)^2} = -0.96 D^2_\beta \quad (208)$$

$$A_B = - \frac{(-0.140)(16.17)(16.17)}{(2.54)^2} = 36.7 D^2_\beta \quad (209)$$

The ratio of A/D provides a better indicator of the comparison of the experimental and theoretical values than the value of A alone. For the Q band, the value of -4.70 compares fairly well with the experimental values which range from about -0.50<sup>20</sup> to -8.1<sup>19</sup>. The value of  $A_B$  is of the right order of magnitude (0.14), but has the wrong sign. As we have shown earlier, this may be due to inaccuracies in the calculated values for the angular momentum between orbitals. One possible cause for error in calculated angular momenta is that Equation (209) uses a single Slater-type orbital for the carbon  $2p_z$  atomic orbital and molecular orbital coefficients,  $k_{ja}$ , of Equation (194), which are obtained from the PPP theory. It is inconsistent to use  $k_{ja}$  that are calculated with a zero differential overlap assumption with overlapping atomic orbitals. Future calculations should subject the atomic orbitals to a Löwdin transformation.<sup>60</sup>

Indeed, A. Kaito, et al., have calculated recently the MCD spectra of porphyrin, protoporphyrin, and porphyrin a using the Löwdin transformation.<sup>76</sup> Unlike previous calculations they obtain the correct signs for the A terms of the Soret region. The delicate nature of the signs of the MCD A

term can be seen by comparing low-spin ferrous protoheme with low-spin ferrous heme a. In this case the removal of a vinyl group with the addition of a formyl group to another positive reverses the signs of the A terms.

Next, let us examine spectra of the metallochlorins. The experimental B values are obtained by Eq. (63), while the theoretical quantities are obtained by Eq. (62). These are listed in Table 9. The first band (calculated to be at 15.64 kK represents the  $Q_y(0-0)$  component of the Q band. The assignment of the  $Q_x(0-0)$  is harder for two reasons. First, the absorption intensity is reduced to the same level as the 0-1 vibrational bands. Second, the MCD spectra of these components can be of either sign. Measurement of the polarizations of these bands would provide better evidence for these assignments; nonetheless, these assignments agree with those of Weiss.<sup>22</sup> These calculations show that the  $Q_x(0-0)$  band should have a weak absorption when compared with the  $Q_y(0-0)$  band and that the  $Q_x(0-0)$  should have an MCD spectrum of the same magnitude but opposite in sign to that of the  $Q_y(0-0)$  band. The Soret region also exhibits the same signs as that of the visible band. The splitting of the Soret band is smaller than the linewidth. When the results are expressed as B terms, we are generally more interested in the signs of these terms than their magnitude, since the calculation involves the summation over dipoles between all states. Table 9 lists an additional band beyond the Soret band. This transition is due primarily to

configuration 2 (Equation 198). This band is not predicted by the four orbital model and is not important in describing the major features of the absorption and MCD spectra of the neutral porphyrins and chlorins.

The last set of neutral compounds studied are the bacteriochlorins. In both the 4-orbital and SCF-MO calculations, the absorption and MCD spectra of the metallobacteriochlorin should be much closer to that of the metallochlorin than to the metalloporphyrin. Table 10 gives the calculated and experimental spectra for the bacteriochlorins. Note that bacteriochlorins exhibit the same signs of the B terms in both the theoretical values and experimental values as was found in the chlorin spectra. The transition,  $N_x$ , tends to broaden the absorption spectrum in the near UV region and to augment the MCD intensity due to the  $B_x$  band. The quantitative agreement between calculations and data is good and provides further support for the assignments.

As these calculations have shown, the observed spectra for the neutral compounds can be divided up into two bands, Q and B. The most obvious differences between the symmetric porphyrins and the metallochlorins and bacteriochlorins is the sign reversal which occurs in both Q and B bands. As we have shown, both the MCD and absorption can be calculated quite simply by Gouterman's four orbital model. This model agrees satisfactorily with the more sophisticated SCF-MO calculations.

Table 10. Neutral Bacteriochlorin Spectra. (B has units of  $(\text{Debye})^2 (\text{Bohr magneton}) (\text{cm}^{-1})$ ; A has units of  $(\text{Debye})^2 (\text{Bohr magneton})$ ; D has units of  $(\text{Debye})^2$ .)

Calculated (Metallobacteriochlorin)

	$\nu (\text{kK})$	D	$B \times 10^3$
$Q_Y$	13.8	16.1	-4.4
$Q_X$	17.2	1.4	6.3
$B_X$	29.8	22.0	-3.6
$N_X$	30.8	6.1	-0.7
$B_Y$	31.0	26.6	2.7

Experimental ( $\text{H}_2\text{TPBc}$ )

	$\nu (\text{kK})$	D	$B \times 10^3$
$Q_Y$	13.5	34	-4
$Q_X$	19.2	34	8
Soret	27.0	200	-12 4

Experimental ( $\text{ZnTPBc}$ )

	$\nu (\text{kK})$	D	$B \times 10^3$
$Q_Y(0-0)$	13.3	32.8	-2.1
$Q_Y(0-1)$	14.6	5.3	-0.3
$Q_X(0-0)$	17.9	19.2	7.3
$B_X$	26.0	43.6	-3.2
$N_X$	26.9	23.7	-1.3
$B_Y$	28.2	52.9	2.3

### Electronic Configurations of Monoanions

The monoanion spectra are more complicated than the neutral spectra due to an increase in the number of configurations which contribute to the observed spectra. There are eight singly excited configurations from the b orbitals to the c orbitals. In addition to these the promotion of the unpaired electron from  $c_1$  to  $c_2$ ,  $d_1$ , or  $d_2$  and the promotion of an electron from a to  $c_1$  or  $c_2$  must be included. There will be fourteen relevant configurations to work with. These are listed in Table 11. Although other configurations were included in the SCF-MO calculations, these configurations do not contribute significantly to the low lying states which were studied. Their inclusion is responsible for some of the states listed in the following tables to deviate slightly from being normalized.

Consider the first two configurations in Table 11. One of these or some linear combination of these two will form the ground state. For  $D_{4h}$  porphyrins the ground state will be degenerate. For chlorins and bacteriochlorins (and as will be shown in the next section, for the porphyrins) the  $c_1$  and  $c_2$  orbitals are not degenerate. Therefore the ground state may be written as

$$\psi_1 = (a^2 b_1^2 b_2^2 c_1), \quad (214)$$

with

Table 11. Monoanion Configurations. In  $D_{4h}$  symmetry  $c_1 = e_{gx}$  and  $c_2 = e_{gy}$ . Configurations 1 and/or 2 form the ground state; 3 and 4 correspond to promoting the unpaired electron to a higher orbital. 5-10 correspond to promoting an electron from a filled orbital to the half filled orbital. 11-14 correspond to promotion from a filled orbital to an empty orbital. 11 and 12 are electronically allowed, while 13 and 14 are forbidden.

No.	Configuration	<u>Pure Configurations</u>		
		Symmetry:	$D_{4h}$	$D_{2h}$ $C_{2v}$
1	$ a^2b_1^2b_2^2c_1 $		$E_{gx}$	$B_{2g}$ $B_1$
2	$ a^2b_1^2b_2^2c_2 $		$E_{gy}$	$B_{3g}$ $A_2$
3	$ a^2b_1^2b_2^2d_1 $		$B_{1u}$	$A_u$ $A_2$
4	$ a^2b_1^2b_2^2d_2 $		$B_{2u}$	$B_{1u}$ $B_1$
5	$ ab_1^2b_2^2c_1^2 $		$B_{2u}$	$B_{1u}$ $B_1$
6	$ ab_1^2b_2^2c_2^2 $		$B_{2u}$	$B_{1u}$ $B_1$
7	$ a^2b_1b_2^2c_1^2 $		$A_{2u}$	$B_{1u}$ $B_1$
8	$ a^2b_1b_2^2c_2^2 $		$A_{2u}$	$B_{1u}$ $B_1$
9	$ a^2b_1^2b_2c_1^2 $		$A_{1u}$	$A_u$ $A_2$
10	$ a^2b_1^2b_2c_2^2 $		$A_{1u}$	$A_u$ $A_2$
11	$\frac{1}{\sqrt{2}}( a^2b_1b_2^2c_1\bar{c}_2  -  a^2b_1b_2^2c_1c_2 )$		$A_{2u}$	$A_u$ $A_2$
12	$\frac{1}{\sqrt{2}}( a^2b_1^2b_2c_1\bar{c}_2  -  a^2b_1^2\bar{b}_2c_1c_2 )$		$A_{1u}$	$B_{1u}$ $B_1$
13	$\frac{1}{\sqrt{6}}(2 a^2b_1b_2^2\bar{c}_1c_2  -  a^2b_1b_2^2c_1\bar{c}_2  -  a^2\bar{b}_1b_2^2c_1c_2 )$		$A_{2u}$	$A_u$ $A_2$
14	$\frac{1}{\sqrt{6}}(2 a^2b_1^2b_2\bar{c}_1c_2  -  a^2b_1^2b_2c_1\bar{c}_2  -  a^2b_1^2\bar{b}_2c_1c_2 )$		$A_{1u}$	$B_{1u}$ $B_1$

$$\psi_2 = (a^2 b_1^2 b_2^2 c_2) \quad (215)$$

being a low-lying excited state. In  $D_{4h}$  and  $D_{2h}$  symmetries, an electronic transition between these two states will be forbidden. This transition is allowed for the  $C_{2v}$  chlorin anion, but is predicted to be in the far IR region and has not yet been observed.

The promotion  $c_1 \rightarrow d_1$  forms the  $1B_{1u}$ ,  $3A_2$ , and  $2B_{1u}$  states for the porphyrin, chlorin, and bacteriochlorin anions respectively. In each case this configuration contributes 60-70% to the state after configuration interaction. Within the limited orbital model, the MCD of the lowest-energy transition will be due to the existence of angular momentum between this configuration and those formed by the  $c_2 \rightarrow d_1$  and the  $c_1 \rightarrow d_2$  configurations. For the porphyrin anion the degeneracy of the  $c$  orbitals causes the first term to predominate. However, for the chlorin and bacteriochlorin anions, the  $c_1 \rightarrow d_2$  configuration is significant.

The configuration formed by promoting the unpaired electron from the  $c_1 \rightarrow d_2$  level will give rise to the  $2B_{2u}(3B_{2u})$ ,  $3B_2(5B_2)$ , and  $2A_u(5A_u)$  states for the porphyrin, chlorin, and bacteriochlorin anions, respectively. In each case there is considerable mixing with the state in parenthesis. The MCD for the porphyrin anion will be dominated by the magnetic moment between the  $c_1$  and  $c_2$  levels because of their near degeneracy.

Configurations 7, 9, 11, and 12 (Table 11) correspond to promoting an the electron in a b orbital to a c orbital when the ground state is configuration 1. Configurations 8, 10, 13, and 14 would be electronically allowed, if the ground state configuration were configuration 2, but are electronically forbidden from configuration 1. In  $D_{4h}$  symmetry both sets of configurations will give rise to one each of the following states:  $A_{1u}$ ,  $A_{2u}$ ,  $B_{1u}$ , and  $B_{2u}$ . After configuration interaction we would expect to have two sets of these states. As in the case of neutral porphyrins the dipoles of the lower energy set will be due to the sum of these terms. The  $B_{1u}$  and  $B_{2u}$  states will mix with the states formed by  $c_1 \rightarrow d_1$  and  $d_2$ , which will increase the intensity of the low energy states of this symmetry. For this reason most of the intensity of the visible-near infrared region of the porphyrin monoanion spectra is due to  $B_{1u}$  or  $B_{2u}$  states, while in the near UV region all four symmetries are important. As the  $c_1$  and  $c_2$  orbitals move apart in energy, the configurations 8, 10, 13, and 14 become less important. In this limit we are left with  $\psi_1 \rightarrow \psi_{7,8,11,12}$ . The configuration interaction for these states will be identical for that of the neutrals. The relative signs of the MCD of these bands should therefore be the same as those for the neutrals. Thus the sign reversal, which is found between the neutral porphyrins and the neutral chlorins and bacteriochlorins, should also be found in their monoanions.

There is one more set of configurations to include in assigning the spectra of these anions. The configurations 5 and 6 (Table 11) for the  $D_{4h}$  porphyrin monoanion are two high in energy to contribute significantly to the observed spectrum. Only in the case of the bacteriochlorin anion where the  $c_1$  orbital energy has been significantly lowered will this set of configurations contribute to the observed spectrum. Even here this contribution will be in the near UV.

#### Zero Field Splitting of Metalloporphyrin Monoanion

MCD spectra of  $ZnEtio^{\dot{-}}$ ,  $ZnTPP^{\dot{-}}$ ,  $H_2TPP^{\dot{-}}$ ,  $H_2Etio^{\dot{-}}$ , and  $CuTPP^{\dot{-}}$  are remarkably similar. In the near infrared spectral region, we observe three features that coincide with absorption maxima (Figure 21). In the present discussion, attention is restricted to the lowest energy transition which, isolated from other bands, appears at 905 nm (11 kK) in  $ZnTPP^{\dot{-}}TBAB^+$  and at 825 nm (12.1 kK) in  $Na^+ZnEtio^{\dot{-}}$ . This band deserves special attention, since its origin is predicted to arise from promotion of the electron in the partially filled  $4e_g$  level to the lowest unfilled orbital, the  $2b_{1u}$  level. The resultant configuration is  $|b_1^2 b_2^2 d_1|$ , and detailed calculations, discussed later, suggest that configuration mixing with other states is minor. If we assume that angular momentum and electric dipole matrix elements between this transition, which is denoted as Band I, and other excited electronic states are negligible, then the states:

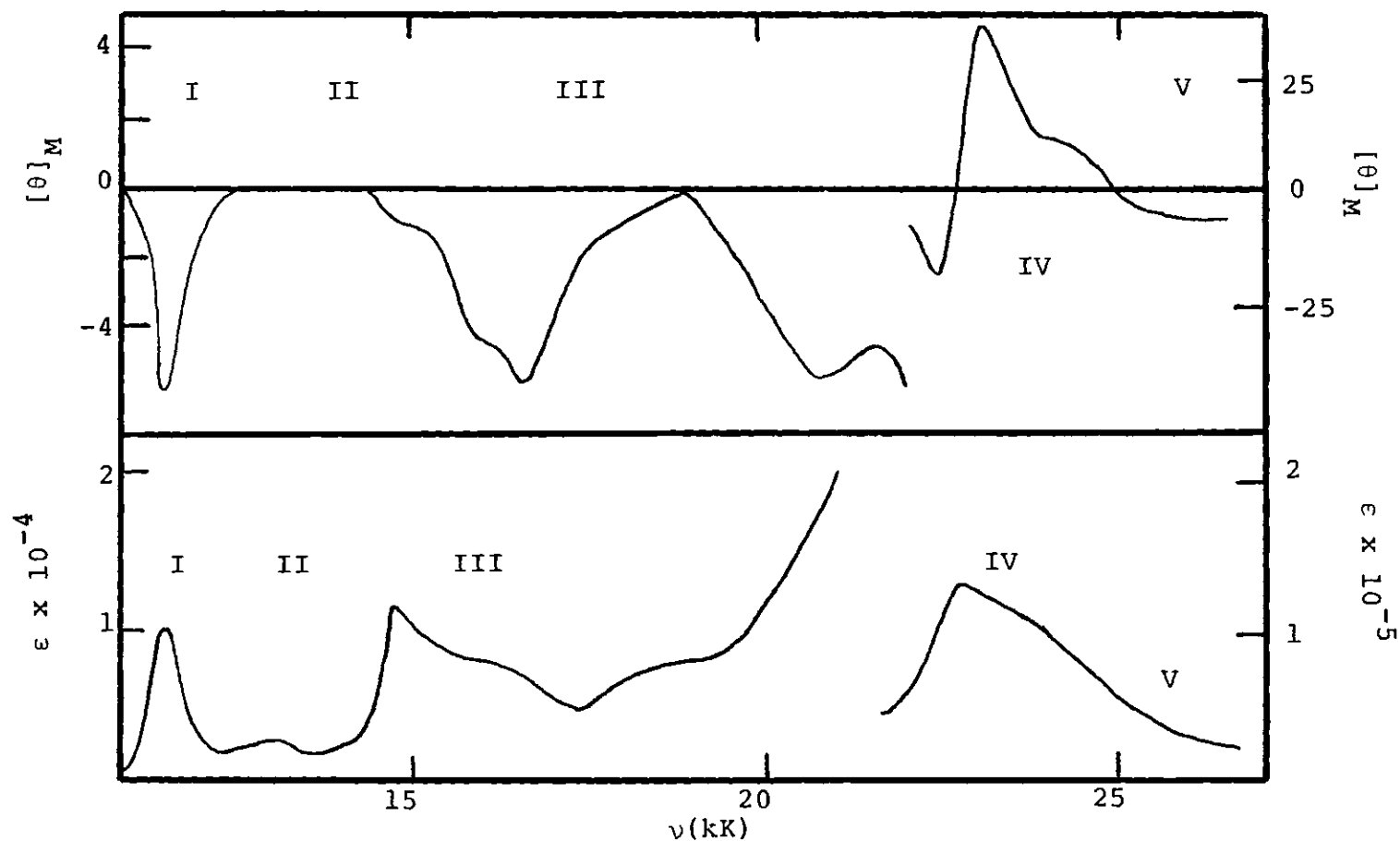


Figure 21. MCD (Upper Figure) and Absorption (Lower Figure) Spectra of CuTPP Monoanion in Dimethylformamide at Room Temperature. The units are:  $[\theta]_M$ ,  $\text{deg cm}^2 \text{ gauss}^{-1} \text{ dmole}^{-1}$ ;  $\epsilon$ ,  $\text{liter cm}^{-1} \text{ mole}^{-1}$ . For purposes of discussion the spectra have been divided into five regions.

$c_1$ ,  $c_2$ , and  $d$  constitute the three orbital model discussed in Chapter II. The salient features of that discussion provide the framework in which Band I is interpreted.

Our approach is to use Equations (151) and (152) to calculate  $\epsilon$  and  $\Delta\epsilon$  by computer integration over the Eulerian angles. A listing of the program is presented in the Appendix. It is generally accepted that the angular momentum,  $M_z$ , of the  $4e_g$  orbitals is ca. 2.2  $\hbar$ ; a result, which is both calculated and derived from analysis of metallo-porphyrin MCD data.<sup>19</sup> Thus, the absorption and MCD spectra are computed for  $1.2 < M_z < 2.6 \hbar$ ; values lying between  $2.2 \pm 0.4 \hbar$  are shown in Figure 22, bracketed by heavy solid lines. Additional parameters are found from the experimental data: 1) Linewidths for  $c_1 \rightarrow d$  and  $c_2 \rightarrow d$  transitions are set at  $300 \text{ cm}^{-1}$  and the dipole intensities are taken to be equal; 2)  $\Delta\epsilon$  is computed for a field strength of 1.0 T; and 3) the transition energy for the  $e_{gx}(c_1) \rightarrow 2b_{1u}(d)$  is set at 11.11 kK.

From the computed  $\Delta\epsilon$  and  $\epsilon$  spectra, the quantities,  $A/D$  and  $(B + C/kT)/D$  are derived by momentum analysis (Equation 18). In the absence of zero-field splitting,  $A/D$  is  $2M_z$  and is independent of temperature, since both states contribute equally to the transition intensity. Similarly,  $(B + C/kT)/D$  reduces to  $C/DkT$ , since no coupling with other excited states exists in the three-state model. A plot of the ratio of the zeroth moments of  $\Delta\epsilon$  and  $\epsilon$ , respectively, yields

$$\frac{10.7 \times 10^4 \langle \Delta \epsilon \rangle}{H \langle \epsilon \rangle} = C/kTD$$

and this quantity as a function of  $T^{-1}$  is exhibited in Figure 22 for various choices of  $M_z$ . Since  $C/D = 2M_z$ , the slope increases with increasing angular momentum in the ground state. With no zero-field splitting, the slope is constant.

In Figure 23, experimental data for the long wavelength band of  $\text{TBA}^+\text{ZnTPP}^{\dot{-}}$  and  $\text{Na}^+\text{ZnEtio}^{\dot{-}}$  in dimethoxyethane is presented. Three separate techniques are employed: gaussian fitting, moment analysis, and an analysis based on Kuhn's dissymmetry factor of the A-term contribution to the MCD spectrum.<sup>83</sup>

A computer program written by Dr. Fujita was used for the gaussian fitting routine. The best single gaussian line function which fitted both the MCD and absorption spectra for this band was used for this analysis. The contribution of the A term was ignored. The values of  $(B + C/kT)$  and D obtained by this method agrees with those found by moment analysis.

Moment analysis for  $B + C/kT$  and the dipole strength consists of integration through the MCD and absorption spectra. Normally, the contribution to a single band in a region of overlapping bands is determined by extrapolation before the integration is performed. However, it is easier to see the error involved in separating these bands, if the integration

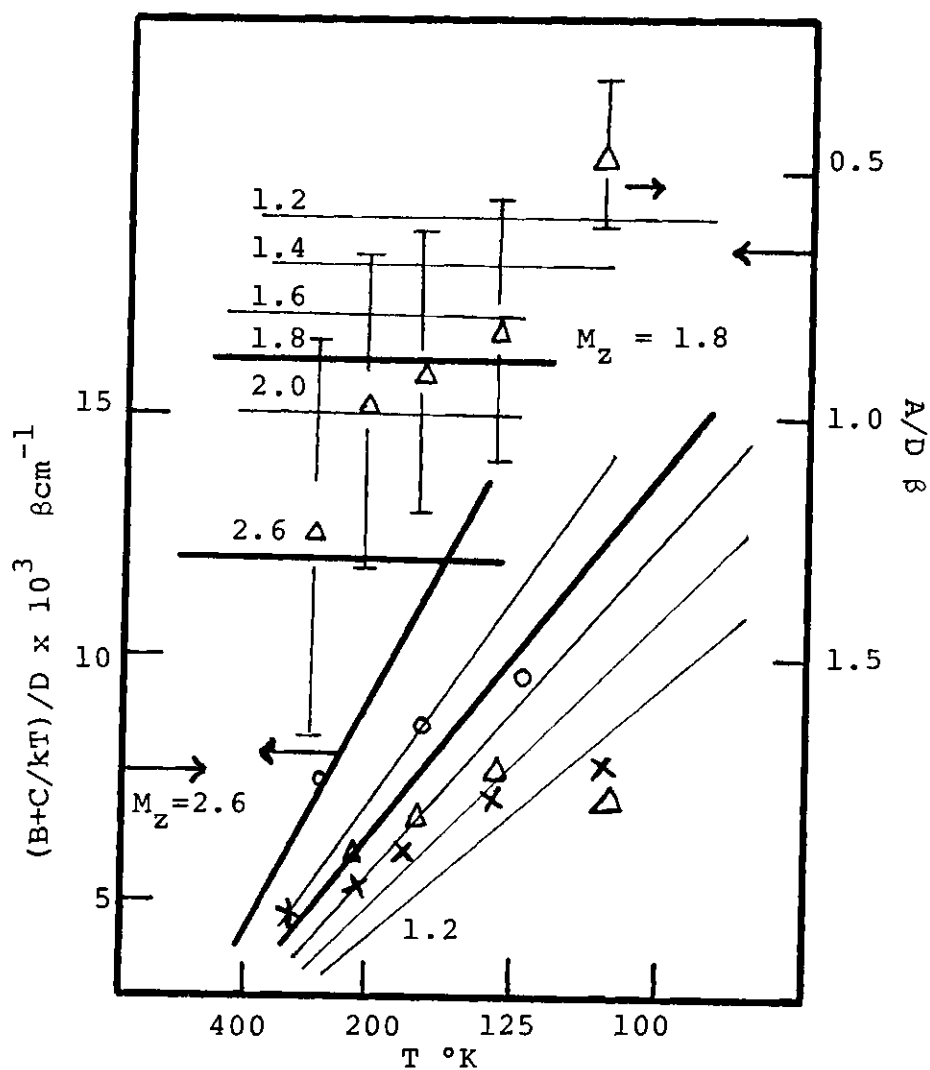


Figure 22. MCD Parameters Vs.  $1/T$  for the Three State Model with No Zero Field Splitting. The lines are calculated values for the various values of  $M_z$ . Experimental data are:  $(B+C/kT)/D$  of  $\text{Na}^+ \text{ZnEtio}^{\cdot-}$ , circles;  $(B+C/kT)/D$  of  $\text{TBA}^+ \text{ZnTPP}^{\cdot-}$ , crosses;  $(B+C/kT)/D$  and  $A/D$  of  $\text{TBA}^+ \text{ZnTPP}^{\cdot-}$  as determined by dissymmetry factor method, triangles. The bars on the upper set of triangles represent a range of bandwidths ( $300+50 \text{ cm}^{-1}$ ). Upper set of data and right-hand scale refer to  $A/D$ ; lower set of data and left-hand scale refer to  $(B+C/kT)/D$ .

is performed first. Therefore, the integrals of the MCD and absorption are given along with the spectra. (See Appendix B for additional details of data analysis.) The spectra and their integrals for  $\text{TBA}^+\text{ZnTPP}^{\dot{-}}$  in 2-methyltetrahydrofuran are given in Figures 23 and 24. The open circles in Figure 22 represent  $(B + C/kT)/D$  determined in this manner for  $\text{Na}^+\text{ZnEtio}^{\dot{-}}$ , and the crosses represent this quantity for  $\text{TBA}^+\text{ZnTPP}^{\dot{-}}$ .

A third method for analyzing this band depends on the MCD spectrum being directly proportional to the absorption spectrum and the first derivative of the absorption spectrum. The MCD parameters may be determined by constructing a plot of  $[\theta]_M/\epsilon$  versus wavenumber (or wavelength). The value of  $(B + C/kT)/D$  is directly proportional to this ratio at the center of the absorption band (the wavenumber corresponding to the maximum value of  $\epsilon$ ).  $A/D$  is directly proportional to the slope times the square of the linewidth. By using only the low energy half of the band, it was possible to avoid much of the overlap on the high energy side. The triangles in Figure 22 are the parameters as determined by this method for  $\text{TBA}^+\text{ZnTPP}^{\dot{-}}$ . Since the  $A/D$  values depend critically on the linewidth, bars are used to show the variation of  $A/D$  values, for a choice of  $300 \pm 50 \text{ cm}^{-1}$ . The quantity,  $(B + C/kT)/D$ , is much less sensitive and is placed on Figure 22 to indicate agreement between this spectral parameter determined by two methods.

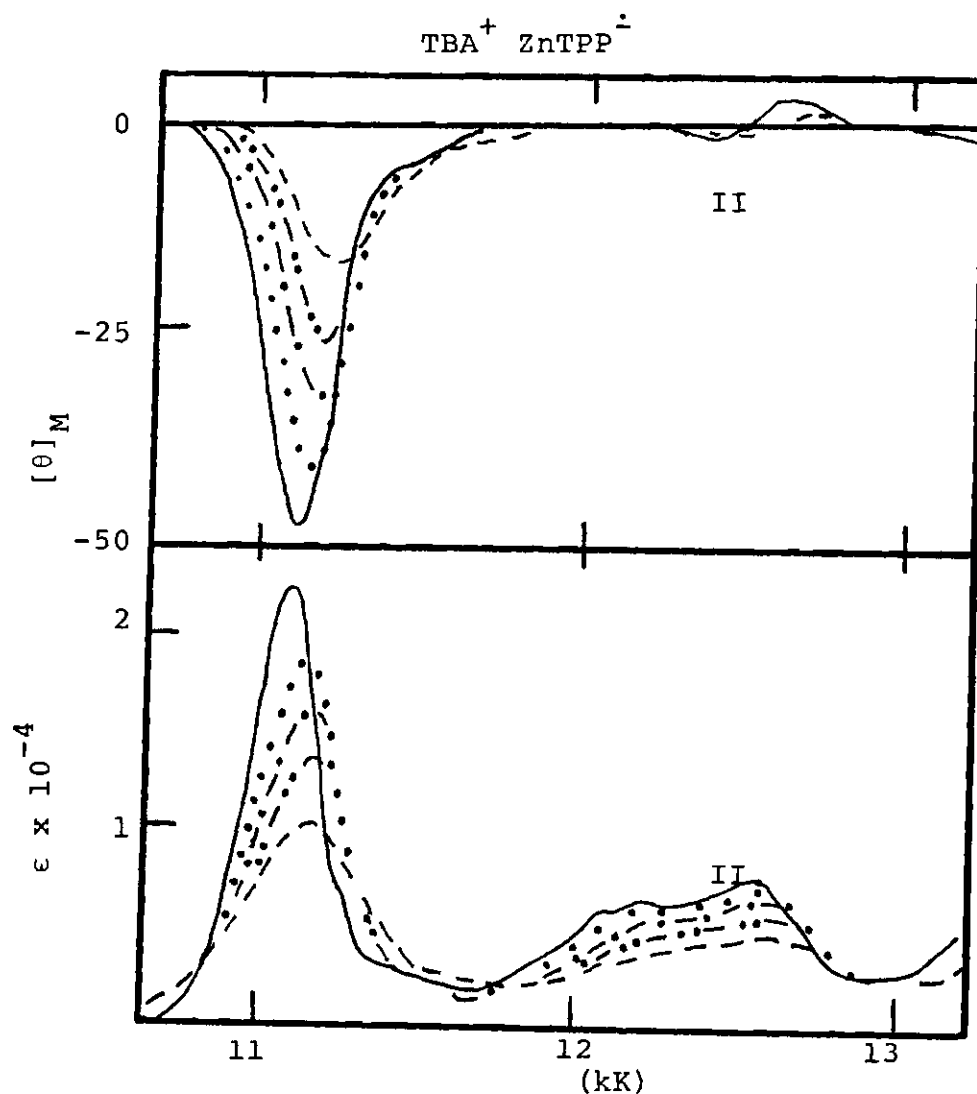


Figure 23. MCD (Upper Figure) and Absorption (Lower Figure) Spectra of  $\text{TBA}^+ \text{ZnTPP}^-$  in 2MTHF; ----, room temperature; - · - · - ·,  $-60^\circ\text{C}$ ; - - - -,  $-105^\circ\text{C}$ ; · · · · ·,  $-140^\circ\text{C}$ ; ———,  $-170^\circ\text{C}$ . The units are:  $[\theta]_M$ ,  $\text{deg cm}^2 \text{ gauss}^{-1} \text{ dmole}^{-1}$ ;  $\epsilon$ ,  $\text{liter cm}^{-1} \text{ mole}^{-1}$ . Band I was analyzed for  $A/D$  and  $(B+C/kT)/D$  values. Band II shows the derivative shape characteristic of two nearby oppositely polarized transitions.

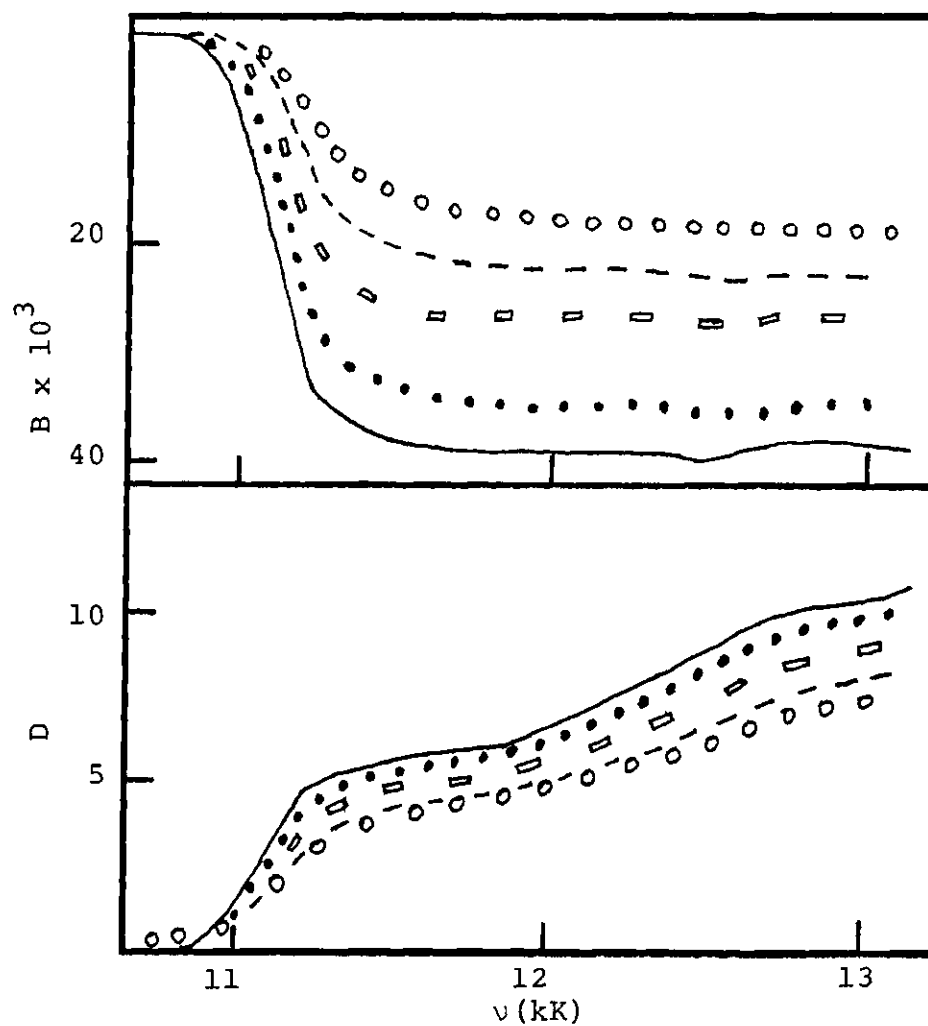


Figure 24. Integrated Spectra of  $\text{TBA}^+ \text{ZnTPP}^-$  in 2MTHF. MCD spectra (upper figure), absorption spectra (lower figure). (ooo, room temperature; ---,  $-60^\circ\text{C}$ ; ····,  $-105^\circ\text{C}$ ; —,  $-140^\circ\text{C}$ ; —,  $-170^\circ\text{C}$ ). The units are: D, Debye<sup>2</sup>; B, Debye<sup>2</sup> Bohr magneton  $\text{cm}^{-1}$ .

Interpretation of Figure 22 is now possible. It is immediately apparent that  $A/D$  is temperature dependent, which is inconsistent with degeneracy in the ground electronic state of the porphyrin monoanion. Although experimental  $C/DkT$  values are scattered, they possibly could be fit with a straight line; however, the intercept yields then a  $4 - 6 \times 10^{-3}$  value of  $B$ . The magnitude of  $B$  is then comparable to  $C/kT$ , which is unlikely in view of the assumed degeneracy of the ground electronic state and calculated value of  $\langle e_{gx} | L_z | e_{gy} \rangle = 2.2 \text{ i}\hbar$ . Although at each temperature the MCD parameters can be obtained from fitting the experimental data with Equations (63) and (64), the interpretation of these parameters leads to inconsistent results. In the following discussion, these experimental MCD parameters will be compared with those obtained by the use of Equations (63) and (64) to fit the spectra calculated from Equations (151) and (152). We will then be able to compare the experimental data with that which would be obtained if the  $^2E_g$  ground state were to split into nondegenerate components.

In Figures 25-27, the  $^2E_g$  state is subjected to increasing zero-field splitting increments. Neither  $A$  nor  $C$  terms are linear in  $T^{-1}$ , and the slopes calculated for both MCD parameters follow experimental trends. For a  $100 \text{ cm}^{-1}$  zero-field splitting,  $A/D$  shown in Figure 25 lies within the range of  $1.8 < M_z < 2.6 \text{ i}\hbar$ , as does the  $C/D$  term for  $\text{ZnEtio}^{\cdot-}$ . However, data for  $\text{ZnTPP}^{\cdot-}$  is consistent with lower angular

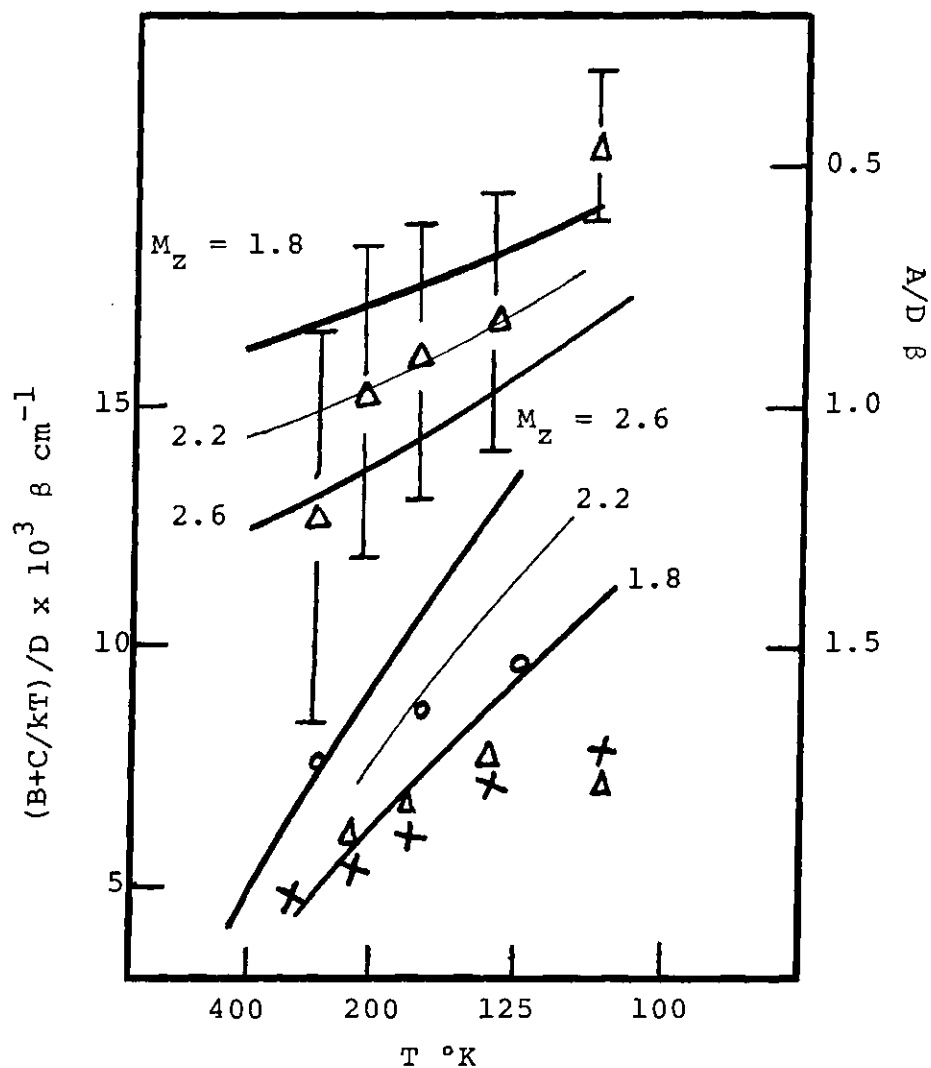


Figure 25. MCD Parameters Vs.  $1/kT$  for the Three State Model with a  $100 \text{ cm}^{-1}$  Zero Field Splitting. The lines are calculated values for the various values of  $M_z$ . Experimental data are:  $(B+C/kT)/D$  of  $\text{Na}^+ \text{ZnEtio}^-$ , circles;  $(B+C/kT)/D$  of  $\text{TBA}^+ \text{ZnTPP}^-$ , crosses;  $(B+C/kT)/D$  and  $A/D$  of  $\text{TBA}^+ \text{ZnTPP}^-$  as determined by dissymmetry factor method, triangles. The bars on the upper set of triangles represent a range of bandwidths ( $300 \pm 50 \text{ cm}^{-1}$ ). Upper set of data and right-hand scale refer to  $A/D$ ; lower set of data and left-hand scale refer to  $(B+C/kT)/D$ .

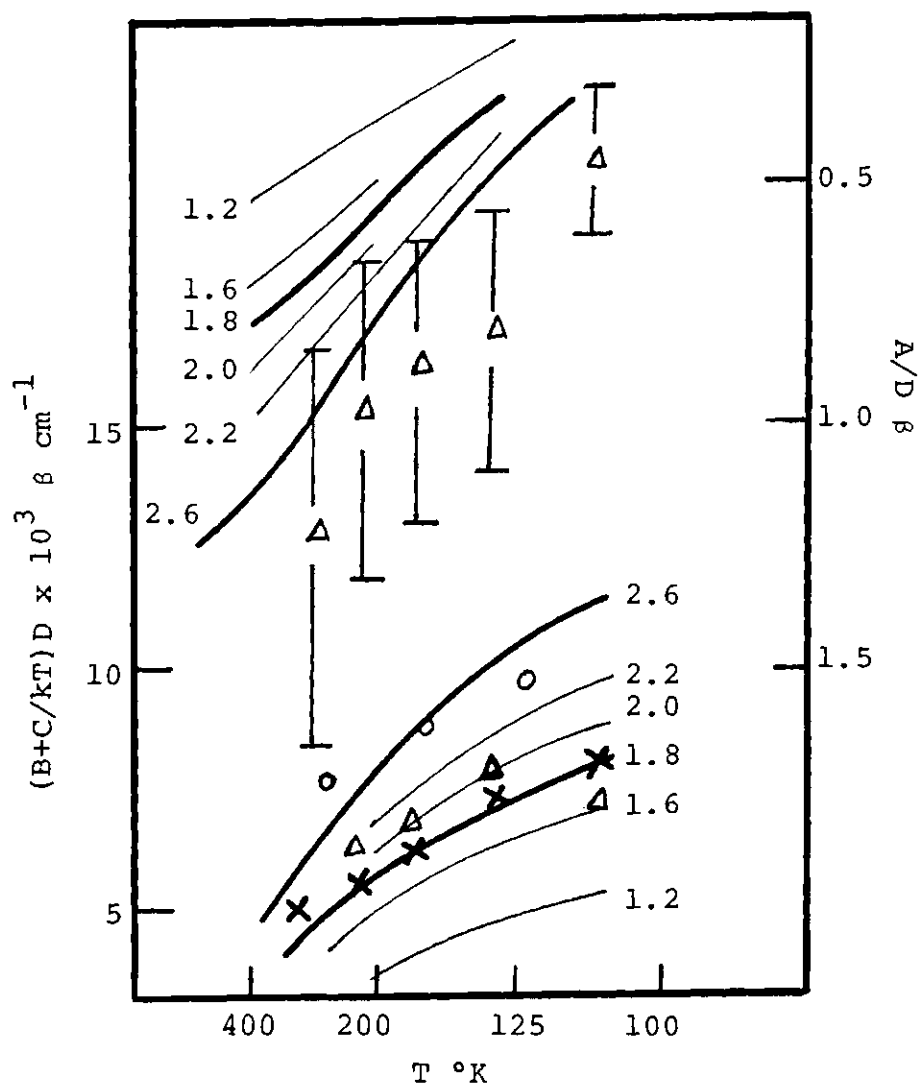


Figure 26. MCD Parameters vs.  $1/kT$  for the Three State Model with a  $200 \text{ cm}^{-1}$  Zero Field Splitting. The lines are calculated values for the various values of  $M_z$ . Experimental data are:  $(B+C/kT)/D$  of  $\text{Na}^+\text{ZnEtio}^-$ , circles;  $(B+C/kT)/D$  of  $\text{TBA}^+\text{ZnTPP}^-$ , crosses;  $(B+C/kT)/D$  and  $A/D$  of  $\text{TBA}^+\text{ZnTPP}^-$  as determined by dissymmetry factor method, triangles. The bars on the upper set of triangles represent a range of bandwidths ( $300+50 \text{ cm}^{-1}$ ). Upper set of data and right-hand scale refer to  $A/D$ ; lower set of data and left-hand scale refer to  $(B+C/kT)/D$ .

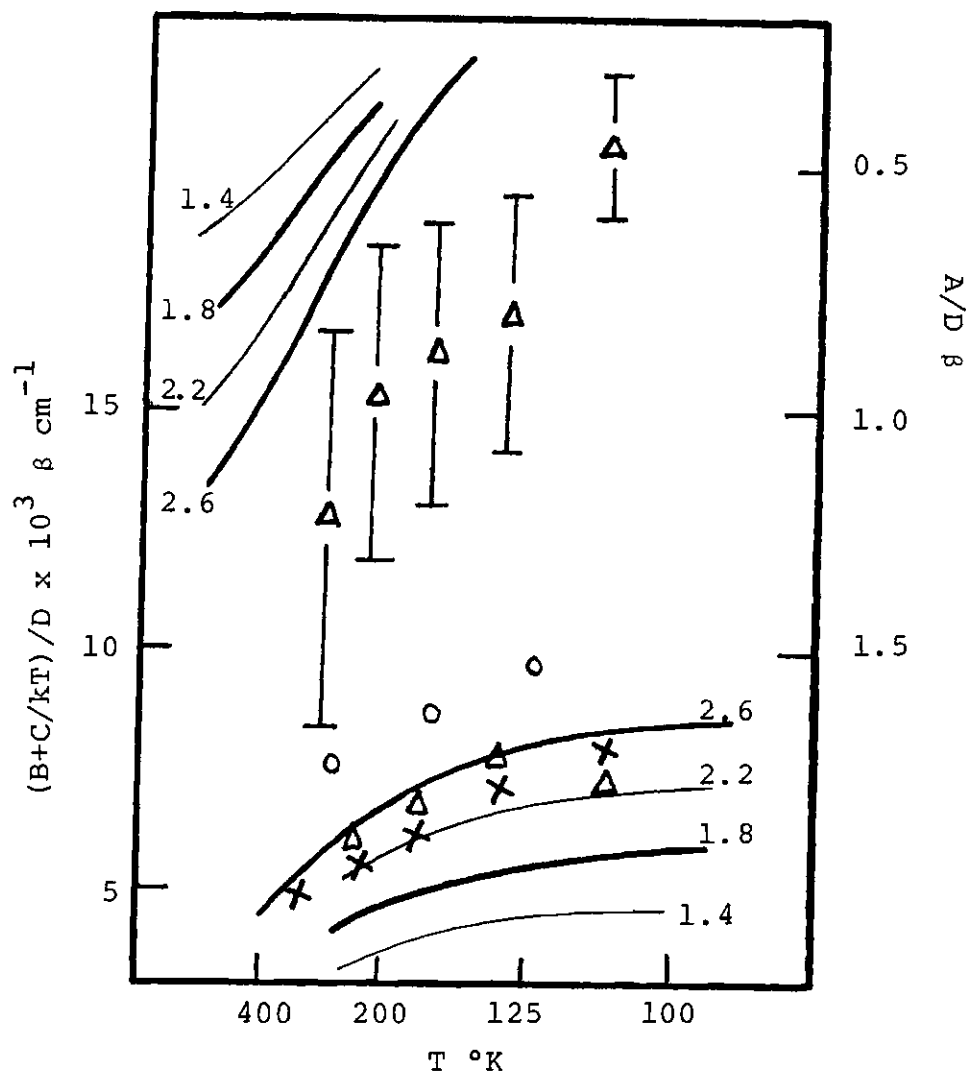


Figure 27. MCD Parameters vs  $1/kT$  for the Three State Model with a  $300 \text{ cm}^{-1}$  Zero Field Splitting. The lines are calculated values for the various values of  $M_z$ . Experimental data are:  $(B+C/kT)/D$  of  $\text{Na}^+\text{ZnEtio}^{\cdot-}$ , circles;  $(B+C/kT)/D$  of  $\text{TBA}^+\text{ZnTPP}^{\cdot-}$ , crosses;  $(B+C/kT)/D$  and  $A/D$  of  $\text{TBA}^+\text{ZnTPP}^{\cdot-}$  as determined by dissymmetry factor method, triangles. The bars on the upper set of triangles represent a range of bandwidths ( $300 \pm 50 \text{ cm}^{-1}$ ). Upper set of data and right-hand scale refer to  $A/D$ ; lower set of data and left-hand scale refer to  $(B+C/kT)/D$ .

momentum (ca.  $1.4 \mu$ ) in the  $^2E_g$  state. Increasing the zero-field splitting to  $200 \text{ cm}^{-1}$  now permits all but two  $(B + C/kT)/D$  values to reside within a range of reasonable  $M_z$  values, and introduces additional curvature into the temperature-dependancy; a feature which is exhibited by the data. The two data points not lying within the selected range of  $M_z$  possibly reflect the following features: At room temperature the ZnEtio monoanion is associated with the sodium counterion, and it is conceivable that the deviation of the high temperature point for this species is due to the presence of residual associated forms. The ZnEtio monoanion also presents a greater problem in that the long wavelength band overlaps the next set of transitions. At the lowest temperature, examination of the experimental spectra shows that the band begins to split and shifts to longer wavelengths. This was not investigated further. Although none of the points for the other experimental quantity,  $A/D$ , lie in this range, this is not a serious problem for two reasons. First, the MCD spectrum is dominated by the C terms. Second, the value of  $A/D$  depends on the square of the linewidth. If the linewidth,  $250 \text{ cm}^{-1}$ , is used instead of  $300 \text{ cm}^{-1}$  in calculating the experimental  $A/D$  values, then all values except one lie in the  $2.2 \pm 0.4 \mu$  range. A comparison of both  $A/D$  and  $(B + C/kT)/D$  values show that whereas a zero field splitting of  $100 \text{ cm}^{-1}$  is much too small, a splitting of  $200 \text{ cm}^{-1}$  may be slightly too large.

Figure 26 exhibits MCD parameters for a zero field splitting of  $300 \text{ cm}^{-1}$ . The A/D values correspond to a linewidth of less than  $250 \text{ cm}^{-1}$  or an angular momentum of at least 5 to 6  $\hbar$ . If the linewidth is  $300 \text{ cm}^{-1}$  or less, then the absorption spectra will be resolved into the two components. Although a very large angular momentum is consistent with the  $(B + C/kT)/D$  values, it is difficult to account for this number theoretically. There are mechanisms that quench orbital angular momentum, but none that increase the expected value by a factor of two or three. As the  $E_{gx}$  and  $E_{gy}$  energies increasingly differ due to zero-field splitting, excited states cannot be ignored. Inclusion of the next two higher states add terms, which should increase the magnitude of the observed  $(B + C/kT)/D$  values. For  $\text{ZnEtio}^-$ , the proximity of the  $2B_{1u}$  and  $1B_{2u}$  states to the  $1B_{1u}$  state makes inclusion of these states necessary to account for the MCD spectrum if the ground state splitting were  $300 \text{ cm}^{-1}$  or larger. Inclusion of these states changes the calculated values by about 2% for  $\text{ZnTPP}^-$  when the ground state splitting is  $300 \text{ cm}^{-1}$ .

The presence of thermally populated states that contribute to the transition amplitude of an excitation will influence the overall appearance of the absorption and MCD spectra. We have shown in the discussion leading to Equation (165) the differing temperature-dependency of A and C terms. Now, for  $\tanh (\Delta E_T^\circ/kT)/\Delta E_T^\circ \frac{d \ln f(v, v_0)}{dv}$ , which occurs at

elevated temperatures, the A term contribution will lead to a net positive  $\Delta OD$  at long wavelengths. This contribution will decrease relative to the C term at reduced temperatures, and Figure 28 exhibits the net  $\Delta OD$  calculated by the three state model. At the lowest temperature the MCD and absorption spectra will bear a mirror-image relationship. The experimental MCD data of  $ZnEtio^{\dot{-}}$ ,  $H_2Etio^{\dot{-}}$ , and  $H_2TPP^{\dot{-}}$  display in Figures 29-32 the predicted positive  $[\theta]_M$  at long wavelengths; however, it is not seen in  $ZnTPP^{\dot{-}}$  (Figure 23).

An additional factor to consider in the analysis of Band I is the contribution of spin orbit coupling to  $E_T^{\circ}$  (see Equation (156)). When the magnetic field becomes small,  $\Delta E_T^{\circ} = M_Z \lambda / 2 \sim 5 \text{ cm}^{-1}$  for parameter choices:  $M_Z = 2$  and  $\lambda \sim 5 \text{ cm}^{-1}$ . For the temperature range examined, the field-independent contribution will be maximized at  $-170^{\circ}C$ : however, the MCD signal of the  $ZnTPP^{\dot{-}}$  remained linear in magnetic field within the  $\pm 3\%$  error of the spectrometer. Thus, we conclude that spin-orbit coupling is unimportant in the present analysis.

In this study we have considered the free ion (acutally a separated ion-pair) in order to avoid the complication of ion-pairing. The influence of ion-pairing can be seen in the study of the MCD of the triphenylene anion by R. E. Koning, et. al.<sup>79</sup> The triphenylene anion was observed to change from the tight to the loose ion pair form as the temperature was lowered. Since the MCD parameters of the two forms are different, the interaction with the cation makes the zeroth

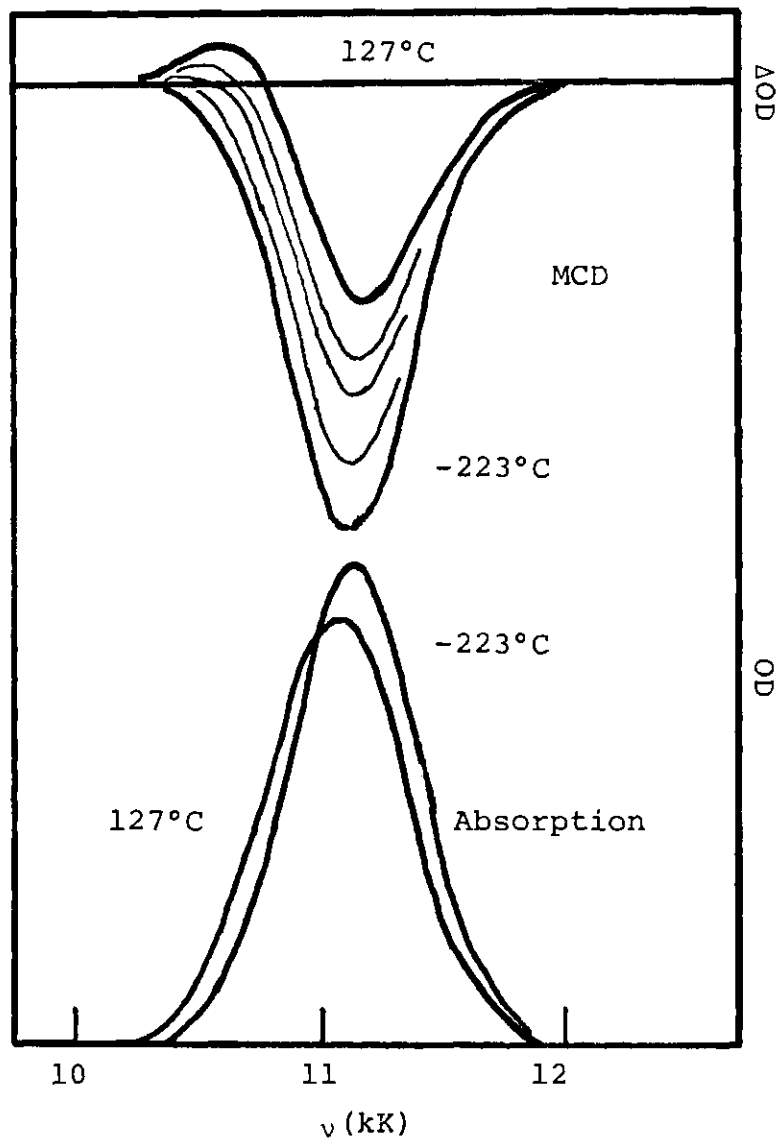


Figure 28. Calculated MCD and Absorption Spectra for the Three State Model. The ground state splitting is  $200 \text{ cm}^{-1}$ , bandwidth is  $300 \text{ cm}^{-1}$ ,  $M_z$  is  $2.2 \mu_B$ , and magnetic field is 1 T. As the temperature decreases the MCD  $\Delta OD$  becomes more negative (127°C, -23°C, -72°C, -148°C, and -223°C) and the absorption spectrum (OD) sharpens slightly (127°C and -223°C).

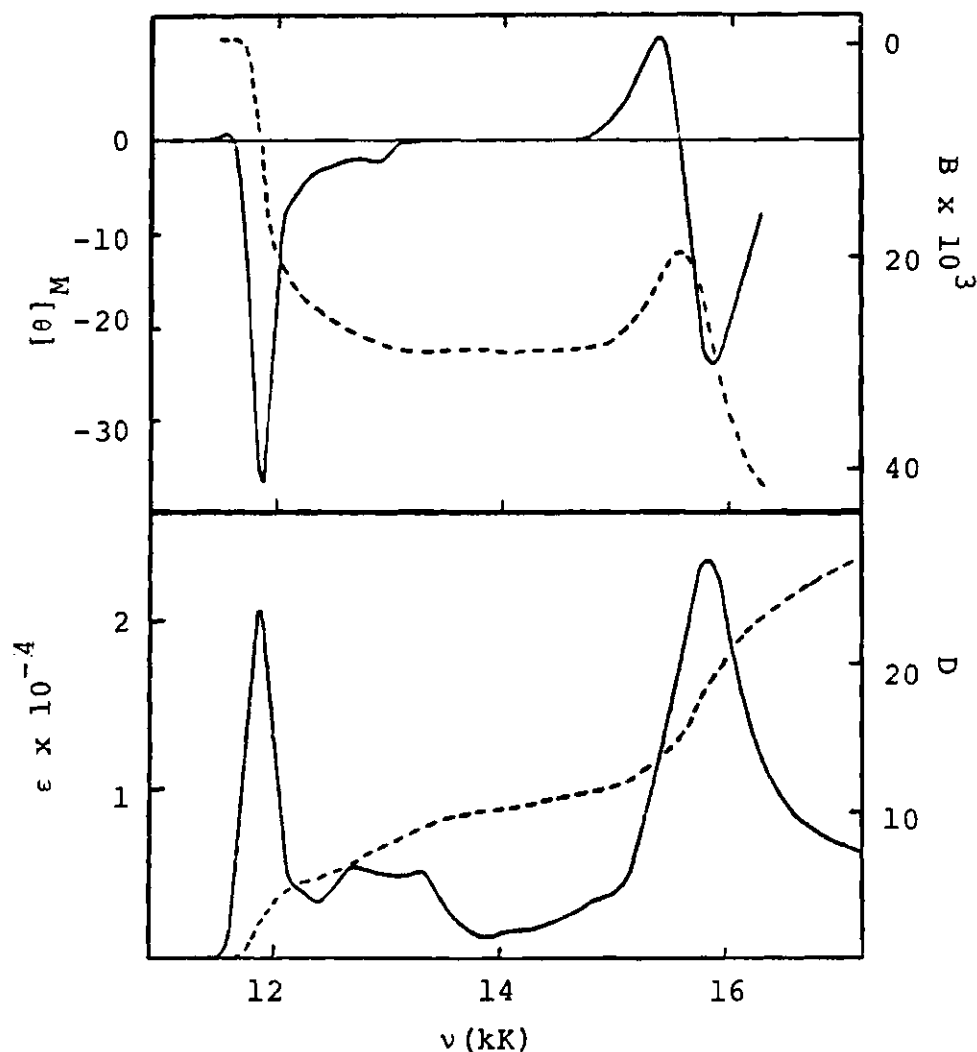


Figure 29. ZnEtio Monoanion at 200°K (MCD spectra (upper figure); absorption spectra (lower figure); units are:  $[\theta]_M$ ,  $\text{deg cm}^2 \text{ gauss}^{-1} \text{ dmole}^{-1}$ ;  $B$ ,  $(\text{Debye})^2$  (Bohr magneton)  $(\text{cm}^{-1})$ ;  $D$ ,  $\text{Debye}^2$ ). The dotted lines represent the integrated intensities. The solvent is a mixture of 2-methyltetrahydrofuran and dimethoxyethane. Note slight positive MCD on long wavelength side of the 12 kK transition.

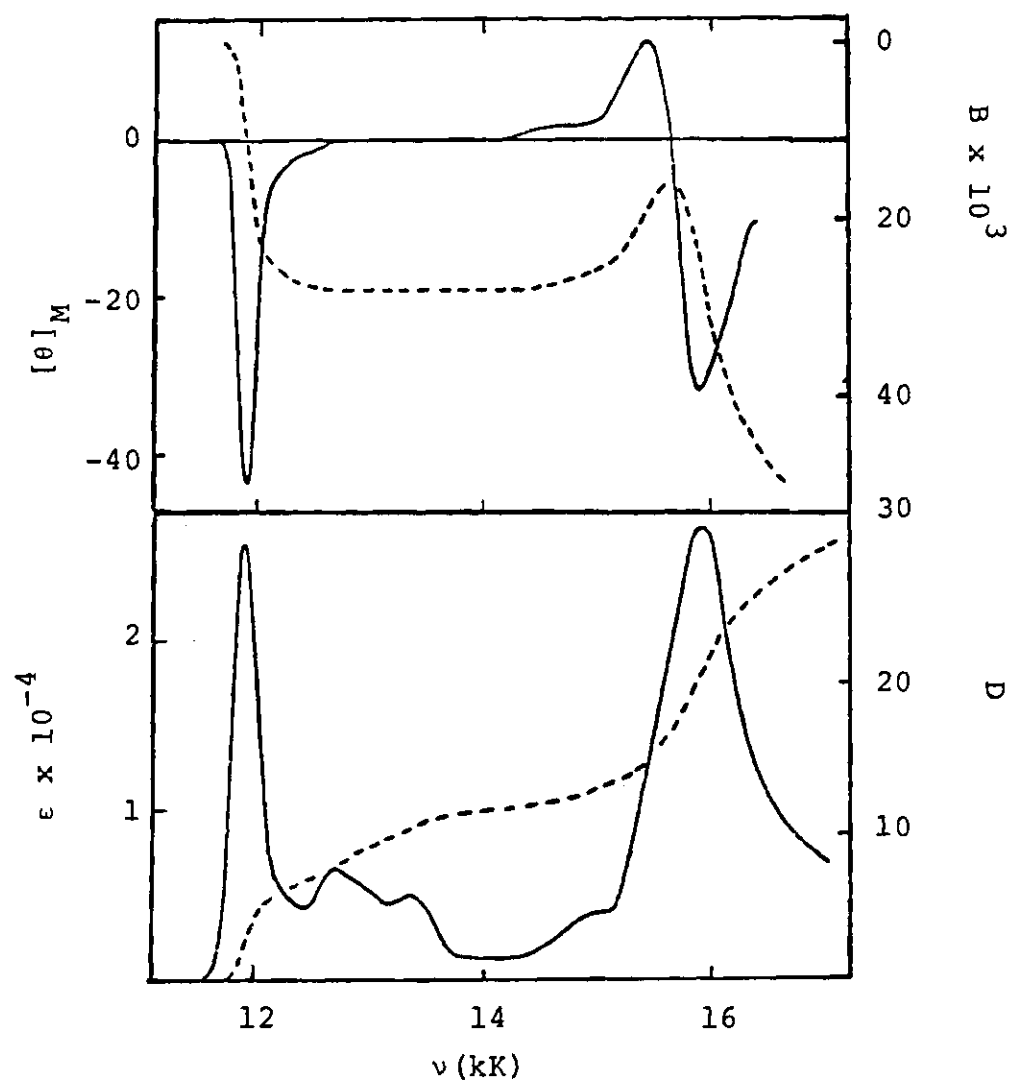


Figure 30. ZnEtio Monoanion at 100°K (MCD spectra (upper figure); absorption spectra (lower figure); units are:  $[\theta]_M$  deg cm<sup>2</sup> gauss<sup>-1</sup> dmole<sup>-1</sup>; B, Debye<sup>2</sup> Bohr magneton cm<sup>-1</sup>; D, Debye<sup>2</sup>). The dotted lines represent the integrated intensities. The solvent is a mixture of 2-methyltetrahydrofuran and dimethoxyethane.

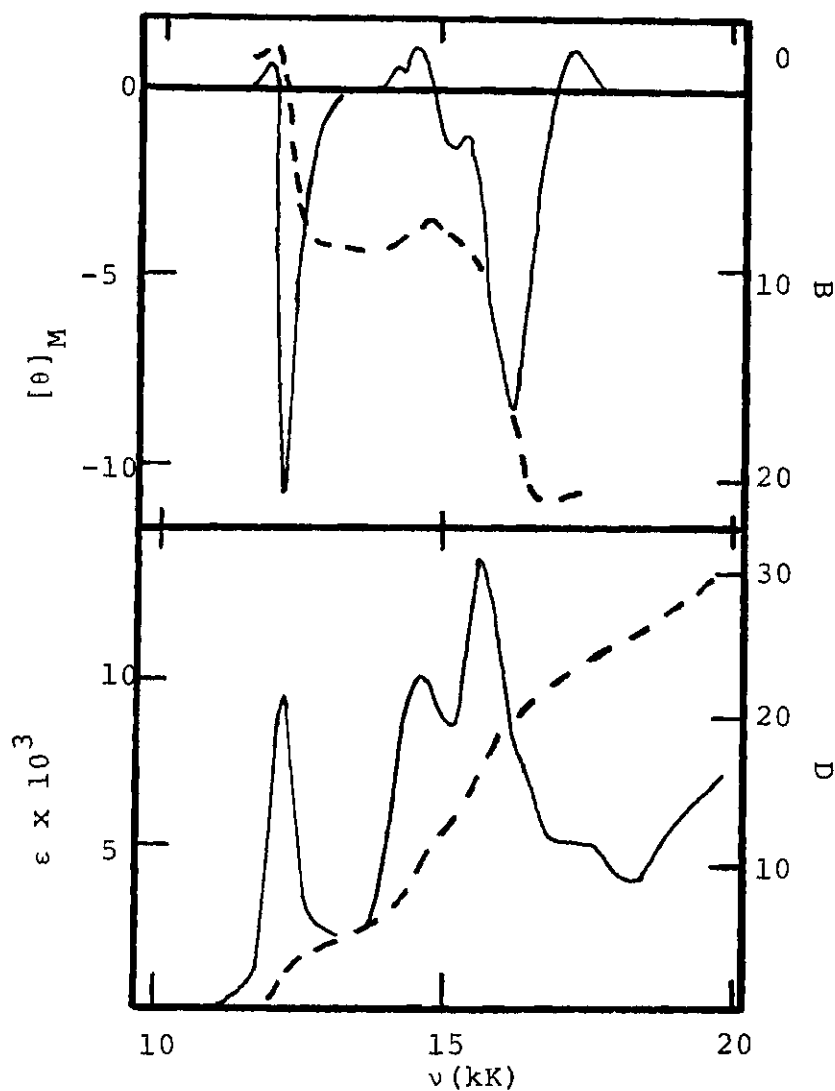


Figure 31.  $H_2Etio$  Monoanion (MCD Spectra (Upper Figure); Absorption Spectra (Lower Figure): Units are:  $[\theta]_M$ ,  $\text{deg cm}^2 \text{ gauss}^{-1} \text{ dmole}^{-1}$ ; B,  $(\text{Debye})^2$  (Bohr magneton)  $(\text{cm}^{-1})$ ; D,  $\text{Debye}^2$ ,  $\epsilon$ ,  $\text{liter cm}^{-1} \text{ mole}^{-1}$ ). This is the tetrapropylammonium salt in dimethylformamide. The spectra were taken at room temperature. Note the slight positive MCD on the long wavelength side of the first transition.

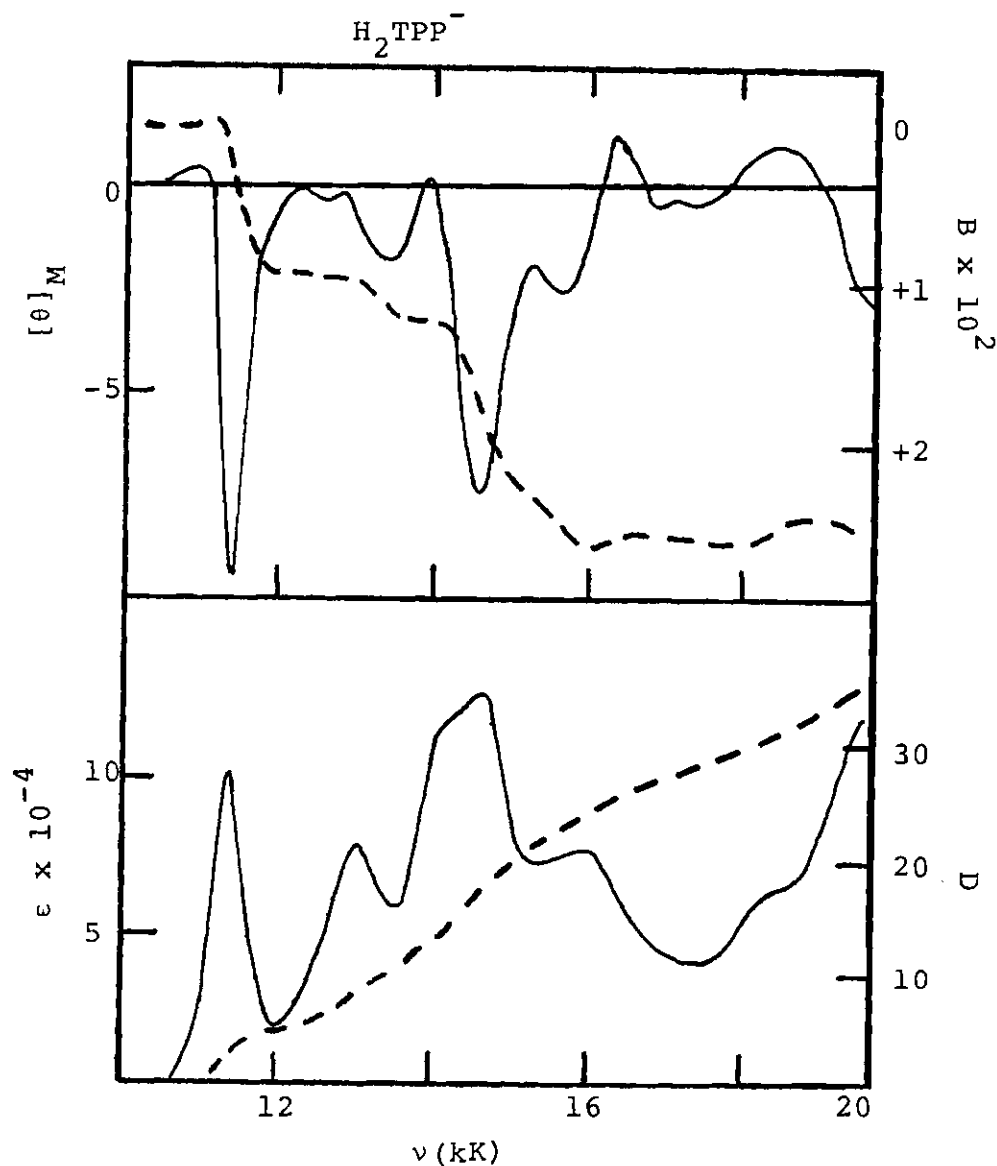


Figure 32.  $\text{H}_2\text{TPP}$  Monoanion (MCD Spectra (Upper Figure); Absorption Spectra (Lower Figure): Units are:  $[\theta]_M$ ,  $\text{deg cm}^2 \text{ gauss}^{-1} \text{ dmole}^{-1}$ ;  $B$ ,  $(\text{Debye})^2$   $(\text{Bohr magneton})(\text{cm}^{-1})$ ;  $D$ ,  $\text{Debye}^2$ ,  $\epsilon$ ,  $\text{liter cm}^{-1} \text{ mole}^{-1}$ ). This is the tetrapropylammonium salt in dimethylformamide. The spectra were taken at room temperature. Note the slight positive MCD on the long wavelength side of the first transition.

moment of the MCD a non-linear function of the reciprocal of the temperature. This non-linearity is due to a relative change in concentration of the two forms and is in addition to that caused by any zero field splitting. An analysis of the effect of the perturbation of the degenerate ground state using the same three state model as derived in this thesis led to results identical to those shown in Figures 9 and 10.

There are several possible causes for the zero field splitting of the ground state. One possibility is the interaction of the cation with the anion. The effect of the sodium cation on the triphenylene anions was calculated by Koning, et. al.<sup>79</sup> The counter ion was placed at a number of positions above the molecular plane moving out from the central three-fold axis. For the tight ion pair the cation was placed  $3 \text{ \AA}$  above the plane. For the loose ion pair, it was placed at  $6 \text{ \AA}$  above the plane. The most stable position for the tight ion pair was with the cation displaced from the center by  $1 \text{ \AA}$ , while in the loose ion pair the most probable position is on the three-fold axis. Regardless of the displacement, the zero field splitting was in general greater for the tight ion pair case than for the loose ion pair. The calculated zero field splitting for the most stable configuration of the tight ion pair was  $690 \text{ cm}^{-1}$ . Upon pulling the cation away from the molecular plane to the loose ion pair distance (remaining off center by  $1 \text{ \AA}$ ), the zero field splitting dropped to  $45 \text{ cm}^{-1}$ . In other words, the closer the cation

approaches the anion, the greater the splitting of the ground state by the counter ion. These calculations agree with the well-known spectral evidence that the change from a tight ion pair to a loose ion pair (or solvent separated ion pair) is greater than going from the loose ion pair to the free ion. Upon cooling the sodium salt of ZnTPP monoanion in 2-MTHF, the optical spectrum changes from that of the tight ion pair to that of the loose ion pair. If it is assumed that the spectral shifts are due to changing the ground state splitting, then we can obtain a crude estimate of the splitting caused by the counter ion. The shifts of the first two bands from 880 to 900 nm and 785 to 800 nm correspond to about  $250\text{ cm}^{-1}$ . The spectra do not change if we pull the center of positive charge further away by varying the counter-ion by forming the tetrapropylammonium salt, the tetrabutylammonium salt, the sodium dimethoxyethane salt, and the sodium crown ether salt. If we assume that the influence on the splitting of the ground state by the counter ion falls off exponentially with distance in the same manner as the calculated splittings for triphenylene anion, then the counter ion will be responsible for about 10% of the observed zero field splitting in the loose ion pair form of  $\text{ZnTPP}^-$ . Thus, the interaction with the counter ion cannot be responsible for the observed zero field splitting of the metal porphyrin monoanions.

### Assignments of Bands II, III, IV, and V in Porphyrin Mono-anion

In Figure 21 absorption bands of the porphyrin mono-anions are classified empirically, according to the transition energy. A more detailed presentation of Bands I-III, which constitute the near infrared region of the spectrum, is shown in Figure 23. General features of the absorption and MCD spectra areas follows:

- a. Bands I (11-12 kK) and III (15-16 kK) have moderate absorption intensity with  $\epsilon = 1-2 \times 10^4$  liter-mole-cm<sup>-1</sup> and negative  $[\theta]_M$ , excepting the low energy component of Band III in ZnEtio<sup>-</sup>. This component displays a positive  $[\theta]_M$ , whose appearance suggests overlapping transitions.
- b. Band II (13-14 kK) exhibits both weak absorption and MCD spectra.
- c. Band IV (23-25 kK) appears in the near uv, in the spectral region associated with the porphyrin Soret band. The extinction coefficient of the most intense absorption is  $1-2 \times 10^5$  liter-mole-cm<sup>-1</sup>. Spectra of all porphyrin radicals examined exhibit one or two supernumerary bands at higher energy. The structure is better resolved at lower temperatures in the instance of Na<sup>+</sup>ZnEtio<sup>-</sup> in a DME/2-MTHF solvent mixture (vide: Figures 33 and 34), MCD spectra (Figures 33-38) are similar for the ions: ZnEtio<sup>-</sup>, ZnTPP<sup>-</sup>, CuTPP<sup>-</sup>, H<sub>2</sub>TPP<sup>-</sup>, and H<sub>2</sub>Etio<sup>-</sup> in that the MCD signal associated with the major absorption peak is negative, and  $[\theta]_M$  values for the remaining absorptions

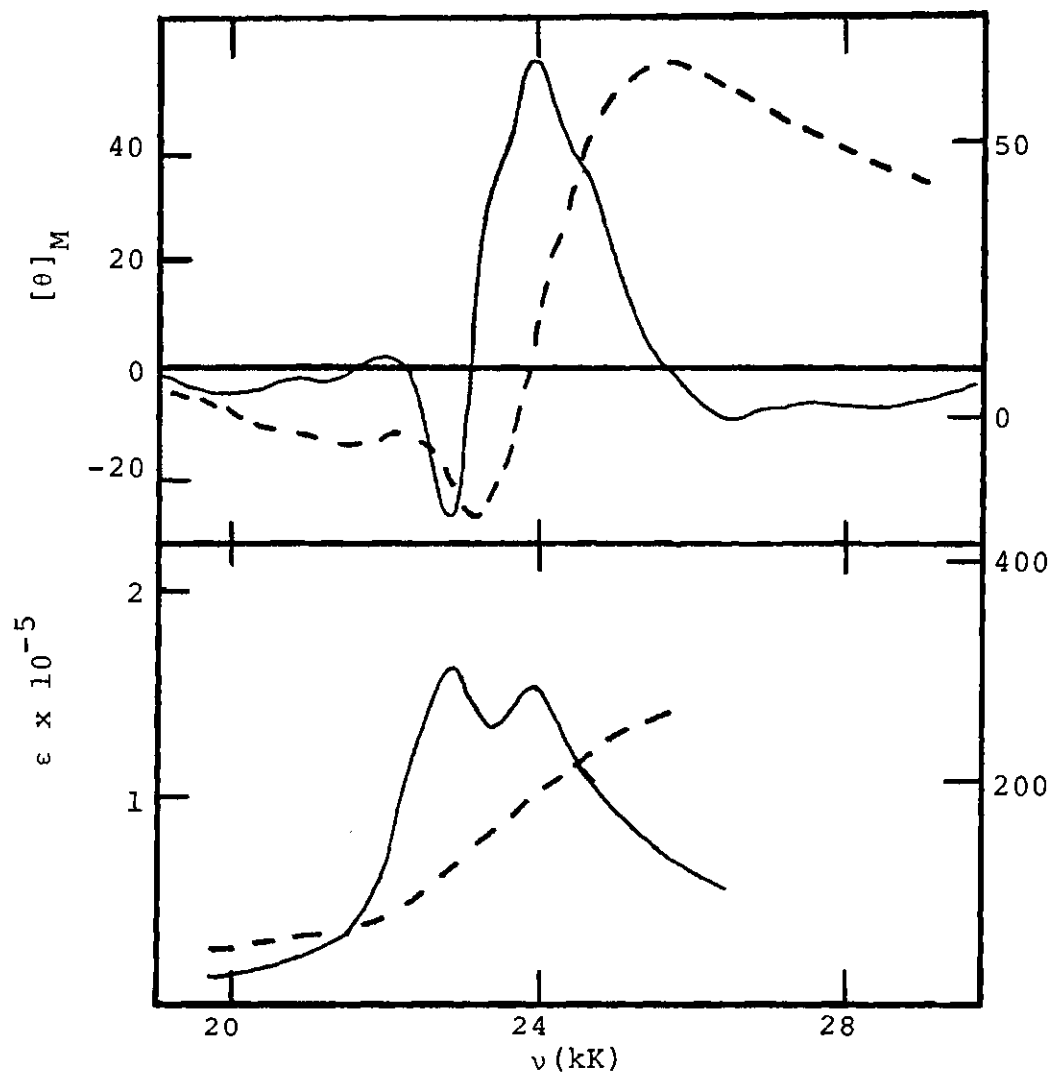


Figure 33. ZnEtio Monoanion at 200°K (MCD Spectra (Upper Figure); Absorption Spectra (Lower Figure); Units are:  $[\theta]_M$  degree  $\text{cm}^2 \text{ gauss}^{-1} \text{ dmole}^{-1}$ ; B, Debye<sup>2</sup> Bohr magneton  $\text{cm}^{-1}$ ; D, Debye<sup>2</sup>;  $\epsilon$ , liter  $\text{cm}^{-1} \text{ mole}^{-1}$ ). Sodium salt is in a mixture of 2-methyltetrahydrofuran and dimethoxyethane. The dotted lines represent the integrated intensities.

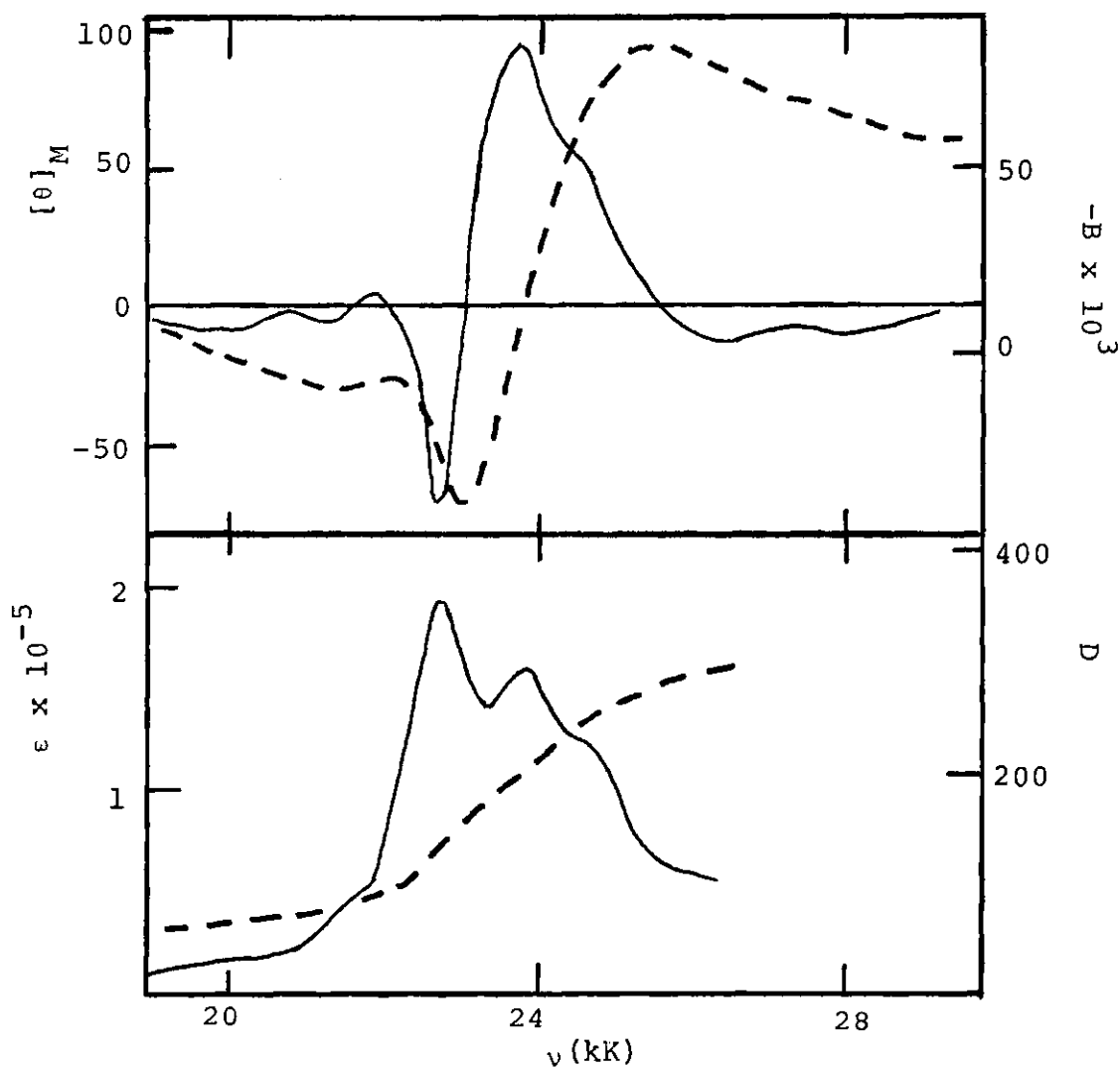


Figure 34. ZnEtio Monoanion Soret at 100°K (MCD Spectra (Upper Figure); Absorption Spectra (Lower Figure): Units are:  $[\theta]_M$ ,  $\text{deg cm}^2 \text{ gauss}^{-1} \text{ dmole}^{-1}$ ;  $B$ ,  $\text{Debye}^2 \text{ Bohr magneton cm}^{-1}$ ;  $D$ ,  $\text{Debye}^2$ ;  $\epsilon$ ,  $\text{liter cm}^{-1} \text{ mole}^{-1}$ ). Sodium salt is in a mixture of 2-methyltetrahydrofuran and dimethoxyethane. The dotted lines represent the integrated intensities.

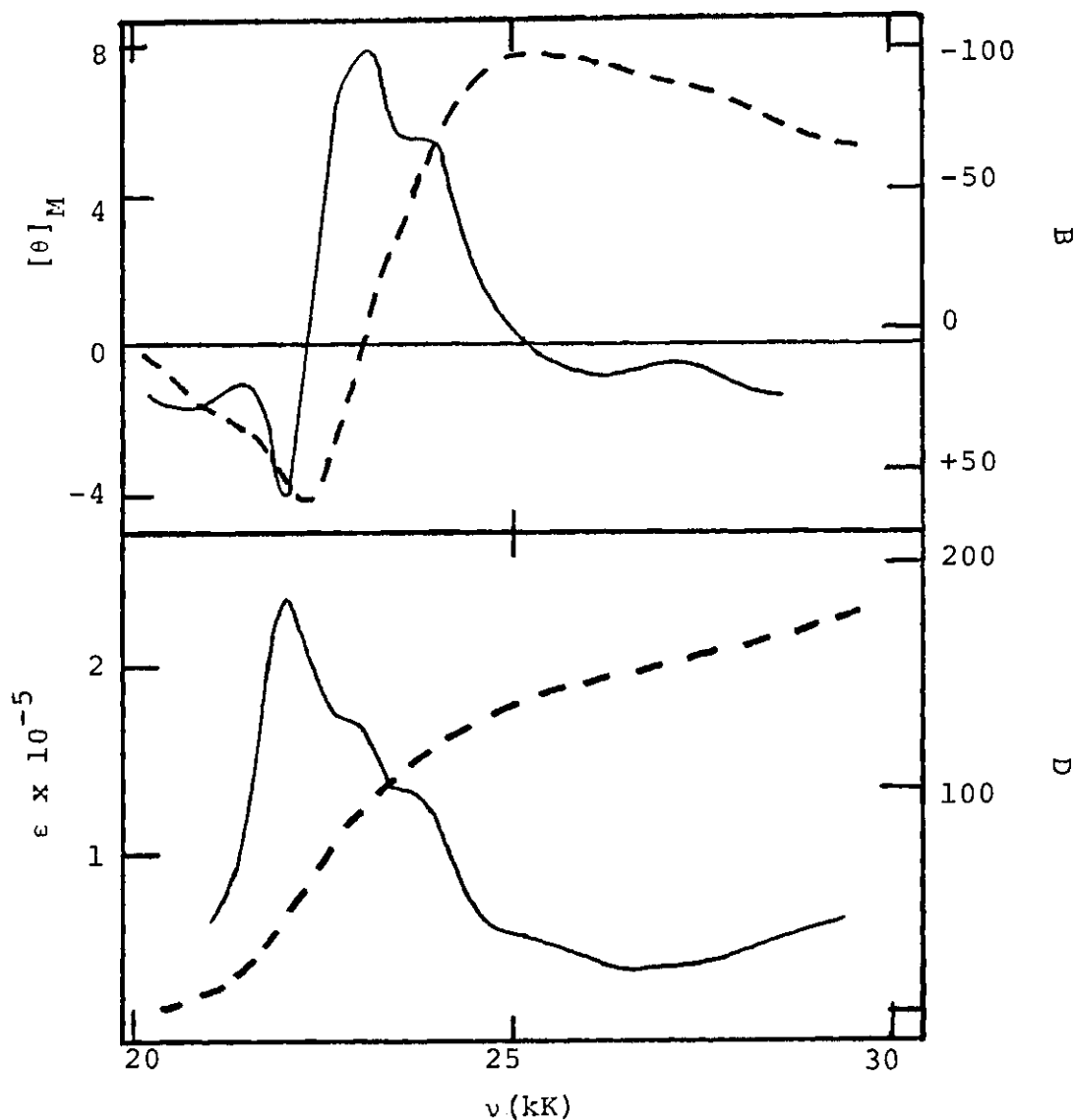


Figure 35. ZnTPP Monoanion Soret at Room Temperature (298°K) (MCD Spectra (Upper Figure); Absorption Spectra (Lower Figure); units are  $[\theta]_M$ , deg  $\text{cm}^2 \text{ gauss}^{-1} \text{ mole}^{-1}$ ;  $\epsilon$ , liter  $\text{cm}^{-1} \text{ mole}^{-1}$ ; D, Debye<sup>2</sup>; B, Debye<sup>2</sup> Bohr magneton  $\text{cm}^{-1}$ ). Sodium salt is in a mixture of dimethoxyethane and 2-methyltetrahydrofuran. The dotted lines represent the integrated intensities.

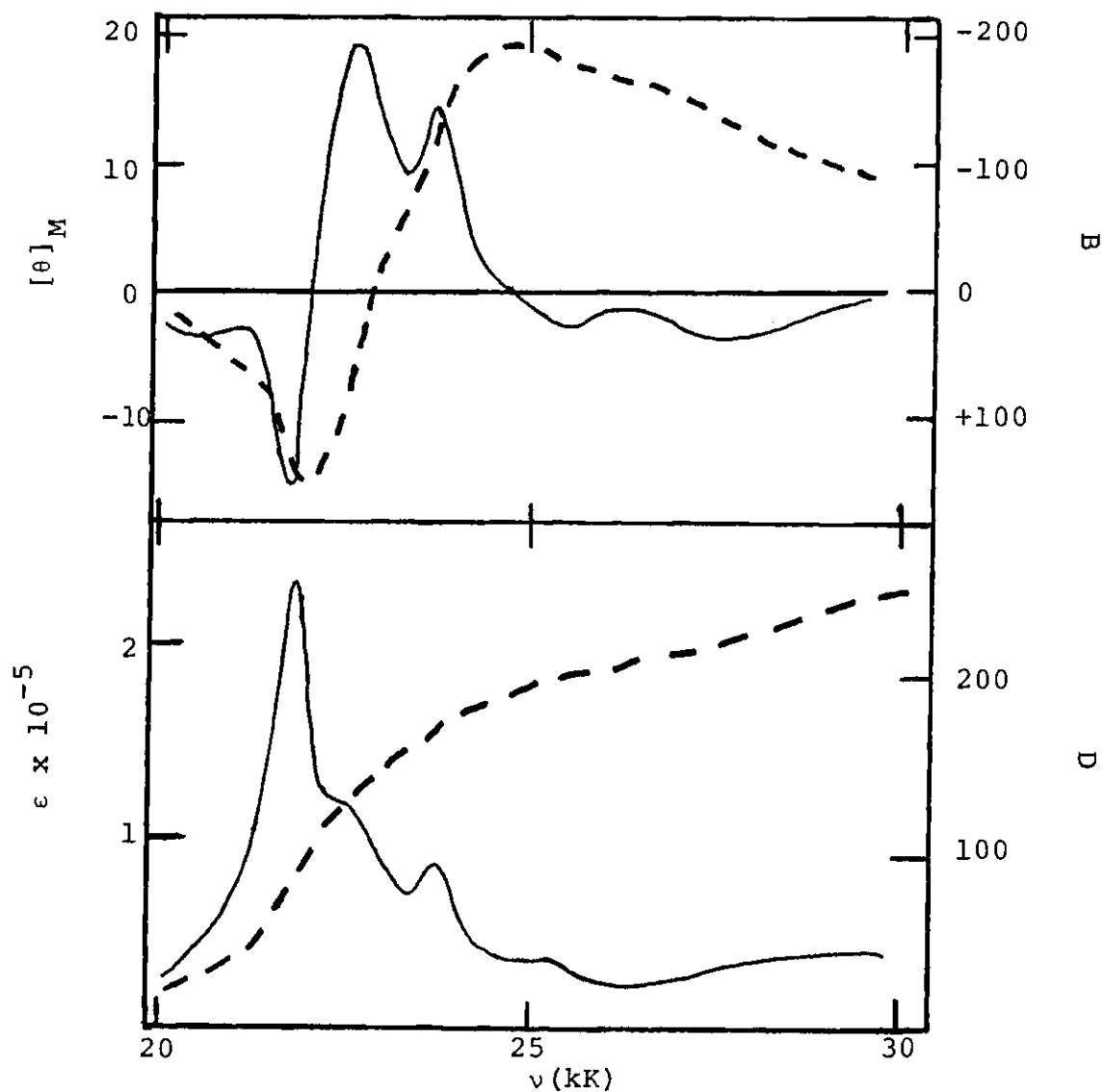


Figure 36. ZnTPP Monoanion Soret at 100°K (MCD Spectra (Upper Figure); Absorption Spectra (Lower Figure); Units are:  $\epsilon$ , liter  $\text{cm}^{-1}$  mole $^{-1}$ ;  $[\theta]_M$ , deg  $\text{cm}^2$  gauss $^{-1}$  dmole $^{-1}$ ; B, Debye $^2$  Bohr magneton  $\text{cm}^{-1}$ ; D, Debye $^2$ ). Sodium salt is in a mixture of 2-methyltetrahydrofuran and dimethoxyethane. The dotted lines represent the integrated intensities.

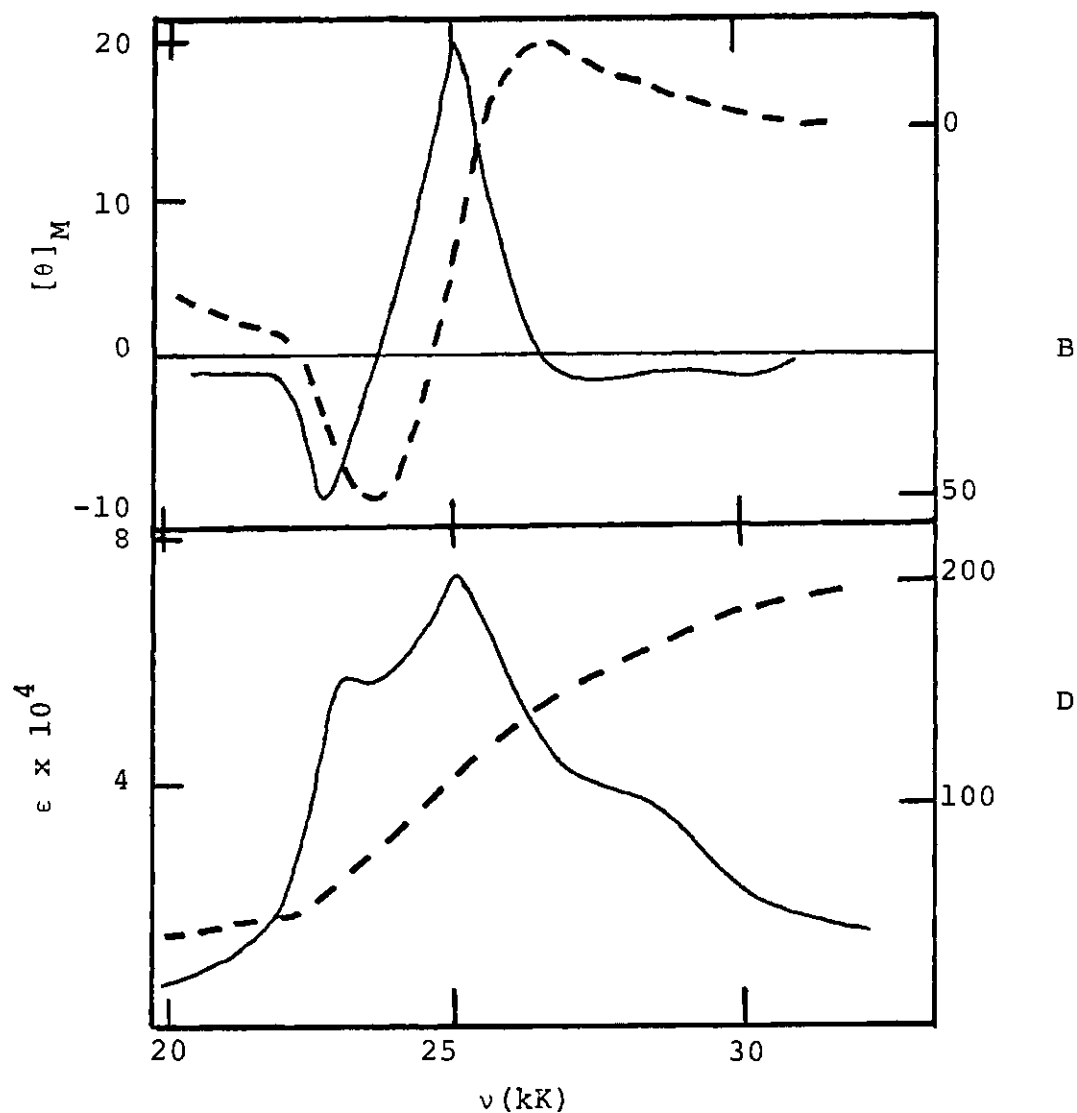


Figure 37.  $\text{H}_2\text{Etio}$  Monoanion Soret at Room Temperature (298°K) (MCD Spectra (Upper Figure); Absorption Spectra (Lower Figure); Units are:  $[\theta]_M$ ,  $\text{deg cm}^2 \text{ gauss}^{-1} \text{ dmole}^{-1}$ ;  $\epsilon$ ,  $\text{liter cm}^{-1} \text{ mole}^{-1}$ ; D,  $\text{Debye}^2$ ; B,  $\text{Debye}^2 \text{ Bohr magneton cm}^{-1}$ ). Tetrapropylammonium salt is in dimethylformamide. The dotted lines represent the integrated intensities.

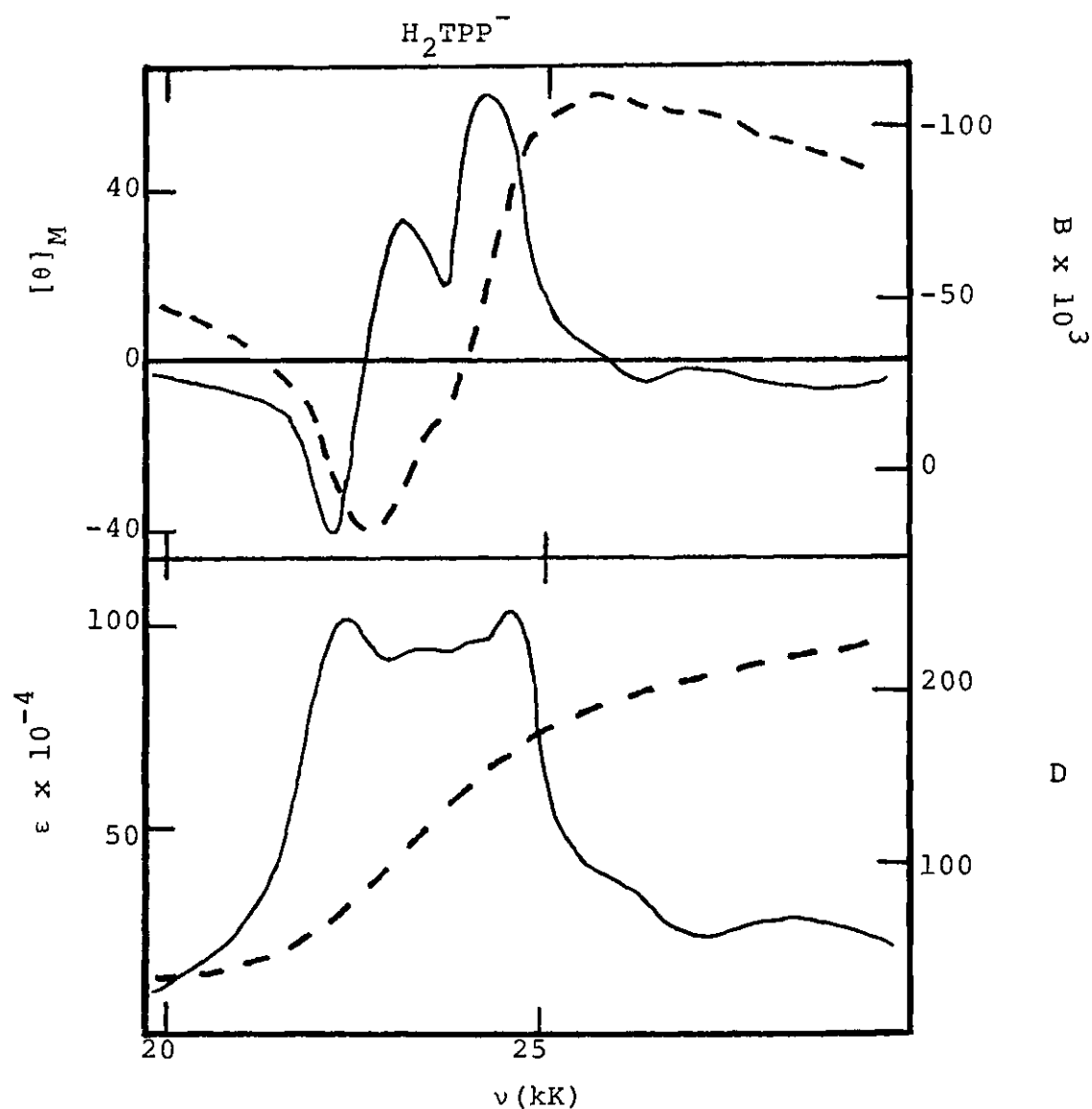


Figure 38.  $\text{H}_2\text{TPP}$  Monoanion Soret at Room Temperature (298°K) (MCD Spectra (Upper Figure); Absorption Spectra (Lower Figure); Units are:  $[\theta]_M$ ,  $\text{deg cm}^2 \text{ gauss}^{-1} \text{ dmole}^{-1}$ ;  $\epsilon$ ,  $\text{liter cm}^{-1} \text{ mole}^{-1}$ ;  $D$ ,  $\text{Debye}^2$ ;  $B$ ,  $\text{Debye}^2 \text{ Bohr magneton cm}^{-1}$ ). Tetrapropylammonium salt is in dimethylformamide. The dotted lines represent the integrated intensities.

at higher energy are positive. These observations suggest at least three overlapping electronic transitions compose Band IV.

- d. Band V (26-30 kK) is diffuse and weak. The MCD spectrum is negative with evidence of two maxima in the MCD spectra of  $\text{H}_2\text{Etio}^-$ ,  $\text{ZnTPP}^-$ ,  $\text{H}_2\text{TPP}^-$ , and  $\text{ZnEtio}^-$ .

Assignments of the anion spectrum make use of the following comparisons between calculated and experimental quantities:

1. energy of the transition
2. dipole strength of the transition
3. sign of  $[\theta]_M$

To a much lesser extent, the magnitude of  $[\theta]_M$  provides a clue to the correctness of the assignment. The reason that it is not more useful is the difficulty in obtaining accurate excited state wavefunctions. Approximate wave functions cannot yield accurate dipole matrix elements nor provide correct differences in the excited state energies, which appear in the theoretical expression for the B term. Compounding this difficulty is the unknown influence of vibronic satellites, which are known to reverse the sign of the MCD signal in the Q(0-1) satellite of neutral porphyrins.<sup>27</sup>

For these reasons, we rely on the three items enumerated above to guide the assignments in the anion spectrum.

The Pariser-Parr-Pople open-shell SCF-MO calculations, parameters, and approximations are described in Chapter II.

No Lowdin orthogonalization is performed. The anion is slightly distorted so as to force the ground state to be  $E_{gx}$ ; this is required for convergence of the SCF calculation. Since zero-field splitting of the ground electronic state is an integral feature of our interpretation of Band I, this distortion is a natural consequence. There is no implication that the rectangular geometry chosen is the correct distortion; indeed, a recent paper on triphenylene anion<sup>79</sup> argues that a solvent-separated counterion provides an electrical field that induces the splitting of the  $^2E_g$  level. The results of the SCF-MO calculations are presented in Tables 12-15. Table 12 lists the transition energy, symmetry type ( $D_{4h}$ ), and major contributing configurations to the state. The phasing between configurations is important and serves to reduce the intensity of Bands I and III, while increasing that of Bands IV and V. This situation is analogous to that found in neutral porphyrins: weak, Q dipole strength and strong Soret absorption. In Table 13 dipole and angular momentum matrix elements are listed. In the PPP model, a magnetic transition moment is found to be calculated more accurately than is an electric dipole transition moment.<sup>32</sup> The quantities are important, since they appear in the triple product of Equation (62) for the B term and give some indication as to relative contributions in the sum-over-states in Equation (63). Additionally, these values are employed to estimate the C term contribution from the near degeneracy of

Table 12. Porphyrin Monoanion States

## Porphyrin Monoanion Configuration Interaction Coefficients

No.	Symmetry	Energy $\nu$ (kK)	Coefficients				
1	$1E_{gx}$		0.999(1)				
2	$1E_{gy}$	1.099	-0.998(2)				
3	$1B_{1u}$	8.379	0.815(3)	0.440(14)	0.247(7)		
4	$1B_{2u}$	14.212	-0.846(9)	0.335(11)	-0.226(13)		
5	$2B_{1u}$	15.037	-0.710(7)	-0.452(12)	0.437(14)	0.305(8)	
6	$1A_{2u}$	16.966	-0.798(10)	0.434(13)	-0.313(9)	0.272(11)	
7	$2B_{2u}$	17.954	-0.629(13)	-0.528(4)	0.471(11)	-0.260(10)	
8	$1A_{1u}$	18.265	0.724(8)	0.444(14)	0.366(7)	0.364(12)	
9	$2B_{1u}$	26.346	-0.594(12)	0.516(7)	-0.498(3)	0.270(14)	
10	$2A_{2u}$	27.642	0.769(11)	0.364(9)	0.322(13)	0.297(10)	0.276(4)
11	$2A_{1u}$	28.461	0.556(14)	0.492(12)	-0.257(3)		
12	$3B_{2u}$	30.136	-0.794(4)	0.504(13)	0.312(10)		

Table 13. Porphyrin Anion Electric and Magnetic Dipoles.  
The units are Debye units and Bohr magneton.

Porphyrin Monoanion  
Dipoles and Polarizations

State	From $E_{gx}$	From $E_{gy}$	States	Magnetic Moments
3	-3.64 x	4.20 y	1,2	-2.07
			3,4	-0.93
4	2.54 y	1.46 x	3,6	-0.19
			3,7	0.46
5	-0.45 x	-0.35 y	3,10	0.39
			3,12	1.72
6	-0.65 y	-0.12 x	4,5	3.70
			4,8	-1.74
7	-3.60 y	-2.51 x	4,9	0.42
			4,11	0.70
8	0.29 x	-2.00 y	5,6	-1.74
			5,7	-2.14
9	15.41 x	-6.48 y	5,10	0.33
			5,12	0.81
10	-12.66 y	8.82 x	6,8	3.22
			6,9	-0.20
11	-3.83 x	-15.16 y	6,11	-0.68
			7,8	-0.27
12	4.82 y	11.68 x	7,9	0.19
			7,11	1.44
			8,10	0.58
			8,12	-0.00
			9,10	0.01
			9,12	-1.16
			10,11	-2.98
			11,12	1.27

Table 14. Metalloporphyrin Monoanion Absorption and MCD Spectra. The B term calculation includes all states (including both components of the split ground state). The C term calculation is based on those dipoles which would determine the C term if the molecule were degenerate. The units are D, Debye<sup>2</sup>; C, Bohr magneton Debye<sup>2</sup>; B, Bohr magneton Debye<sup>2</sup> cm<sup>-1</sup>. The values in parenthesis are from reference 72 and have been converted to these units.

Calculated Porphyrin Monoanion Spectra

No.	Group	Symmetry	$\nu$ (kK)	D (polarization)	Bx10 <sup>3</sup>	C Term
2		1E <sub>gy</sub>	1.1			
3	I	1B <sub>1u</sub>	8.4 (8.5)	13.24 (8.76) x	27.2	15.8
4	II	1B <sub>2u</sub>	14.2 (13.4)	6.45 (5.07) y	3.9	3.8
5	II	2B <sub>1u</sub>	15.0 (13.8)	0.20 (0.0) x	6.3	-0.2
6	III	1A <sub>2u</sub>	17.0 (16.1)	0.42 (0.0) y	-0.6	0.1
7	III	2B <sub>2u</sub>	18.0 (17.1)	12.96 (12.4) y	17.5	9.4
8	III	1A <sub>1u</sub>	18.3 (17.6)	0.08 (0.46) x	2.1	0.6
9	IV	3B <sub>1u</sub>	26.3 (26.6)	237.34 (84.8) x	213.8	103.4
10	IV	2A <sub>2u</sub>	27.6 (26.5)	160.36 (85.3) y	-394.0	-115.7
11	IV	2A <sub>1u</sub>	28.5 (26.3)	14.69 (66.4) x	79.8	-60.2
12	V	3B <sub>2u</sub>	30.1 (29.0)	23.45 (88.0) y	68.7	58.6

Table 14. (Continued)

Experimental (CuTPP <sup>-</sup> at Room Temperature)			
Group	$\nu$ (kK)	D	$(B+C/kT) \times 10^3$
I	11.5	6.5	9.1
II	13.0	2.1	-
III	15.0	20.0	18.1
IV	22.0	126.8	16.8
	-	-	-41.6
	24.0	20.5	-10.4
V	26.0	24.0	7.8
Experimental (ZnEtio <sup>-</sup> at 100°K)			
Group	$\nu$ (kK)	D	$(B+C/kT) \times 10^3$
I	12	7.3	56
II	13	7.3	-
III	15	1.6	-2
	15.5	4.8	-15.8
	16	8.3	42.1
IV	23.5	244	39
	23.9	-	-132
Experimental (ZnEtio <sup>-</sup> at 200°K, $\nu$ (kK) is for the band at 100°K)			
Group	$\nu$ (kK)	D	$(B+C/kT) \times 10^3$
I	12	5.8	29
II	13	4.5	-
III	15.5	17.4	-14.7
	16	-	25.4
IV	23.5	109	17
	23.9	109	-82
Experimental (ZnTPP <sup>-</sup> at 298°K)			
Group	$\nu$ (kK)	D	$(B+C/kT) \times 10^3$
IV	22.0	158	30
	22.9	-	-106
	23.6	-	-38
Experimental (ZnTPP <sup>-</sup> at 100°K, $\nu$ (kK) is for the band at 298°K)			
Group	$\nu$ (kK)	D	$(B+C/kT) \times 10^3$
IV	22.0	105	119
	22.9	53	-220
	23.6	26	-110

Table 15. Experimental Metal-Free Porphyrin Monoanion Spectra.  
 (See Table 14 for calculated spectra.) The units  
 are D, Debye<sup>2</sup>; B, Bohr magneton Debye<sup>2</sup> cm<sup>-1</sup>.

Group	$\nu$ (kK)	$H_2Etio^-$		$\nu$ (kK)	$H_2TPP^-$	
		D	$B \times 10^3$		D	$B \times 10^3$
I	12.2	6	9	11.4	6	8.8
II & III	16.7	8	-2	13.1	5	2.4
	-	-	2	14.6	22	14
	17.2	11.7	13			
IV & V	23.3	71.0	28	22.2	100	95
	25.2	51.6	-68	23.1	-	-54
	28.2	21.5	10	23.6	-	-
	29.8	10.8	3	24.2	100	-95

the  $1E_{gx}$  and  $1E_{gy}$  energies.

In Tables 14 and 15, calculated properties and experimental quantities of the porphyrin anions are listed. As discussed earlier in Chapter II, the C term contribution to B has a definite sign, positive (corresponding to negative  $[\theta]_M$ ) for  $B_{1u}$  and  $B_{2u}$  states and negative for  $A_{1u}$  and  $A_{2u}$  states. If we compare the sign of the C term entry in the calculated results with that found experimentally, then the comparison is quite good. Thus, Bands I, III, and V will be dominated by positive  $(B + C/kT)$  terms, while Band IV will exhibit, in order of increasing transition energy, a positive term followed by two negative terms of comparable magnitude. Indeed, this general pattern is closely followed in the MCD spectra of all anions. Band II is predicted to consist of low intensity transitions to a  $1B_{2u}$  and  $2B_{1u}$  state. Band III comprises three transitions:  $E_g \rightarrow A_{2u}$ ,  $2B_{2u}$ , and  $A_{1u}$ . The majority of the dipole transition appears in the  $2B_{2u}$  state, and this accounts for the dominant  $[\theta]_M$  seen in the anions. The  $ZnEtio^+$  MCD spectrum at 100°K does display two components at 15 and 15.5 kK with a positive  $[\theta]_M$  signs. Possibly the A-symmetry states have gained sufficient dipole intensity to now be observed. The fact that two such components are seen supports the assignment. Inasmuch as they appear to the red of the  $2B_{2u}$  transition, we cannot consider them as vibrational components.

Band IV is predicted to consist of three transitions:

$2B_{1u}$ ,  $2A_{2u}$ , and  $2A_{1u}$ , in order of increasing energy. The signs of the MCD signal supports this assignment as does the approximate equality of the magnitude of  $[\theta]_M$ . Band V is assigned to a  $B_{2u}$  state. At transition energies on the order of 30 kK, it is difficult to speculate on the origin of the other component seen at higher energies in  $ZnEtio^-$ ,  $ZnTPP^-$ ,  $H_2TPP^-$ , and  $H_2Etio^-$ . The band is weak and diffuse with signs of  $[\theta]_M$  consistent with B-symmetry excited state.

General agreement between relative dipole strength of the assigned states and that observed is found. Thus, Band I is predicted to be weaker by a factor of 0.03 than the composite Band IV, while the experimental ratio is  $\sim 0.03$ . The experimental intensity of Band III relative to Band I is  $\sim 3$ , while the calculated ratio is 1.0. Band II is predicted to be weaker than Band I by one-half. In  $CuTPP^-$  the factor one-third is found, but in  $ZnEtio^-$  at 100°K, the intensity of Band II has increased to that of Band I. Again,  $ZnEtio^-$  displays absorption and MCD spectra slightly different from those of  $CuTPP^-$  or  $ZnTPP^-$ . The difference is found also in the intensities of Q(0-0) in neutral metallooctaalkyl and tetraphenylporphyrins and is related by Gouterman<sup>70,71</sup> to inductive effects of the peripheral substituents on the relative energy gap between  $1a_{1u}$  and  $3a_{2u}$  molecular orbital energies.

The previous discussion assumes that  $[\theta]_M$  is dominated by the C term contribution. In other words, we are assuming

that each excited state is isolated from its neighbors. In the instance of Band I, it is easy to show that 85% of the calculated B term value arises from just three states:  $1E_{gx}$ ,  $1E_{gy}$ , and  $1B_{1u}$ . However, this assumption is certainly not true for the closely-clustered states composing Bands III and IV. Now, errors in calculating dipole moment matrix elements with correct signs and magnitudes and energy differences become important; the latter especially so. For this reason, the calculated B term values of Table 14 are at best suggestive. This point has been noted previously.<sup>79</sup> There are two improvements that might enhance the quality of the computed B terms: (1) employment of the Lowdin orthogonalization procedure, which is theoretically sound for the zero differential overlap approximation of the PPP theory, and (2) use of CNDO/S<sup>80</sup> wavefunctions for the excited state.

#### Chlorin and Bacteriochlorin Anion Assignment

In their general features, the absorption spectra of these anions are similar. The longest wavelength absorptions at 13-14 kK in the tetraphenylchlorin anion and at 10-12 kK in the tetraphenylbacteriochlorin anion series are the most intense bands in the visible and near infrared region of the spectrum. Other absorption bands in this spectral region are diffuse and overlapping; however,  $ZnTPBC^-$  and  $H_2TPBC^-$  exhibits a well-defined peak at 13.4-13.6 kK. Between 20 and 25 kK and to lower energies of the strong uv absorption, the bacteriochlorin anions display moderate absorption; this feature is

absent or not pronounced in the tetraphenylchlorin anions. Metal anion radicals evince a strong, structureless peak in the near uv region, while two absorption maxima are noted for the free base anion.

In contrast to the relatively structureless absorption spectra, the MCD spectrum of the metallochlorin anions may be classified into three main groups, with further subdivision into Bands Ia, Ib, IIa, IIb, IIIa, and IIIb. The classification is shown in Figure 39 of  $\text{ZnTPC}^-$ . Bands Ia and Ib appear with opposite signs at 13.2 and 13.8 kK in  $\text{ZnTPC}^-$  and at 13.6 and 14.8 kK in  $\text{CuTPC}^-$  (Figure 40). This feature is absent in the  $\text{H}_2\text{TPC}^-$  MCD spectrum shown in Figure 41; instead,  $[\theta]_M$  of Band Ib is positive. The same classification appears in the MCD spectrum of  $\text{ZnTPBC}^-$ , shown in Figure 42 and repeats itself in Figure 43, where the MCD spectrum of  $\text{H}_2\text{TPBC}^-$  is displayed. Bands Ia and Ib of the bacteriochlorin anions are now similar for both the metal salt and free base compound.

Bands IIa and IIb are characterized in both tetraphenylchlorin and tetraphenylbacteriochlorin anion radicals by negative  $[\theta]_M$ . In the metallochlorin complexes the separation in energy of the two transitions is ca. 1.5 kK, while it is ca. 6 kK in the  $\text{TPBC}^-$  complexes. In the chlorin anion spectra (excluding  $\text{H}_2\text{TPC}^-$  from this discussion) Bands IIa and IIb correspond to absorption maxima, while Band IIb correlates with the onset of diffuse absorption in  $\text{ZnTPBC}^-$  and

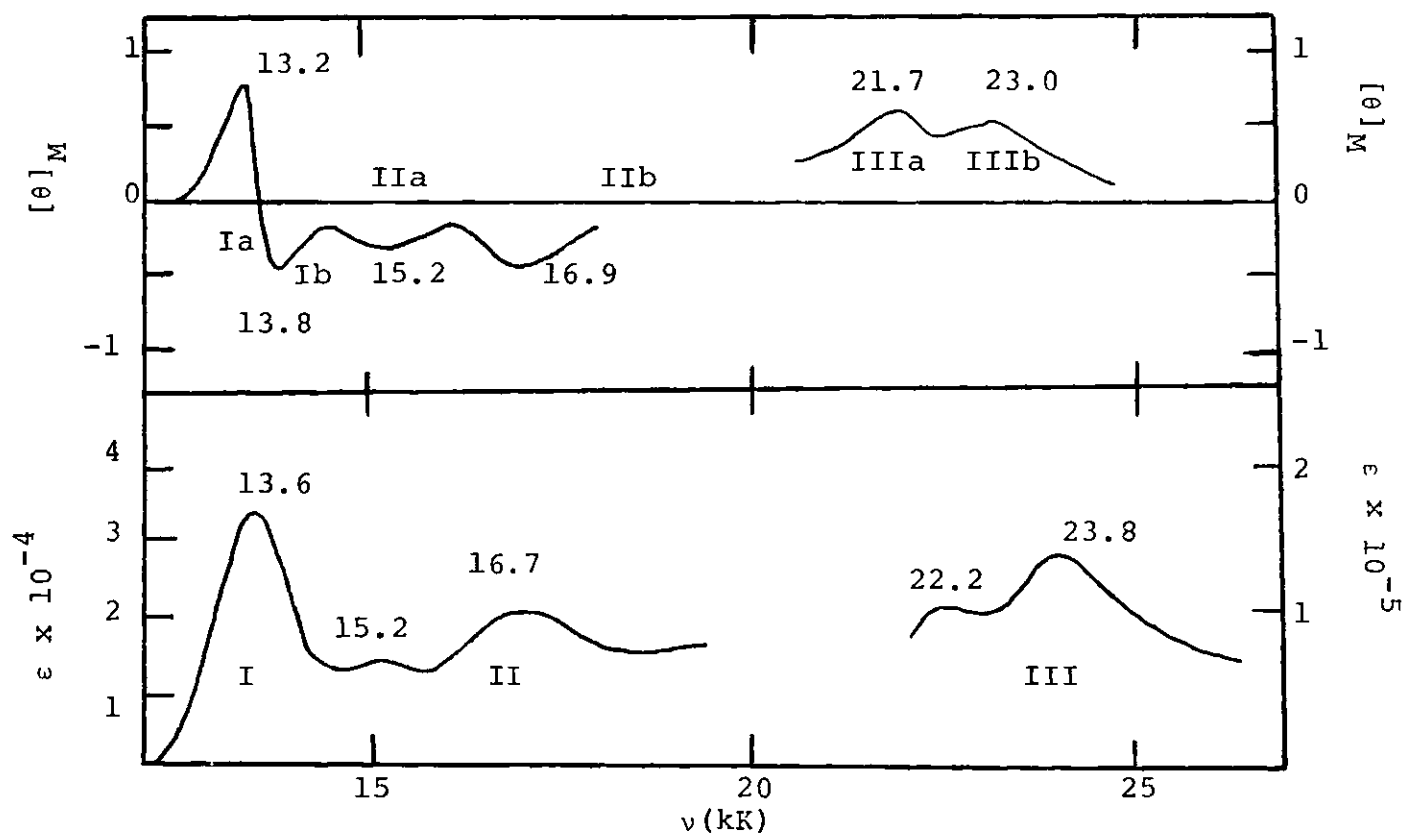


Figure 39. ZnTPC Monoanion (MCD Spectra (Upper Figure, Maxima and Minima are Indicated); Absorption Spectra (Lower Figure, maxima are Indicated)). This is the tetrapropylammonium salt in dimethylformamide. The units are:  $[\theta]_M$ ,  $\text{deg cm}^2 \text{ gauss}^{-1} \text{ dmole}^{-1}$ ;  $\epsilon$ ,  $\text{liter cm}^{-1} \text{ mole}^{-1}$ . These spectra were taken at room temperature ( $25^\circ\text{C}$ ). For purposes of discussion the spectra have been divided up into three regions.

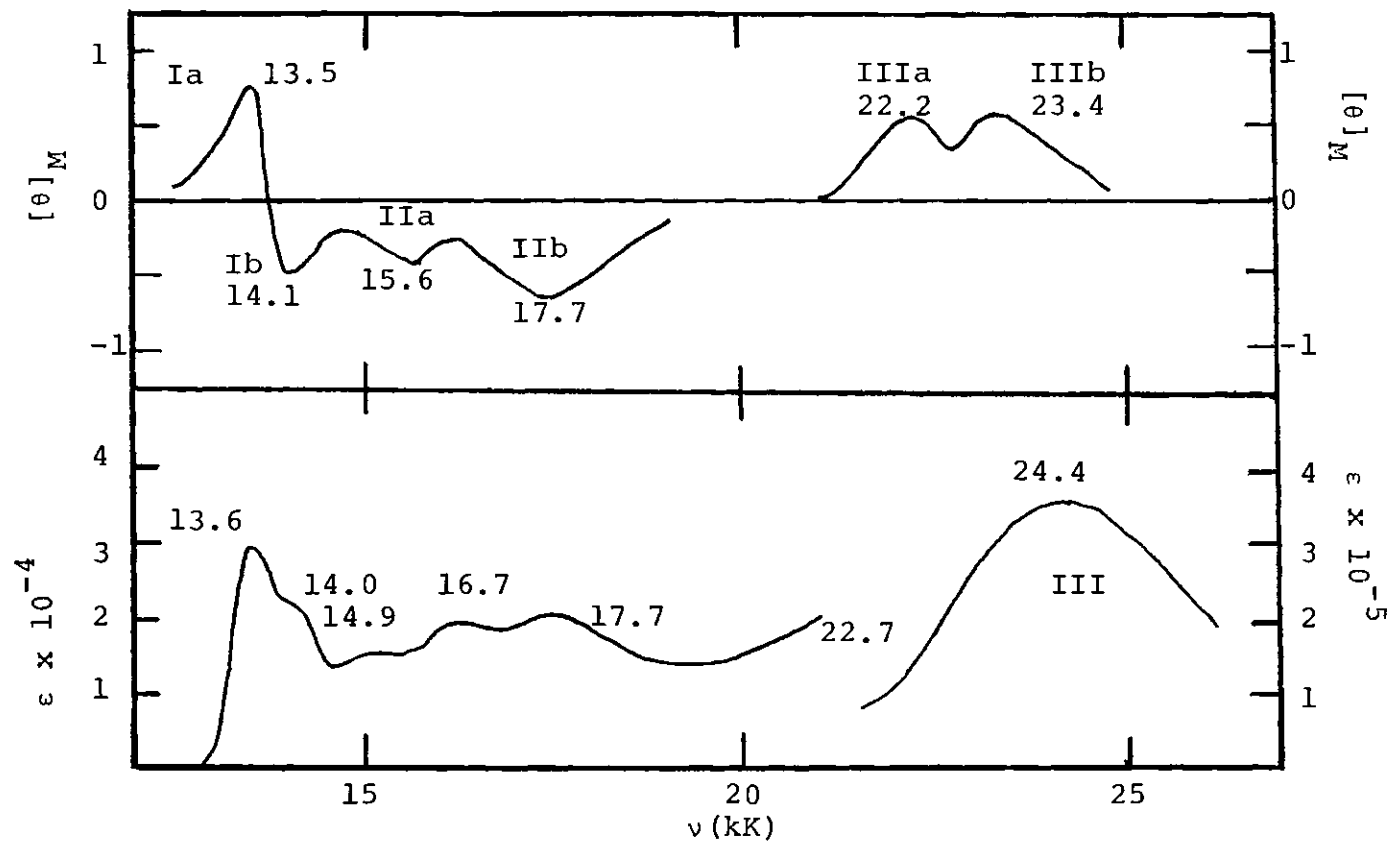


Figure 40. CuTPC Monoanion. MCD spectra (upper figure, maxima and minima are indicated); absorption spectra (lower figure, maxima are indicated). This is the tetrapropylammonium salt in a mixture of dimethylformamide and tetrahydrofuran. The units are:  $[\theta]_M$ ,  $\text{deg cm}^2 \text{ gauss}^{-1} \text{ dmole}^{-1}$ ;  $\epsilon$ ,  $\text{liter cm}^{-1} \text{ mole}^{-1}$ . The spectra were taken at room temperature (25°C). For purposes of discussion the spectra have been divided up into three regions.

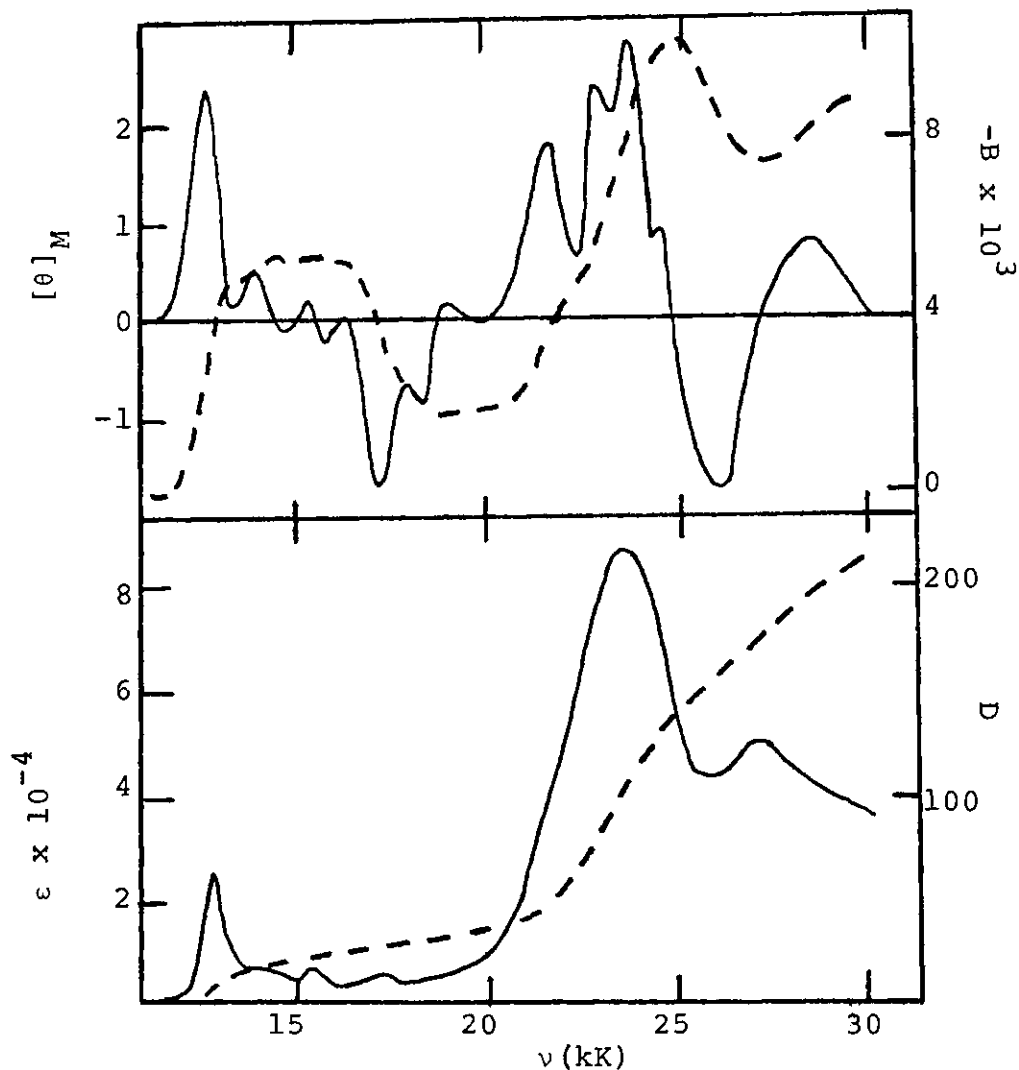


Figure 41.  $\text{H}_2\text{TPC}$  Monoanion. MCD spectra (upper figure); and absorption spectra (lower figure). Units are:  $\epsilon$ , liter  $\text{cm}^{-1}$  mole $^{-1}$ ;  $[\theta]_M$ , deg  $\text{cm}^2$  gauss $^{-1}$  dmole $^{-1}$ ;  $B$ , Debye $^2$  Bohr magneton  $\text{cm}^{-1}$ ;  $D$ , Debye $^2$ . The dotted lines are the integrated intensities. This is the tetrapropylammonium salt in dimethylformamide. The spectra were taken at room temperature (25°C).

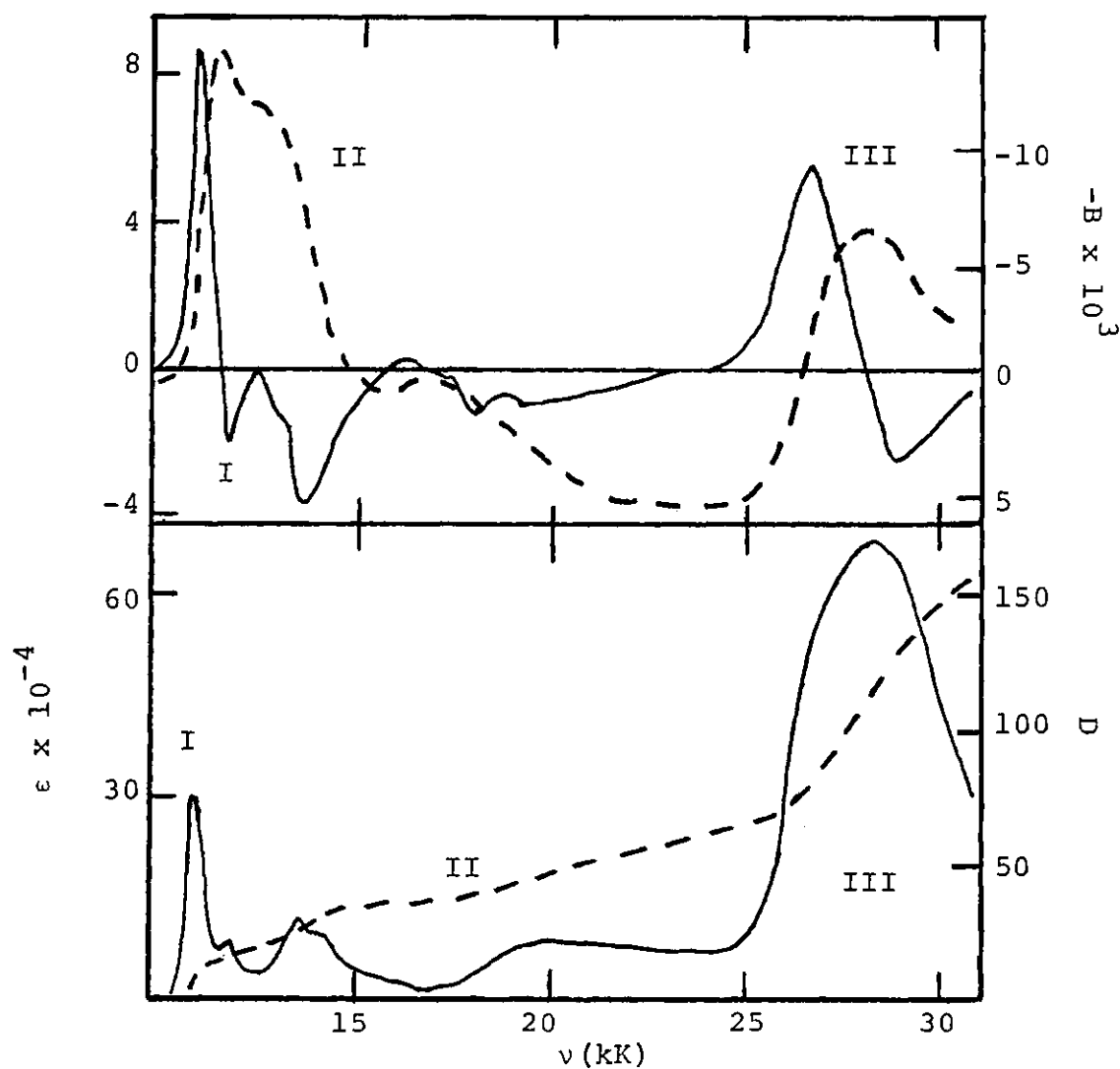


Figure 42. ZnTPBc Monoanion (MCD Spectra (Upper Figure); Absorption Spectra (Lower Figure); Units are:  $\epsilon$ , liter  $\text{cm}^{-1}$  mole $^{-1}$ ;  $[\theta]_M$ , deg  $\text{cm}^2$  gauss $^{-1}$  d mole $^{-1}$ ; B, Debye $^2$  Bohr magneton  $\text{cm}^{-1}$ ; D, Debye $^2$ ). The dotted lines are the integrated intensities. This is the tetrapropylammonium salt in dimethylformamide. The spectra were taken at room temperature (25°C). For purposes of discussion the spectra have been divided up into three regions.

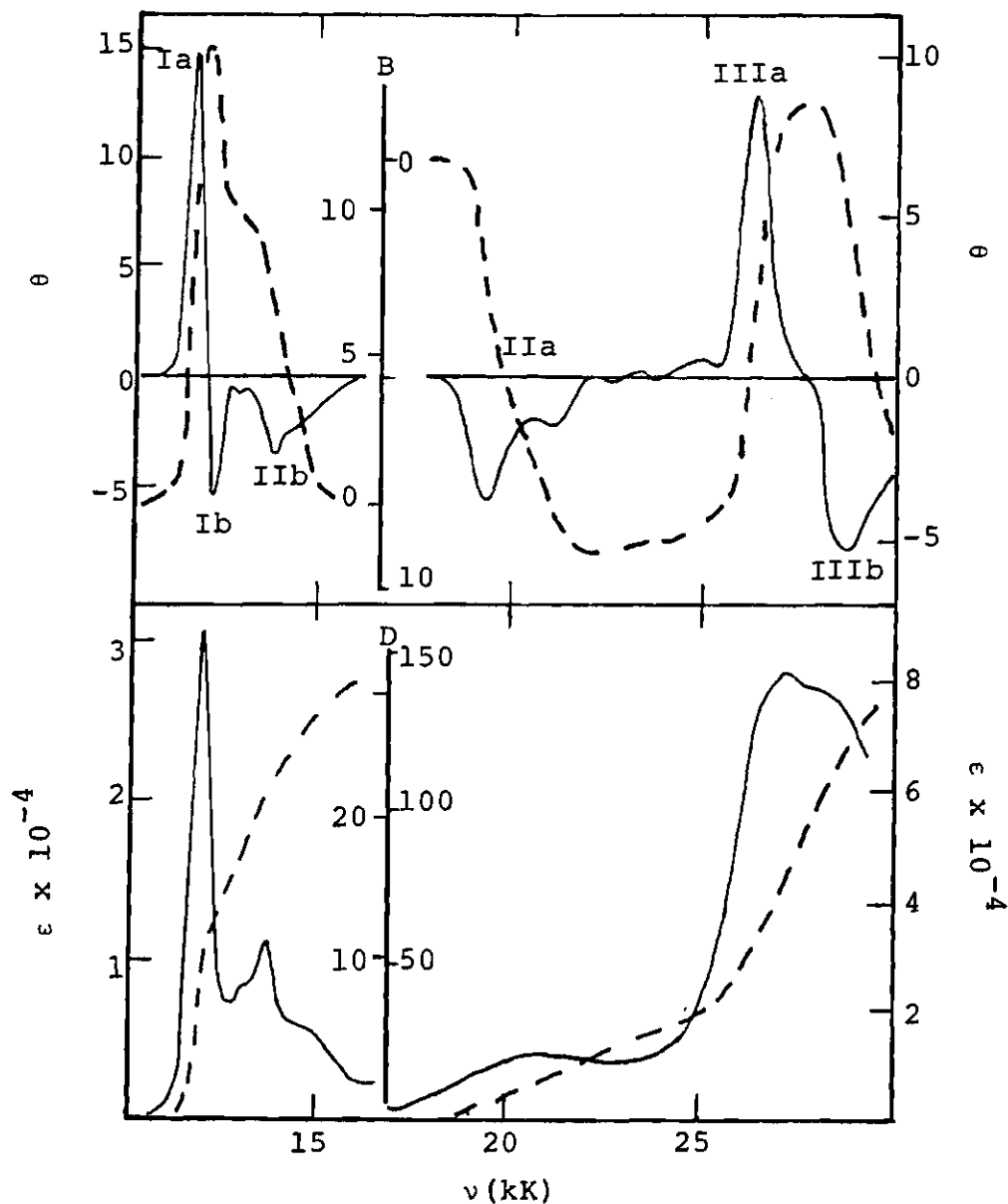


Figure 43.  $\text{H}_2\text{TPBc}$  Monoanion (MCD spectra (upper figure); absorption spectra (lower figure); units are  $\epsilon$ , liter  $\text{cm}^{-1}$  mole $^{-1}$ ;  $[\theta]_M$ , deg  $\text{cm}^2$  gauss $^{-1}$  dmole $^{-1}$ ; B, Debye $^2$  Bohr magneton  $\text{cm}^{-1}$ ; D, Debye $^2$ ). The dotted lines are the integrated intensities. This is the tetrapropylammonium salt in dimethylformamide. The spectra were taken at room temperature (298°K).

$\text{H}_2\text{TPBC}^-$  spectra. We note that this diffuse absorption is not reported by Maslov<sup>81</sup> in a study of the photodichroism of  $\text{Na}_2\text{TPBC}^-$  in a mixture of DMF and THF at  $-196^\circ\text{C}$ . The reason for this difference is not understood, since other features of Maslov's absorption spectrum agree well with the data of Figures 42 and 43. Bands IIIa and IIIb of  $\text{ZnTPC}^-$  or  $\text{CuTPC}^-$  MCD spectra are shifted with respect to the absorption maxima. Both bands appear in the near uv and display positive  $[\theta]_M$ . A hint of the difficulty facing us in our interpretation appears in the MCD spectrum of  $\text{H}_2\text{TPC}^-$ ; there is evidence of at least six different transitions, and many may be distinct electronic transitions. Bands IIIa and IIIb are present in the spectra of tetraphenylbacteriochlorins, but Band IIIb is characterized by a negative  $[\theta]_M$ .

Since no temperature-dependent study of the spectra was made with the DMF solution, which freezes into a polycrystalline solid, we cannot rigorously exclude the possibility of ion-pairing. However, with the exception of Band IIIb in  $\text{ZnTPBC}^-$ , there is excellent correspondence between our room temperature spectra and Maslov's low temperature spectra of  $\text{Na}_2\text{TPBC}^-$ <sup>81</sup> and  $\text{Na}_2\text{chlorin}^-$ <sup>82</sup>. For this reason, we treat the experimental absorption and MCD spectra as if they arise from a single species.

Our task in analyzing these spectra is simplified somewhat by the natural grouping of calculated transition energies into three, distinct spectral regions. This theoretical

classification also appears in the PPP calculations of anion radicals, carried out by Maslov.<sup>72</sup> In Table 16, the results of this computation on the metallated complex anions are presented. In the chlorin anion, eleven optically accessible states appear below 33 kK. The state at 5.6 kK is predicted to be weakly dipole allowed, but no experimental transition is assigned to this infrared transition. States 3 and 4, 5 and 6, and 7-12 are segregated by energy into three groups. For the bacteriochlorin anion states 2 and 3, 4 and 5, and 6-10 are divided into three groups by their transition energies.

Bands Ia and Ib are calculated to be polarized in the y and x directions, respectively, in agreement with the results of the photodichroic experiment and in agreement with Maslov's calculations. Importantly, the signs of the B terms of the two transitions are correctly computed in the PPP model as seen by comparison of theoretical and experimental results in Table 17 for the chlorin monoanion and in Table 18 for the bacteriochlorin anion. The configurations responsible for the excited states are promotions from the filled orbitals,  $b_1$  or  $b_2$  to the half-filled level,  $c_1$ . This pattern contrasts with the  $c_1 \rightarrow d_1$  or  $c_2 \rightarrow d_1$  promotions responsible for Band I or the porphyrin anions and is caused by the increased splitting in energy, of  $b_1$ ,  $b_2$ ,  $c_1$ ,  $c_2$ , and  $d$  by removing two or four carbon atoms from the  $\pi$  electron system. The splitting is shown graphically in Figure 15. The magnitude of the computed

Table 16. Metallochlorin and Metallobacteriochlorin Anion States.

Chlorin Monoanion (The hydrogenated pyrrole is on the + x axis.)

State	Energy $\nu$ (kK)	Configuration Interaction Coefficients <sup>a</sup>				
1	0.0	-0.987(1)				
2	5.60 y <sup>b</sup>	0.956(2)	0.206(9)			
3	13.86 y	-0.892(9)	0.300(3)			
4	15.01 x	0.924(7)	0.224(12)			
5	19.07 y	0.832(3)	0.406(13)	0.271(11)		
6	21.92 x	-0.539(4)	-0.463(12)	0.650(14)		
7	25.65 x	-0.701(12)	-0.506(14)	0.373(8)		
8	26.02 y	0.713(11)	-0.500(10)	0.384(13)	-0.252(5)	
9	29.54 x	0.751(4)	-0.461(12)	-0.262(7)		
10	30.37 y	0.562(13)	0.378(3)	-0.325(5)	-0.479(11)	

Bacteriochlorin Monoanion (The hydrogenated pyrroles are on the x axis.)

State	Energy $\nu$ (kK)	Configuration Interaction Coefficients				
1	0.0	-1.000(1)				
2	9.84 y	-0.960(9)				
3	13.76 x	0.936(7)				
4	18.38 x	0.606(4)	-0.672(14)	0.406(12)		
5	20.99 y	-0.780(3)	-0.514(13)	-0.304(11)		
6	30.15 x	-0.315(7)	-0.426(4)	0.837(12)		
7	30.53 y	0.592(13)	-0.513(10)	-0.435(6)	-0.389(11)	
8	31.86 x	0.566(4)	0.652(14)	0.442(8)	0.215(12)	
9	32.09 y	0.790(11)	-0.494(10)	0.262(13)		

a) The quantities in parentheses are the configurations listed in Table 11.

b) Polarization of transition with x axis parallel to axis bisecting dihydro pyrrol ring.

Table 17. Chlorin Monoanion Spectra. The units are D, Debye<sup>2</sup>; B, Debye<sup>2</sup> Bohr magneton cm<sup>-1</sup>. The values in parenthesis are from reference 72.

Calculated						
No.	Group	Symmetry	$\nu$ (kK)	D(polarization)	$B \times 10^3$	
2		1A <sub>2</sub>	5.6 (5.0)	4.83 (3.9) y	-0.78	
3	Ia	2A <sub>2</sub>	13.86(13.2)	21.91(13.1) y	-34.22	
4	Ib	2B <sub>2</sub>	15.01(15.3)	16.18(11.5) x	35.34	
5	IIb	3A <sub>2</sub>	19.07(16.5)	23.97(15.7) y	17.98	
6	IIa	3B <sub>2</sub>	21.92(19.0)	2.14( 0.5) x	-5.37	
7	III	4B <sub>2</sub>	25.65(24.3)	41.42( 3.2) x	0.78	
8		4A <sub>2</sub>	26.02(24.7)	34.90(15.4) y	-12.95	
9		5B <sub>2</sub>	29.54(26.3)	101.33(42.2) x	36.82	
10		5A <sub>2</sub>	30.37(28.0)	73.10(28.1) y	-3.90	

Experimental ZnTPC <sup>-</sup>				Experimental CuTPC <sup>-</sup>		
Assignment	$\nu$ (kK)	D	$B \times 10^3$	$\nu$ (kK)	D	$B \times 10^3$
Ia	13.2	7.6	-0.70	13.6	5.1	-0.72
Ib	13.8	6.2	0.45	14.8	7.2	0.55
IIa	15.1	4.4	0.31	16.2	7.1	0.42
IIb	16.7	13.7	0.62	17.5	14.6	1.16
III	22.0	26.0	-1.60	22.2	32.8	-1.05
	22.9	60.4	-0.81	23.4	95.2	-0.93
	34.4	11.4	-0.10			

Table 18. Bacteriochlorin Monoanion Spectra. The units are D, Debye<sup>2</sup>; B, Debye<sup>2</sup> Bohr magneton cm<sup>-1</sup>. The values in parenthesis are from reference 72.

Calculated Metallo Monoanion

No.	Band	Symmetry	$\nu$ (kK)	D (polarization)	Bx10 <sup>3</sup>
2	Ia	1B <sub>1u</sub>	9.84 (9.0)	45.18(45.9) y	-11.81
3	Ib	1A <sub>u</sub>	13.76 (13.8)	14.42(14.3) x	11.79
4	IIa	2A <sub>u</sub>	18.38 (16.2)	0.16( 0.0) x	0.48
5	IIb	2B <sub>1u</sub>	20.99 (19.0)	22.35(14.3) y	11.00
6	IIIa	3A <sub>u</sub>	30.15 (28.3)	132.35(16.8) x	-141.95
7	IIIb	3B <sub>1u</sub>	30.53 (29.4)	72.09(17.7) y	24.92
8	IIIa	4A <sub>u</sub>	31.86 (29.2)	2.91(79.0) x	-99.85
9	IIIb	4B <sub>1u</sub>	32.09 (32.2)	87.79(93.8) y	-5.02

Experimental ZnTPBC<sup>-</sup>

Experimental H<sub>2</sub>TPBC<sup>-</sup>

Assignment	$\nu$ (kK)	D	Bx10 <sup>3</sup>	$\nu$ (kK)	D	Bx10 <sup>3</sup>
Ia	10.8	17.0	-13.2	11.8	19 <sup>a</sup>	-15.3
Ib	11.6	4.0	2.1	12.0		5.5
IIa	13.6	17.5	11.5	13.4	13	9.8
IIb	20.0	21.6	4.5	19.3	22	9.4
IIIa	26.7	47.9	-10.1	26.4	74	-10.8
IIIb	29.0	60.2	4.6	38.9	74	10.8

a) The value of 19 (Debye)<sup>2</sup> corresponds to both transitions.

B terms is in poor agreement with that found experimentally for  $\text{ZnTPC}^-$  or  $\text{CuTPC}^-$ , but is in better agreement with the data for  $\text{ZnTPBC}^-$  or  $\text{H}_2\text{TPBC}^-$ . As discussed earlier for metalloporphyrin anions, the presence of numerous excited states renders an a priori computation of B from Equation (62) difficult. In Tables 19 and 20 we have listed the electric dipole moment and magnetic moment matrix elements between the states after extensive CI. It is evident the similarity in magnitudes of the magnetic moment matrix elements between closely-lying electronic states prevents us from choosing a few dominant terms in the sum yielding B.

Calculated spectra for both chlorin and bacteriochlorin anions indicate that Group II comprises two transitions: in chlorin anions excited state energies (dipole strengths) are predicted to reside at 19.1 (24 D) and 21.9 kK (2.1 D), and in bacteriochlorin anion excited state energies are computed to be at 18.4 (0.16 D) and 21.0 (1.3 D) kK. Since Band IIb in  $\text{ZnTPC}^-$  (Figure 39) and  $\text{CuTPC}^-$  (Figure 40) is stronger, we so assign it to the 19.1 kK transition. The calculated positive B value agrees with that found experimentally. Our calculation yields too small a dipole strength for Band IIa; however, Maslov's calculation has the intensity of Band IIa factor of 1.4 greater than that of Band IIb. Again the sign of B for Band IIa is positive, which is consistent with the MCD spectra of  $\text{CuTPC}^-$  and  $\text{ZnTPC}^-$ .

Bands IIa and IIb of  $\text{ZnTPBC}^-$  (Figure 42) and  $\text{H}_2\text{TPBC}^-$

Table 19. Electric and Magnetic Dipoles Between Chlorin Monoanion States. The units are Debye units and Bohr magneton.

Dipole Moments and Magnetic Momentum Between Various States  
Chlorin Monoanion

Dipoles and Polarizations		Magnetic Moment	
1,2	2.20 y	1,2	1.63
1,3	4.68 y	1,3	1.51
1,4	4.02 x	2,4	
1,5	-4.90 y	3,4	-2.26
1,6	-1.46 x	3,6	-1.88
1,7	-6.44 x	4,5	-1.54
1,8	5.91 y	4,8	-0.66
1,9	10.07 x	5,6	0.69
1,10	-8.55 y	5,7	-0.54
		5,9	0.94
		6,8	-0.79
		6,10	0.64
		7,8	0.28
		7,10	0.93
		8,9	0.31
		9,10	-0.29

Table 20. Electric and Magnetic Dipoles Between Bacteriochlorin Monoanion States. The units are Debye units and Bohr magneton.

Dipoles and Polarizations		Magnetic Moment	
1,2	2.64 y	2,3	-2.16
1,3	1.49 x	2,4	-2.59
1,4	0.16 x	2,5	-0.55
1,5	1.86 y	2,8	0.71
1,6	-4.53 x	3,5	2.15
1,7	3.34 y	3,7	-1.56
1,8	0.67 x	3,9	0.34
1,9	-3.69 y	4,5	0.90
		4,7	-0.63
		4,9	0.68
		5,6	-0.35
		5,8	1.08
		6,7	-0.51
		6,9	0.01
		7,8	2.01
		8,9	-1.15

(Figure 43) are similarly assigned to an x-polarized and y-polarized transition, respectively. The calculated transition energies differ by 3 kK, while the experimental difference is 6 kK. It is possible that the extensive configuration interaction exhibited in Table 16 for states 4 and 5 of the bacteriochlorin anion is responsible for the poor comparison between theory and experiment. However, our calculated separation of 3 kK compares favorably to the value reported by Maslov of 2.7 kK for this quantity. B values are again of the correct sign but the magnitudes are in poor agreement with the data.

The ultraviolet region is especially complicated due to the appearance of a cluster of transitions with similar energies. Evidence in favor of the severe overlapping appears in the  $\text{H}_2\text{TPC}^-$  spectrum (Figure 41) spectrum, in which seven maxima and minima are discernible. The two maxima composing Bnad III MCD spectra of  $\text{ZnTPC}^-$  (Figure 39) or  $\text{CuTPC}^-$  (Figure 40) do not coincide with the absorption maxima; a feature consistent with numerous overlapping MCD transitions. An apparent red shift in the MCD spectra possibly reflects the fact that the states at 25.2, 26.1, and 26.6 kK have weaker dipole strength than those at 30.8 and 31.2 kK, yet have appreciable magnetic rotation strength as demonstrated in Table 17. Also partial cancellations between overlapping MCD spectra of opposite signs can readily yield apparent shifts in the net MCD spectrum. Dipole strengths listed in Table 17 and reported

by Maslov suggest that two maxima will appear in the absorption spectra of chlorin anions with a 5 kK separation. The experimental separation is only 1 kK in  $\text{CuTPC}^-$ ,  $\text{ZnTPC}^-$  and the anion radical of disodium chlorin<sup>82</sup>. Nonetheless, the dominant positive  $[\theta]_M$ , which is found experimentally, is also calculated in the  $\pi$ -electron approximation.

In contrast, MCD spectra of  $\text{ZnTPBC}^-$  (Figure 42) and  $\text{H}_2\text{TPBC}^-$  (Figure 43) show B terms of opposite signs. These bands, denoted as Bands IIIa and IIIb, are assigned to composite transitions. Thus, Band IIIa comprises two transitions. In Table 18, the transitions are at 30.15 kK and 31.86 kK; however, the polarization of Band IIIa is x and that of Band IIIb is y. Considering, also that the resolved maxima at  $-196^\circ\text{C}$  in  $\text{Na}_2\text{TPBC}^-$  are of near equality in intensity, a more consistent ordering of states is assignment of the x polarized transitions at 30.2 and 31.9 kK to Band IIIa and the y polarized transitions at 30.5 and 32.1 kK to Band IIIb. With this grouping, Band IIIa still yields a positive  $[\theta]_M$ , and the computation results in a negative  $[\theta]_M$  for Band IIIb.

As noted earlier by Maslov,<sup>72</sup> the absorption spectra of the chlorin and bacteriochlorin anions are more similar to one another than to that of the porphyrin anion. The assignments advanced here support that suggestion, and the use of MCD spectroscopy provides corroborative evidence in the form of  $[\theta]_M$  signature. Thus, one has qualitative compatibility in polarization, MCD, and absorption data. The lack of quanti-

tive agreement is not surprising given the known behavior of PPP theory to overestimate excited state energy separations in neutral porphyrins and the extreme sensitivity of B to such differences.

### Porphyrin Dianion

The dianion MCD and absorption spectra, shown in Figures 44-46 indicate that there are two major features, Band I and Band II. In Band I, the dianions absorb in a broad region between 15 to 20 kK. Three peaks are apparent in the visible region in both the absorption and MCD spectra. In view of the regularity of their spacing, we assign the transitions to a 0-0 band with decreasing intensity in the 0-1 and 0-2 satellites. Three pieces of evidence favor this assignment and are, 1) the calculated MCD spectrum shows at most two electronic transitions in this region with opposite signatures for MCD spectra; this is incompatible with assignment of each band to an electronic transition; 2) the spacing between peaks is 1.4 kK which is the same as found for the energy differences between Q(0-0) and Q(0-1), or Q(0-2) bands in the neutral porphyrin spectra; and 3) the fluorescence polarization data<sup>82</sup> of Na<sub>2</sub>ZnEtio at -190°K indicate that all three absorptions exhibit the same degree of polarization (49%). The high polarization is consistent with D<sub>2h</sub> or lower symmetry in the excited state and would exclude electronic transitions of different polarization. The degree of polarization drops to 10% when excitation is in the uv transition, which is the second

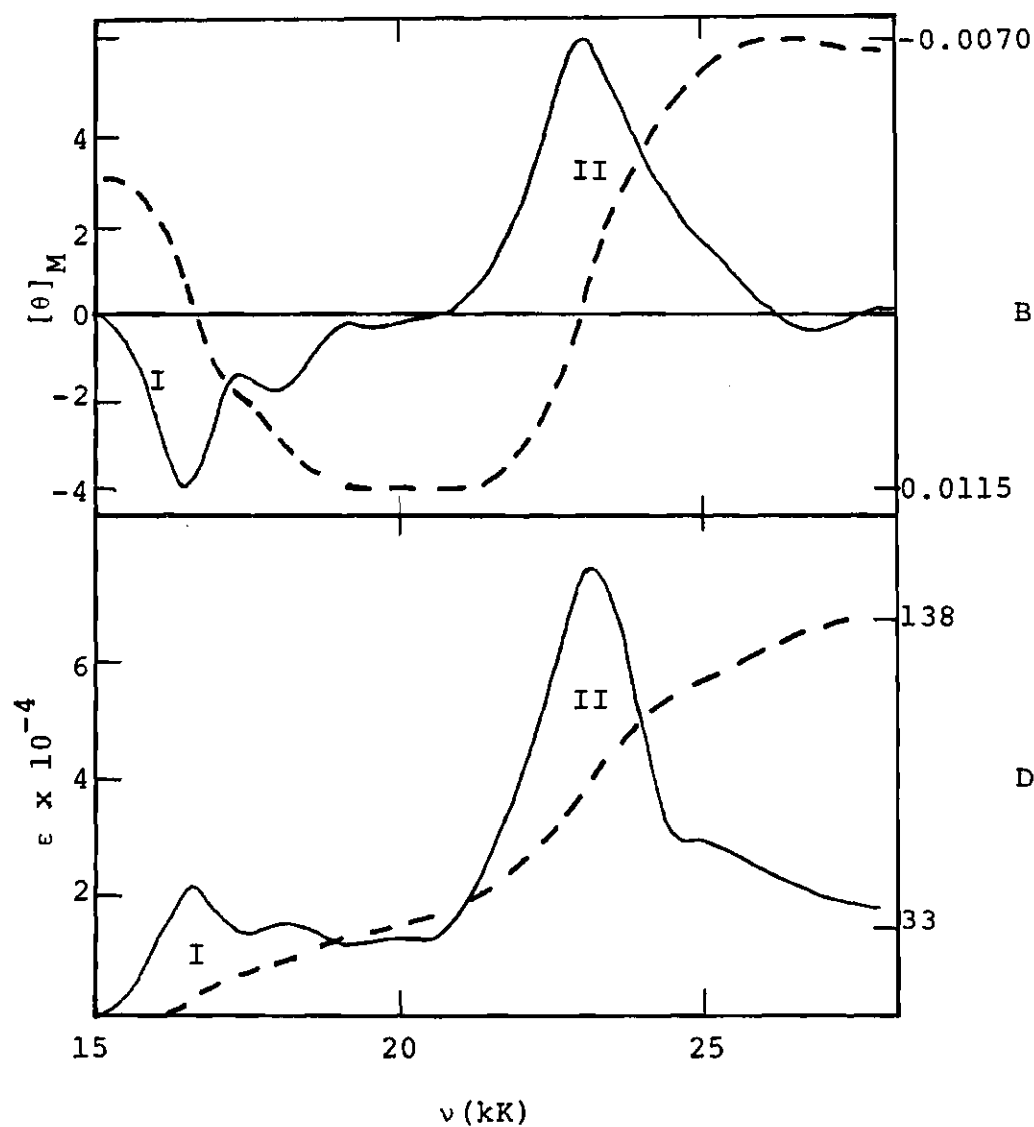


Figure 44. Disodium ZnTPP Dianion. MCD spectra (upper figure); absorption spectra (lower figure). Units are  $\epsilon$ , liter  $\text{cm}^{-1}$  mole $^{-1}$ ;  $[\theta]_M$ , deg  $\text{cm}^2$  gauss $^{-1}$  dmole $^{-1}$ ; B, Debye $^2$  Bohr magneton  $\text{cm}^{-1}$ ; D, Debye $^2$ . The dotted lines are the integrated intensities. Sodium salt is in 2-methyltetrahydrofuran at room temperature. For purposes of discussion the spectra have been divided into two regions.

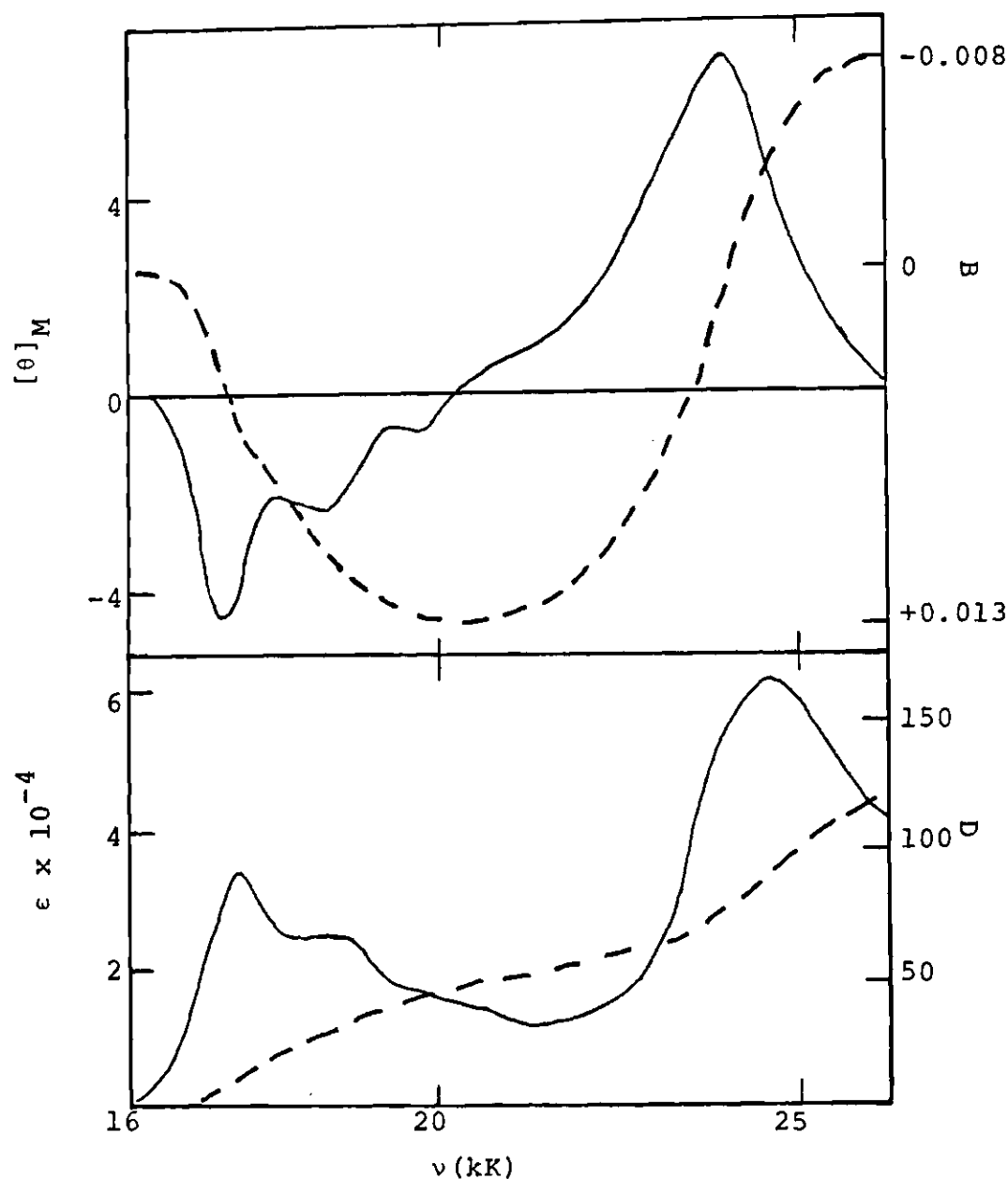


Figure 45. Disodium ZnEtio Dianion. MCD spectra (upper figure) and absorption spectra (lower figure). Units are  $\epsilon$ , liter  $\text{cm}^{-1}$  mole $^{-1}$ ;  $[\theta]_M$ , deg  $\text{cm}^2$  gauss $^{-1}$  dmole $^{-1}$ ; B, Debye $^2$  Bohr magneton  $\text{cm}^{-1}$ ; D, Debye $^2$ . The dotted lines are integrated intensities. Sodium salt is in 2-methyltetrahydrofuran at room temperature.

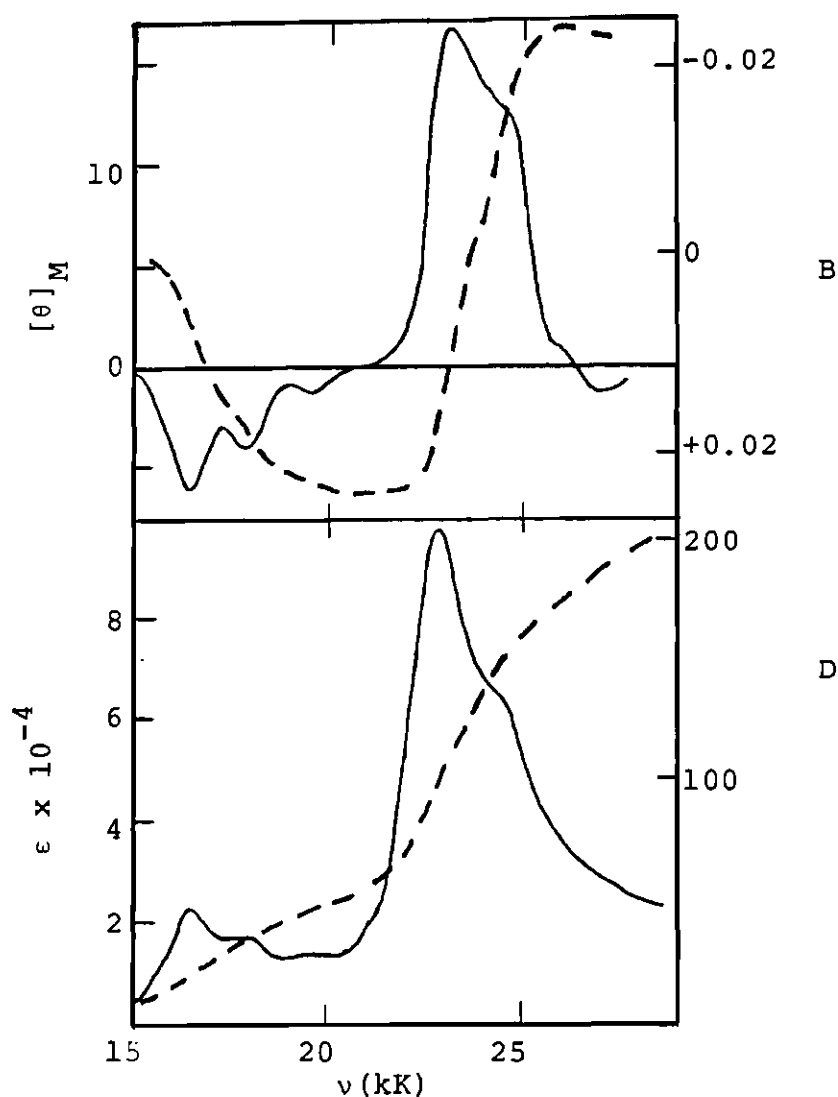


Figure 46. Bis-tetrapropylammonium  $\text{H}_2\text{TPP}$  Dianion. MCD spectra (upper figure); absorption spectra (lower figure. Units are  $\epsilon$ , liter  $\text{cm}^{-1}$  mole $^{-1}$ ;  $[\theta]_M$ , deg  $\text{cm}^2$  gauss $^{-1}$  dmole $^{-1}$ ; B, Debye $^2$  Bohr magneton  $\text{cm}^{-1}$ ; D, Debye $^2$ . The dotted lines are the integrated intensities. The tetrapropylammonium salt is in dimethylformamide at room temperature. For purposes of discussion the spectra have been divided into two regions. The absorption and MCD spectra of Band II are too large due to contamination with phlorin.

major spectral feature, located between 21 and 25 kK. The low extent of fluorescence polarization in Band II is consistent with at least two underlying electronic transitions of opposite polarization. Thus, the Soret-like absorption cannot be assigned to a single electronic transition.

From examination of the data of Figures 44-46, it is apparent that excited state degeneracy is absent; otherwise, A term behavior, analogous to that observed in neutral metalloporphyrins would be seen. Also, C term contributions to the magnetic ellipticity are excluded, since the states arising from the configuration  $b_1^2 b_2^2 c^2$  are  $^1A_{1g}$ ,  $^1B_{1g}$ ,  $^1B_{2g}$ , and  $^3A_{2g}$ . None are orbitally degenerate. The  $^2A_{2g}$  state is excluded on the basis of pmr data that require spin pairing.<sup>83</sup>

In the absence of external forces, one would expect the  $^1B_{1g}$  state to lie lowest due to favorable interelectronic terms. However, it is more likely that solvent or counterion molecules exert an external field which causes molecular distortion and stabilizes a particular state. The role of the counter ions is not essential to the spectral properties described earlier. Thus, the  $H_2TPP^{2-}$  dianion in DMF with tetrapropylammonium counter ions exhibits MCD spectra similar to the ion paired  $Na_2ZnTPP$  or  $Na_2ZnEtio$  species in THF. Cooling of  $Na_2ZnTPP$  to  $-170^\circ C$  causes the spectra to shift to lower transition energies; however, no new bands appear in either MCD or absorption spectra. For the zinc complex, bands appearing at 16.5 and 17.9 kK at room temperature shift to

14.8 and 16.3 kK, respectively. There is no decrease in the bandwidth of the transitions. The shift to lower transition energies is consistent with a shift in equilibrium to less ion-pairing. Band II has an absorption maximum at 22.4 kK which shifts to 21.2 kK, and a shoulder at 25 kK, in Figure 44, is prominent at 24.5 kK at  $-170^{\circ}\text{C}$ . The 24.5 kK transition is characterized by a negative  $[\theta]_M$ .

The MCD data, therefore, are in agreement with fluorescent depolarization ratios. Band I appears to be a single electronic transition with vibrational satellites; however, the failure to observe significant sharpening of spectral bands at reduced temperatures argues for significant vibronic interactions in this region. Band II exhibits at least two transitions: 21.2 and 24.5 kK in  $\text{Na}_2\text{ZnTPP}$  at  $-170^{\circ}\text{C}$ . The 3.3 kK separation argues against the second maximum being a vibrational satellite.

Electronic structure of the porphyrin dianion is discussed in terms of the six orbitals used to describe the mono-anion. In  $D_{4h}$  symmetry fully occupied orbitals are  $1a_{1u}$  and  $3a_{2u}$ , the doubly degenerate  $4e_g$  level has two electrons, and the lowest unoccupied orbitals are  $2b_{1u}$  and  $3b_{2u}$ . There are three possible singlet configurations which can be formed by placing the two electrons in the  $e_g$  orbitals:  $^1A_{1g}$ ,  $^1B_{1g}$ , and  $^1B_{2g}$ . Four low-lying, doubly-degenerate, optically accessible states shown in Figure 47 can be formed by the excitations  $e_g \rightarrow b_{1u}$ ,  $b_{2u}$  and  $a_{1u}$ ,  $a_{2u} \rightarrow e_g$ . If the  $e_g$  orbitals are now split

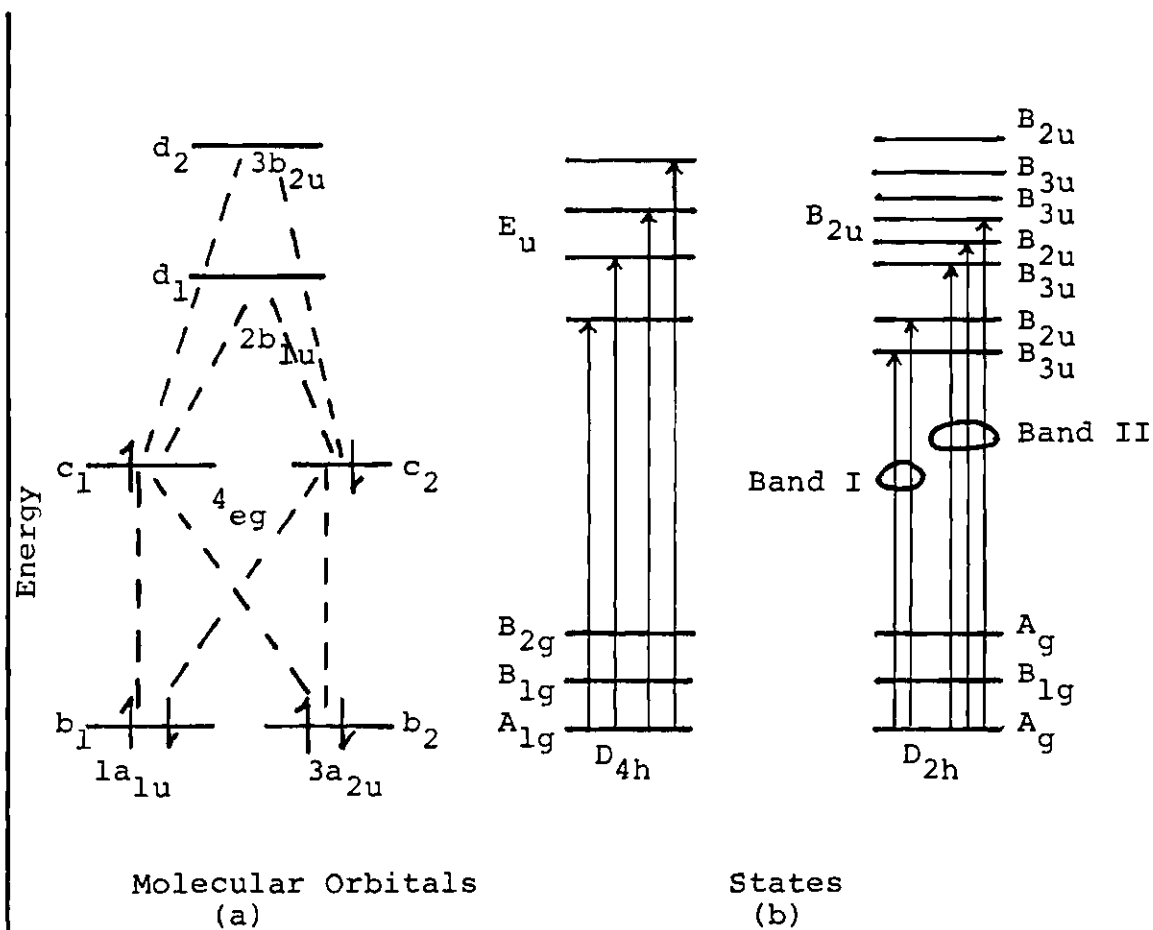


Figure 47. Six Orbital Model of Porphyrin Dianion States. (a) Molecular orbital diagram, (b) singlet excited states and transitions.

into an x component and a y component, which are represented by  $c_1$  and  $c_2$ , respectively, then the ground state configuration in  $D_{2h}$  symmetry will be

$$1) \quad |b_1^2 b_2^2 c_1^2| : A_{1g}$$

and the first excited state configuration will be

$$2) \quad \frac{1}{\sqrt{2}} (|b_1^2 b_2^2 c_1 \bar{c}_2| + |b_1^2 b_2^2 c_2 c_1|) : B_{1g}$$

The lowest, optically accessible, singly excited configurations are

$$3) \quad \frac{1}{\sqrt{2}} (|b_1^2 b_2^2 c_1 \bar{d}_1| - |b_1^2 b_2^2 \bar{c}_1 d_1|) : B_{3u}$$

$$4) \quad \frac{1}{\sqrt{2}} (|b_1^2 b_2^2 c_1 \bar{d}_2| - |b_1^2 b_2^2 \bar{c}_1 d_2|) : B_{2u}$$

$$5) \quad \frac{1}{\sqrt{2}} (|b_1^2 c_1^2 b_2 \bar{c}_2| - |b_1^2 c_1^2 \bar{b}_2 c_2|) : B_{3u}$$

$$6) \quad \frac{1}{\sqrt{2}} (|b_2^2 c_1^2 b_1 \bar{c}^2| - |b_2^2 c_1^2 \bar{b}_1 c_2|) : B_{2u}$$

Doubly excited states cannot be ignored, and five excitations:

$$7) \quad \frac{1}{\sqrt{2}} (|b_1^2 b_2^2 c_2 \bar{d}_1| - |b_1^2 b_2^2 \bar{c}_2 d_1|) : B_{2u}$$

$$8) \quad \frac{1}{\sqrt{2}} (|b_1^2 b_2^2 c_2 \bar{d}_2| - |b_1^2 b_2^2 \bar{c}_2 d_2|) : B_{3u}$$

$$9) \quad \frac{1}{2} (|b_1 b_2^2 \bar{c}_1 c_2^2| - |\bar{b}_1 b_2^2 c_1 c_2^2|) : B_{3u}$$

$$10) \quad \frac{1}{\sqrt{2}} (|b_1^2 b_2 c_1 c_2^2| - |b_1^2 b_2 c_1 c_2|) : B_{2u}$$

$$11) \quad |b_1^2 b_2^2 c_2^2| : A_{1g}$$

are especially important. Excitations 7)-10) are analogues of the singly excited states (3-6) listed above, in which  $c_1$  and  $c_2$  reverse roles.

In Equation (62) the B term depends upon excited state and ground state terms. If there is a state with energy  $E_k$  which is close to the ground state,  $|a\rangle$ , then  $B(a-j)$  will have a major contribution from

$$\frac{\langle k | \mu_z | a \rangle}{E_k - E_a} \{ \langle a | m_x | j \rangle \langle j | m_y | k \rangle - \langle a | m_y | j \rangle \langle j | m_x | k \rangle \}$$

For the porphyrin dianion, state 2) of  $B_{1g}$  symmetry satisfies this role. In Table 21, its energy is listed as 2.11 kK. Depending upon the extent of configuration interaction or a forced distortion into  $D_{2h}$  symmetry in which the porphyrin bond lengths are changed by 1%, its energy varies between 1.1 and 4.2 kK. The later value is for the  $\Delta\alpha = 11.0$   $H_2TPP$  model.<sup>56</sup> The results of the PPP calculation are presented in Table 24 for a molecule which has  $D_{4h}$  geometry, but whose nitrogen ionization potentials differ by 0.02 eV. In this way the wavefunctions are forced to transform as representations of the  $D_{2h}$  point group. Fifty-six configurations are employed.

The essential predictions tabulated are insensitive to moderate distortion or increasing number of interacting

Table 21. Porphyrin Dianion States and Spectra-Calculations and Data. B is in Debye<sup>2</sup> Bohr magneton cm<sup>-1</sup>. D is in Debye<sup>2</sup>.

<u>Calculations</u>						
Band	State <sup>a</sup>	Energy	C.I. Coefficients	Polarization	D	Bx10 <sup>3</sup>
	1	0	1.00(1)	-	-	-
	2	2.11	0.96(2)	-	0	0
	3	5.02	0.94(11)	-	0	0
I	4	15.19	0.80(3)	x	19.4	65
I	5	17.34	-0.64(7), 0.50(6), 0.48(10)	y	14.6	-23
II	6	25.98	0.74(5), 0.53(3)	x	86.6	-106
II	7	26.95	0.66(7)	y	27.2	43
II	8	28.45	0.75(6)	y	19.8	6
	9	33.4	0.95(4)	y	49.3	-8

Band	State <sup>c</sup>	Energy	C.I. Coefficients	Polarization	D	Bx10 <sup>3</sup>
	1	0	1.00(1)	-	-	-
	2	1.95	0.98(2)	-	0	0
	3	4.01	0.96(11)	-	0	0
I	4	15.10	0.80(3)	x	23.1	128
I	5	15.98	0.49(6), 0.51(10), -0.64(7)	y	27.4	-55
II	6	25.61	0.81(5), 0.54(3)	x	161.7	-64
II	7	28.06	0.86(6)	y	63.7	-4
	8	31.7	0.93(4)	y	74.6	77

<u>Experimental</u>		
Na <sub>2</sub> ZnTPP	D	Bx10 <sup>3</sup>
Band I	33	11.3
Band II	105	-18.5
Na <sub>2</sub> ZnEtio		
Band I	55	13
Band II	110	-21
(TPA) <sub>2</sub> H <sub>2</sub> TPP		
Band I	60	25

a) Fifty-six configurations

b) Quantities in parentheses are states described in text

c) Eighteen configurations

states. In the visible region an x,y pair of polarized transitions appear with similar dipole strengths. The first transition has B signature in agreement with that observed. Next, the 2.15 kK separation in the transition energies to states 4 and 5 and the opposite signature of B should give rise to positive  $[\theta]_M$  component in the visible; however, this anticipated behavior is not seen. This point will be discussed later. The computed values of B are 65 and  $-23 \times 10^3$ , which is larger than the  $11 - 25 \times 10^3 \beta D^2$  found experimentally, and are not reduced upon increasing the energy of state 2 to 4.2 kK. In Band II, the dominant MCD sign will be negative, in agreement with the data. Three transitions are calculated to appear within 2.5 kK of each other. The low, fluorescent depolarization ratio supports at least two transitions of opposite polarization appearing here. State 6 listed in Table 24 has the greatest dipole strength, and the spectra shown in Figures 44-46 exhibit coincident MCD and absorption peaks at 23-24 kK. As in the case of Band I, the higher energy transitions labelled states 7 and 8 are calculated with the incorrect MCD signature. As discussed earlier, the low-temperature spectrum provides a positive  $[\theta]_M$  (negative B) to the transition found at 25 kK.

Somewhat better agreement in Band II is provided by a calculation with C.I. among eighteen states including the important doubly excited configurations. The results are listed in Table 24. Now, the x,y polarized states 6 and 7 have

the same, correct sign of B, and state 8 is characterized by a positive B. Negative  $[\theta]_M$  at energies  $\geq 27$  kK, in Figures 44 and 46, support the prediction.

Nonetheless, all calculations conflict with data for Band I; there is no experimental corroboration for two electronic transitions in this band.

Two possibilities are suggested for the disagreement in Band I between theory and experiment. The molecule may distort into a roof-like configurations by bending dipyrromethene units along the  $C_2'$  axis connecting opposite methine bridges. In this instance,  $\sigma$ - $\pi$  separability is not maintained, and the PPP calculations do not apply to such a distortion. A second possibility is extensive vibronic interaction among the x,y components of states 4 and 5 of Table 21. It is easy to show that  $b_{1g}$  vibrations ( $D_{2h}$ ) couple the x and y states. The effect of such coupling will be to increase the energy gap between the 0-0 origins of the states and provide a mechanism for diffuse intensity; this occurring via an increased density of optically active vibronic states. The diffuse bands in Band I spectra contrast sharply with those observed in neutral metalloporphyrins and suggest vibronic coupling is operative.

## CHAPTER IV

## CONCLUSIONS

The magnetic circular dichroism spectra were obtained for the neutral and anionic forms of a series of porphyrins, chlorins, and bacteriochlorins. The experimental spectra were then analyzed in order to obtain information about the electronic structure of the compounds. The major conclusions of this analysis are:

- a. The calculated MCD spectra of the neutral chlorins and bacteriochlorins should be inverted for both Q and B bands, respectively, when compared to the MCD spectra of neutral porphyrins. Within the four orbital model, the MCD spectral signs depend on the difference between the energy separation of the two lowest virtual orbitals and the energy separation of the two highest filled orbitals. (However, the calculation for the B band is sensitive to the values of the magnetic dipoles.) The sign inversion was found experimentally.
- b. As was found for the neutral compounds, the spectra of the chlorin and bacteriochlorin monoanions have a greater resemblance to each other than to the spectra of the porphyrin monoanions. Although most of the assignments agreed with those of V. G. Maslov,<sup>72</sup> there were some dif-

Page missing from thesis

## APPENDIX A

Program CTERM calculates the total absorption, the four individual absorption coefficients, and the MCD for a transition from an approximately degenerate ground state to a non-degenerate excited state. The parameters include the intensity, energy, and linewidth for the two transitions, the magnetic field, the magnetic moment between the almost degenerate states, the temperature, and the wavenumber values. Patterson's integration technique<sup>84</sup> permits the evaluation of the integration error at each point. The moments of the spectra are calculated at the same time as the spectra are calculated. These moments are then converted to central moments to obtain the A, B, + C/kT, and D terms and the center of the band.

```

PROGRAM CTERM(INPUT,OUTPUT,TAPE20=INPUT,TAPE21=OUTPUT)
C   CALCULATES MCL C TERM ALLOWING FOR THE REMOVAL OF THE
C   DEGENERACY OF THE GROUND STATE.
C   THE INTEGRATION IS BY PATTERSON'S METHOD.
C   THE ERROR IS THE DIFFERENCE BETWEEN THE 63 PT AND 31 PT
C   AND BETWEEN THE 63 AND 15 PT FORMULA.

  DIMENSION TITLE(12),IRAY(6),W1(32),W2(16),W3(8),EA(6,32),X(32),
1EB(6,3),EC(6)
  DATA IRAY/6*(-0)/,PI2/1.570796326795/,BETA/4.669018E-05/
  DATA (W1(I),I=1,32)/5.637762836038E-02,5.6277699831254E-02,
15.5978436510476E-02,5.5481404356559E-02,5.4789210527963E-02,
25.3905499335266E-02,5.2834946790117E-02,5.1583253952049E-02,
35.0157139305900E-02,4.8564330406573E-02,4.6813554990628E-02,
44.4914531653632E-02,4.2877960025008E-02,4.0715510116944E-02,
53.8439810249456E-02,3.6064432780783E-02,3.3603877148208E-02,
63.1073551111688E-02,2.8489754745834E-02,2.5869679327215E-02,
72.3231446639910E-02,2.0594233915913E-02,1.7978551568128E-02,
81.5406750466560E-02,1.2903800100351E-02,1.0498246909621E-02,
98.2230079572359E-03,6.1155068221173E-03,4.2176304415589E-03,
12.5790497946857E-03,1.2651565562301E-03,3.6322148184553E-04/
  DATA (W2(I),I=1,16)/1.1275525672077E-01,1.1195687302095E-01,
11.0957842105593E-01,1.0566989358024E-01,1.0031427861180E-01,
29.3627109981265E-02,8.5755920049990E-02,7.6879620499004E-02,
36.7207754295991E-02,5.6979509494123E-02,4.6462893261758E-02,
43.5957103307129E-02,2.5807598096177E-02,1.6446049854388E-02,
58.4345657393211E-03,2.5447807915619E-03/
  DATA (W3(I),I=1,8)/2.2551049979821E-01,2.1915685840159E-01,
12.0062852937699E-01,1.7151190913639E-01,1.3441525524378E-01,
29.2927195315125E-02,5.1603282997089E-02,1.7001719629940E-02/
  DATA (X(I),I=1,32)/0.0,5.6344313046593E-02,1.1248894313319E-01,
11.6823525155221E-01,2.2338668642897E-01,2.7774982202183E-01,
23.3113539325798E-01,3.8335932419973E-01,4.3424374934680E-01,
34.8361802694584E-01,5.3131974364438E-01,5.7719571005205E-01,
46.2110294673723E-01,6.6290966002478E-01,7.0249620649153E-01,
57.3975604435270E-01,7.7459666924148E-01,8.0694053195022E-01,
68.36725938168870E-01,8.63907938193690E-01,8.88459232872260E-01,
79.1037115695700E-01,9.29654857429740E-01,9.4634285837340E-01,
89.60491268708020E-01,9.7218287474858E-01,9.81531149553740E-01,
99.88684757547430E-01,9.93831963212760E-01,9.9720625937222E-01,
19.99098124967670E-01,9.99872888120360E-01/
  DATA S/0.2115710938/
  IRAY(4)=0
  CALL SYSTEMC(115,IRAY)
1  FORMAT(12A6)
2  FORMAT(1X,12A6)
3  FORMAT(1X,5HRX IS,E18.8,10X,5HEX IS,E18.8,10X,7HDELA IS,E18.8)
4  FORMAT(1X,5HRY IS,E18.8,10X,5HEY IS,E18.8,10X,7HDEL2 IS,E18.8)
5  FORMAT(1X,14HMAGNETIC FIELD,E18.8,5HGAUSS,10X,5HMHZ IS,E18.8)
6  FORMAT(1X,3(10X,E20.8,4HCM-1))
7  FORMAT(1X,11HTEMPERATURE,10X,E18.8)
8  FORMAT(1X,2E15.6,2E9.2,E15.6,2E9.2)
9  FORMAT(1X,4(E15.6,2E8.1))
10 FORMAT(1X,5E20.7)
11 FORMAT(11,12A6)
13 FORMAT(1X,I10)
12 FORMAT(1X,I1,12A6)
14 FORMAT(1X,5E15.6)
C   READ DATA
C
100 READ(20,1) TITLE
101 READ(20,*) RX,EX,DEL1
    READ(20,*) RY,EY,DEL2
    READ(20,*) XH,ZM
    READ(20,*) V1,V2,V3
    WRITE(21,2) TITLE
    WRITE(21,3) RX,EX,DEL1

```

```

WRITE(21,4) RY,EY,DEL2
WRITE(21,5) XH,ZM
WRITE(21,6) V1,V2,V3
C
C   INITIAL CALCULATIONS
C
E0=0.5*(EY+EX)
DEN=0.5*(EY-EX)
BHMZ=(BETA*ZH*XH)**2
IF(V3.EQ.0.0) V3=V2-V1
RXY=ABS(RX*RY)
RX=RX**2
RY=RY**2
IF(DEL1.LE.1.0E-99) DEL1=1.0
DT1=S/DEL1
DEL1=-1.0/(DEL1**2)
IF(DEL2.LE.1.0E-99) DEL2=1.0
DT2=S/DEL2
DEL2=-1.0/(DEL2**2)
IF(V1.LT.V2) GO TO 110
ZH=V1
V1=V2
V2=ZH
110 IF(V3.GT.1.0E-99) GO TO 111
WRITE(21,10) V1,V2,V3,RX,RY
111 NUMBER=(1.0+(V2-V1)/V3)
IF(NUMBER.GT.1000.OR.NUMBER.LT.1) GO TO 999
IF(BHMZ.LT.1.0E-99.OR.XH.LT.1.0E-99) GOTO500
C
C   READ TEMPERATURE
C
150 READ(20,*) TEMP
WRITE(21,7) TEMP
IF(TEMP.LE.1.0E-99) GO TO 999
DO 155 I=1,6
EC(I)=0.0
155 CONTINUE
TEMP=-2.877+06/TEMP
E=V1-V3
DO 161 IK=1,NUMBER
DO 161 J=1,6
EB(J,1)=0.0
161 CONTINUE
F1=E*3300.0/XH
E=E+V3
DO 200 I=1,32
XX=PI2*(X(I)+1.)
SINX=SIN(XX)
COSX=COS(XX)**2
BHM=BHMZ*COSX
DET=SQRT(DEN**2+BHM)
V2=(4EN+4ET)**2
IF(V2.LE.1.0E-80.OR.BHM.LE.1.0E-85) GO TO 123
ALSQ=V2/(V2+BHM)
GAMSQ=1.0-ALSQ
B3=(DEN+DET)*COSX*SQRT(BHMZ)*4.0*RXY/(V2+BHM)
GOTO124
123 ALSQ=1.0
GAMSQ=0.0
B3=0.0
124 G=SINX/(EXP(TEMP*DET)+1.0)
FA=DT1*G*EXP(DEL1*(E-E0-DET)**2)
FB=DT2*G*EXP(DEL2*(E-E0+DET)**2+TEMP*DET)
B1=(RX*ALSQ+RY*GAMSQ)*(1.0+COSX)
B2=(RY*ALSQ+RX*GAMSQ)*(1.0+COSX)
EA(1,I)=FA*(B1+B3)
EA(2,I)=FA*(B1-B3)

```

```

EA(3,I)=FB*(B2-B3)
EA(4,I)=FB*(B2+B3)
EA(5,I)=E*(FA*B1+FB*B2)
EA(6,I)=F1*B3*2.0*(FA-FB)
DO 199 J=1,6
  EB(J,1)=EB(J,1)+EA(J,I)*W1(I)
199 CONTINUE
200 CONTINUE
  DO 202 J=1,6
    EB(J,1)=EB(J,1)-EA(J,1)*W1(1)*0.5
    EB(J,2)=-W2(1)*EA(J,1)*0.5
    EB(J,3)=-W3(1)*EA(J,1)*0.5
202 CONTINUE
    DO 220 I=1,6
      DO 210 J=1,16
        K=(2*J)-1
        EB(I,2)=EB(I,2)+EA(I,K)*W2(J)
210 CONTINUE
        DO 205 J=1,8
          K=(4*J)-3
          EB(I,3)=EB(I,3)+EA(I,K)*W3(J)
205 CONTINUE
220 CONTINUE
        DO 230 I=1,6
          EB(I,2)=EB(I,1)-EB(I,2)
          EB(I,3)=EB(I,1)-EB(I,3)
230 CONTINUE
          WRITE(21,8) E,EB(5,1),EB(5,2),EB(5,3),EB(6,1),EB(6,2),EB(6,3)
          WRITE(21,9) ((EB(I,K),K=1,3),I=1,4)
          DO 241 J=1,3
            EC(J)=EC(J)+EB(5,1)*(E**(J-2))*V3
            N=J+3
            EC(N)=EC(N)+EB(6,1)*(E**(J-2))*V3
241 CONTINUE
499 CONTINUE
          WRITE(21,14) (EC(I),I=1,6)
          FA=EC(2)/EC(1)
          EC(1)=EC(1)/108.9
          EC(2)=EC(4)/33.53
          EC(3)=(EC(5)-FA*EC(4))/33.53
          EC(4)=EC(3)/EC(1)
          EC(5)=EC(2)/EC(1)
          WRITE(21,14) FA,(EC(I),I=1,5)
          GO TO 150
500 READ(20,*) TEMP
      WRITE(21,7) TEMP
      IF(TEMP.LE.1.0E-99) GO TO 999
      TEMP=-2.877406/TEMP
      E=V1-V3
      G=EXP(TEMP*DEN)
      TEST=0.0
      C2=2.6666666666667/(1.+G)
      DO 600 IK=1,NUMBER
        E=E+V3
        F1=EXP(DELT1*(E-E0)**2)
        F2=EXP(DELT2*(E-E0)**2)
        FA=RX*C2*F1*DT1*E
        FB=RY*C2*F2*DT2*E
        EP=0.5*(FA+FB)
        WRITE(21,10) E,EP,TEST,FA,FB
600 CONTINUE
      GO TO 500
999 READ(20,11) I,TITLE
      WRITE(21,12) I,TITLE
      IF(I.EQ.1) GO TO 101
      STOP
      END

```

## APPENDIX B

The experimental MCD spectrum is given by

$$\frac{[\theta]_M}{\nu} = -33.53 \sum_i [(B_i + C_i/kT) f_i(\nu_{oi}, \nu) + A_i \frac{df_i(\nu_{oi}, \nu)}{d\nu}]$$

and the absorption spectrum by

$$\frac{\epsilon}{\nu} = 108.9 \sum_i D_i f_i(\nu_{oi}, \nu)$$

where  $f_i(\nu_{oi}, \nu)$  is a function of  $\nu$  centered about  $\nu_{oi}$ .<sup>6,8</sup> The summation is over all resolved or partially resolved transitions among the groups discussed in Chapter II. The MCD spectrum can be divided up into two portions, one part  $(B_i + C_i/kT)$  directly proportional to the absorption spectrum and the other  $(A_i)$  to the first derivative of the absorption spectrum. The first part can be further divided into a temperature dependent term  $(C_i)$  and a temperature independent term  $(B_i)$ . These A, B, C, and D terms are entirely experimental quantities. The correlation between this set of experimental parameters would be straightforward if the nature of the line-shape functions were known.

One method commonly used to obtain these parameters is to assume a mathematical form for  $f_i(\nu_{oi}, \nu)$ . Normally the data is fit with a number of Lorentzian (polynomial) or Gaussian (exponential) functions<sup>8</sup> using a least squares or some other

procedure. Unfortunately there is usually no sound theoretical reason for the type or number of lineshape functions used. Also the results obtained by this method are not necessarily unique.

A second technique which is used to analyze data is moment analysis.<sup>8, 50</sup> This method is superior to that of curve fitting in that there are no adjustable parameters. If  $\rho(v)$  is a bell shaped curve centered about  $v_0$ , the central moments are defined by

$$\langle \rho \rangle \equiv \int \rho(v) (v-v_0)^n dv.$$

The zeroth moment  $\langle \rho \rangle_0$ , gives the area of  $\rho(v)$ ;  $\langle \rho \rangle_1$  gives the center or  $v_0$ ;  $\langle \rho \rangle_2$  characterizes the width of the distribution; and the third moment,  $\langle \rho \rangle_3$ , gives the asymmetry of  $\rho(v)$ .

Central moments of the MCD and absorption spectra are

$$\langle \epsilon \rangle_n = \int_{\text{band}} \frac{\epsilon}{v} (v-v_0)^n dv = \int_{\text{band}} \frac{\epsilon}{\lambda} \left( \frac{1}{\lambda} - \frac{1}{\lambda_0} \right)^n d\lambda$$

and

$$\langle [\theta]_M \rangle = \int_{\text{band}} \frac{[\theta]_M}{v} (v-v_0)^n dv = \int_{\text{band}} \frac{\epsilon}{\lambda} \left( \frac{1}{\lambda} - \frac{1}{\lambda_0} \right)^n d\lambda$$

where  $\lambda$  is the wavelength.

The center of the absorption band is found by setting the first moment of absorption equal to zero, i.e.,

$$v_0 = \int_{\text{band}} \epsilon dv / \int_{\text{band}} \frac{\epsilon}{v} dv,$$

or

$$\nu_0 = \int_{\text{band}} \left(\frac{\epsilon}{\nu}\right) d\lambda / \int_{\text{band}} \left(\frac{\epsilon}{\lambda^2}\right) d\lambda.$$

Three of the parameters may be determined by simple integration and do not depend on  $\nu_0$ ,

$$B + \frac{C}{kT} = -\langle [\theta]_M \rangle_0 / 33.53$$

$$D = \langle \epsilon \rangle_0 / 108.9$$

The A term will be more complex,

$$A = -(\langle [\theta]_M \rangle_1 / 33.53) - (B_1 - \hbar\nu_0 B - \frac{C_1 - \hbar\nu_0 C}{kT}) / 33.53$$

$B_1$  and  $C_1$  are necessary to compensate for a shift in the average position of the MCD spectrum when compared with the absorption spectrum. If it is assumed that this shift is small, then

$$A = -\langle [\theta]_M \rangle_1 / 33.53.$$

In order to carry out these integrations, the bands are separated by some means (such as assuming Gaussian or Lorentzian tails) before performing the numerical calculations. Since the higher moments depend critically on the tails of the lineshape function, it is generally impractical to use higher than first moments.

A third method is based on Kuhn's dyssymmetry factor.<sup>83</sup>

$$\frac{[\theta]_M}{\epsilon} = \sum_i A_i f'_i + (B_i + C_i/kT) f_i,$$

then a plot of  $[\theta]_M/\epsilon$  versus either  $\lambda$  or  $\nu$  through one band should give a straight line. The slope gives  $A_i$ , while the ratio at the absorption maximum gives  $(B_i + C_i/kT)$ . If the ratio is not a straight line, then more than one component is present.

A fourth method of obtaining the experimental parameters is to plot the integrated intensities versus wavenumber. The  $B+C/kT$  and  $D$  terms will be proportional to the differences in these values on either side of the band. A derivative shaped MCD spectrum will give a bell shaped curve whose area is proportional to the  $A$  term. The procedure used here was to fit the experimental data point with a natural cubic spline (the routine is from P. J. Davis and P. Rabinowitz, "Methods of Numerical Integration").<sup>84</sup> A plot of the integral of this function versus  $\nu$  gives both the MCD and absorption parameters.

```

PROGRAM DRAW(INPUT,OUTPUT,TAPE 20)
DIMENSION Z(101),Y(250),X(250),Z(250),T(250),H(250),TITLE(12)
DIMENSION E(250),Y1(250),Y2(250),Y3(250),V1(10),V2(10)
DIMENSION V3(10),INUM(10),V4(10),V5(10),V6(10)
DIMENSION V7(10),V8(10),V9(10)
DATA Q/101*1H /,ST/1H+/,RN/1H*/,RI/1HI/,RBR/1H /
21 FORMAT(3F15.6)
22 FORMAT(I1,3F15.6)
23 FORMAT(12A6)
24 FORMAT(1H,5H*****,1X,12A6,1X,5H*****///)
25 FORMAT(4E20.6)
26 FORMAT(1X,F15.4,5X,101A1)
BITE=0.0298240381
DITE=0.0091827365
40 READ(20,23) TITLE
PRINT 24,TITLE
IT=1
41 READ(20,22) INUM(IT),V1(IT),V2(IT),V3(IT)
PRINT 22, IT,V1(IT),V2(IT),V3(IT)
IF(INUM(IT).LE.0) GO TO 45
READ(20,21) V4(IT),V5(IT),V6(IT)
READ(20,21) V7(IT),V8(IT),V9(IT)
IT=IT+1
GO TO 41
45 I=1
42 READ(20,21) X(I),Y(I),Z(I)
IF(X(I).LE.0.0) GO TO 43
X(I)=1.E07/X(I)
Y(I)=Y(I)/X(I)
Z(I)=Z(I)/X(I)
I=I+1
GO TO 42
43 M2=I-2
IT=IT-1
DO 888 K=1,IT
IF(INUM(K).EQ.3) GO TO 884
880 S=0.0
DO 1 I=1,M2
M(I)=X(I+1)-X(I)
R=(Y(I+1)-Y(I))/M(I)
Y2(I)=R-S
1 S=R
S=0.0
R=0.0
Y2(1)=0.0
Y2(M2+1)=0.0

```

```

      DO 2 I=2,M2
      Y2(I)=Y2(I)+R*Y2(I-1)
      T(I)=2.*(X(I-1)-Y(I+1))-R*S
      S=H(I)
2    R=S/T(I)
      DO 3 J=2,M2
      I=M2+2-J
3    Y2(I)=(H(I)*Y2(I+1)-Y2(I))/T(I)
      DO 4 I=1,M2
      S=H(I)
      R=Y2(I+1)-Y2(I)
      Y3(I)=R/S
      Y2(I)=3.*Y2(I)
4    Y1(I)=(Y(I+1)-Y(I))/S-(Y2(I)+R)*S
      E(1)=0.0
      DO 5 I=1,M2
      S=X(I+1)-X(I)
5    E(I+1)=E(I)+(((Y3(I)*.25*S+Y2(I)/3.)*S+Y1(I)*.5)*S+Y(I))*S
881  IF(INUM(K).EQ.3) GO TO 887
882  I=1
      J=1
105  IF(V1(K).GE.X(1)) GO TO 106
      V1(K)=V1(K)+V3(K)
      GO TO 105
106  V=V1(K)
103  IF(V-X(J)) 102,101,100
100  J=J+1
      GO TO 103
101  T(I)=Y(J)*V
      H(I)=E(J)*DITE
104  I=I+1
      V=V+V3(K)
      IF(V.GT.V2(K)) GO TO 150
      GO TO 103
102  R=V-X(J-1)
      T(I)=V*(Y(J-1)+R*(Y1(J-1)+R*(Y2(J-1)+R*Y3(J-1))))
      H(I)=.5*Y1(J-1)+E*(Y2(J-1)/3.0+0.25*Y3(J-1)*R)
      H(I)=E(J-1)+R*(Y(J-1)+R*H(I))
      H(I)=H(I)*DITE
      GO TO 104
150  HMAX=0.0
      TMAX=T(1)
      V=V1(K)-V3(K)
      I=I-1

```

```

      DO 151 J=1,I
      V=V+V3(K)
      H(J)=H(J)-H(1)
      R=1.0E+07/V
      PRINT25,      R,V,T(J),H(J)
      HMAX=AMAX1(H(J),HMAX)
151  TMAX=AMAX1(T(J),TMAX)
      IF(V4(K).LE.0.0) GO TO 153
      PRINT 25,HMAX,TMAX,V4(K),V7(K)
      HMAX=V7(K)
      TMAX=V4(K)
153  V=V1(K)-V3(K)
      DO 152 J=1,I
      IA=1.0+100.0*H(J)/HMAX
      IB=1.0+100.0*T(J)/TMAX
      Q(1)=RI
      Q(101)=RI
      Q(IA)=RN
      Q(IB)=ST
      V=V+V3(K)
      PRINT26,      V,Q
      Q(1)=RBR
      Q(IA)=RBR
      Q(IB)=RBR
      Q(101)=RBR
152  CONTINUE
883  IF(INUM(K).EQ.2) GO TO 888
884  NAME=M2+1
      DO 200 I=1,NAME
      Y(I)=Z(I)
200  CONTINUE
885  INUM(K)=3
886  GO TO 880
887  I=1
      J=1
305  IF(V1(K).GE.X(1)) GO TO 306
      V1(K)=V1(K)+V3(K)
      GO TO 305

```

```

306 V=V1(K)
303 IF (V-X(J)) 302,301,300
300 J=J+1
    GO TO 303
301 T(I)=Y(J)*V
    H(I)=E(J)*9ITE
304 I=I+1
    V=V+V3(K)
    IF (V.GT.V2(K)) GO TO 350
    GO TO 303
302 R=V-X(J-1)
    T(I)=V*(Y(J-1)+R*(Y1(J-1)+R*(Y2(J-1)+R*Y3(J-1))))
    H(I)=.5*Y1(J-1)+R*(Y2(J-1)/3.0+0.25*Y3(J-1)*R)
    H(I)=E(J-1)+R*(Y(J-1)+R*H(I))
    H(I)=H(I)*3ITE
    GO TO 304
350 HMAX=0.0
    TMAX=T(1)
    HMIN=0.0
    TMIN=T(1)
    V=V1(K)-V3(K)
    I=I-1
    DO 351 J=1,I
        V=V+V3(K)
        H(J)=H(J)-H(1)
        R=1.0E+07/V
        PRINT 25, R,V,T(J),H(J)
        HMAX=AMAX1(H(J),HMAX)
        TMAX=AMAX1(T(J),TMAX)
        HMIN=AMIN1(H(J),HMIN)
351 TMIN=AMIN1(T(J),TMIN)
    IF (V5(K).LE.0.0) GO TO 353
    PRINT 25,TMAX,TMIN,V5(K),V6(K)
    TMAX=V5(K)
    PRINT 25,HMAX,HMIN,V8(K),V9(K)
    HMAX=V8(K)
    HMIN=V9(K)
    TMIN=V6(K)
353 V=V1(K)-V3(K)

```

```
DO 352 J=1,I
  IA=1.0+100.0*((H(J)-HMIN)/(HMAX-HMIN))
  IB=1.0+100.0*((T(J)-TMIN)/(TMAX-TMIN))
  Q(1)=RI
  Q(51)=RI
  Q(101)=RI
  Q(IA)=RN
  Q(IB)=ST
  V=V+V3(K)
  PRINT 26,      V,Q
  Q(IA)=RBR
  Q(IB)=RBR
  Q(1)=RBR
  Q(51)=RBR
  Q(101)=RBR
352 CONTINUE
888 CONTINUE
996 PRINT 24,      TITLE
  STOP
END
```

## BIBLIOGRAPHY

1. C. G. Darwin and W. H. Watson, Roy. Soc. Proc. A., 114, 474 (1927).
2. T. M. Lowry, "Optical Rotatory Power," Dover 1964 (1935), New York, N. Y.
3. J. R. Partington, "An Advanced Treatise on Physical Chemistry," 4, (1953), Longmans, Green and Co., London.
4. E. Dratz, Ph. D. Dissertation, (1966), U. Calif., Berkeley.
5. A. D. Buckingham and P. J. Stephens, Ann. Rev. Phys. Chem., 17, 399 (1966).
6. P. N. Schatz and A. J. McCaffery, Quart. Rev., 23, 552 (1969).
7. D. J. Caldwell and H. Eyring, "The Theory of Optical Activity," (1971), J. Wiley and Sons, Inc., New York, N. Y.
8. P. J. Stephens, Ann. Rev. Phys. Chem., 25, 201 (1974).
9. P. Day (ed.), "Electronic States of Inorganic Compounds: New Experimental Techniques," (1975), D. Reidel Publ. Co., Boston.
10. J. Michl, Spectroscopy Letters, 10, 509 (1977).
11. M. V. Vol'kenshtein and Y. A. Sharnox, Priroda, 5, 30 (1977).
12. V. A. Shuvalov, A. A. Asadov, and I. N. Kraknmaleva, FEBS Letters, 76, 240 (1977).
13. M. Gouterman and D. Holten, Photochemistry and Photobiology, 25, 85 (1977).
14. J. Fajer, A. Forman, M. S. Davis, L. D. Spaulding, D. C. Brune, and R. H. Felton, J. Am. Chem. Soc., 99, 4134 (1977).
15. G. N. Sinyakov, G. P. Gurinovich, V. G. Maslov, and A. N. Sidorov, Zhurnal Prikladnoi Spektroskopii, 14, 849 (1971).
16. K. M. Smith (ed.), "Porphyrins and Metalloporphyrins," (1975) Elsevier Publishing Co., Inc., New York, N. Y.

17. Ann. New York Acad. Sci., 224 (1975).
18. P. J. Stephens, W. Suetaak, and P. N. Schatz, J. Chem. Phys., 44, 4592 (1966).
19. A. J. McHugh, M. Gouterman, and C. Weiss. Theoret. Chim. Acta, 24, 346 (1972).
20. R. Gale, A. J. McCaffery, and M. D. Rowe, J. Chem. Soc. Dalton Trans., 596 (1972).
21. C. Weiss, Ann. New York Acad. Sci., 224, 204 (1975).
22. C. Weiss, J. Mol. Spectroscopy, 44, 37 (1972).
23. B. Briat, D. A. Schooley, R. Records, E. Bunnenberg, and C. Djerassi, J. Amer. Chem. Soc., 89, 6170 (1967).
24. C. Houssier and K. Sauer, J. Amer. Chem. Soc., 92, 779 (1970).
25. J. Breton and M. Hilaire, C. R. Acad. Sc. Paris, D., 278, 678 (1972).
26. C. Gall and D. Simkin, Can. J. of Spectroscopy, 61, 203 (1976).
27. R. E. Linder, G. Barth, E. Bunnenberg, C. Djerassi, L. Seamans, A. Moscowitz, J. Chem. Soc., Perkin Trans. II, 1712 (1974).
28. P. J. Zanstra, D. J. Scholtens and R. E. Koning, J. Chem. Physics, 57, 3821 (1972).
29. A. Tajiri, H. Uchimura, and M. Hatano, Chem. Letters, 1021 (1975).
30. N. Teramae, K. Yazawa, S. Higuchi, and S. Tanaka, Bunseki Kagaku, 24, 641 (1975).
31. R. J. van der Wal and P. J. Zandstra, J. Chem. Phys., 64, 2261 (1976).
32. H. P. J. M. Dekkers and Ms. E. C. M. Kielman-Van Luyt, Molecular Physics, 30 (1976).
33. A. Honma and S. Ooaku, Nippon Butsurigakkai, 41, 152 (1976).
34. P. J. Zandstra and B. C. van Zorge, J. Chem. Phys., 59, 5201 (1973).

35. D. E. Downie, Ph. D. Dissertation, (1970), U. of Calif., Berkeley.
36. R. Serber, Phys. Rev., 41, 489 (1932).
37. R. E. Linder, Ph. D. Dissertation, (1969), Texas A&M.
38. F. A. Modine, Phys. Rev. B, 8, 854 (1973).
39. J. A. Glaze and J. C. Kemp, Phys. Rev., 178, 1502 (1969).
40. V. G. Maslov, Opt. Spectrosc., 37, 1010 (1974).
41. F. Woldbye in "Techniques of Inorganic Chemistry," H. B. Jonassen and A. Weissberger (eds.) 249.
42. L. Velluz, M. Legrand, and M. Grosjean, "Optical Circular Dichroism," (1965), Academic Press, New York, N. J.
43. R. H. Webb, "Elementary Wave Optics," (1969), Academic Press, New York, N. Y.
44. D. Caldwell, Molecular Physics, 33, 495 (1977).
45. G. B. Airy, Phil. Mag. (iii), 28, 469 (1846).
46. G. R. Fowles, "Introduction to Modern Optics," (1968).
47. R. A. Jenkins and H. A. White, "Fundamentals of Optics," (1976) McGraw-Hill, New York, N. Y.
48. J. C. Sutherland, D. Axelrod, and M. P. Klein, J. Chem. Phys., 54, 288 (1971).
49. P. J. Stephens, R. L. Mowery, and P. N. Schatz, J. Chem. Phys., 55, 224 (1971).
50. W. H. Beyer (ed.), "Standard Mathematical Tables," 474, (1976), CRC Press, Inc., Cleveland.
51. J. Fajer, B. H. J. Bielski, and R. H. Felton, J. Phys. Chem., 72, 1281 (1968).
52. R. Pariser and R. G. Parr, J. Chem. Phys., 21, 466 (1952).
53. J. A. Pople, Trans. Faraday Soc., 50, 901 (1954).
54. C. C. J. Roothaan, Rev. Mod. Phys., 32, 179 (1960).
55. O. W. Adams and P. G. Lykos, J. Chem. Phys., 34, 1444 (1961).

56. C. Weiss, H. Kobayashi and M. Gouterman, J. Mole. Spectroscopy, 16, 415 (1965).
57. J. C. Sutherland and M. P. Klein, J. Chem. Phys., 57, 76 (1972).
58. G. Jansen, Ph. D. Dissertation, (1977), Leiden.
59. G. W. Canters, J. Van Egmond, T. J. Schaafsma, I. Y. Chan, W. G. Van Dorp, and J. H. Van der Waals, Ann. New York Acad. Sci., 206, 711 (1973).
60. M. Gouterman, Ann. New York Acad. Sci., 206, 70 (1973).
61. J. P. Riehl and F. S. Richardson, J. Chem. Phys., 65, 1011 (1976).
62. H. Goldstein, "Classical Mechanics," 197, (1959), Addison-Wesley, Reading, Mass.
63. A. D. Adler, F. R. Longo, F. Kampas, and J. Kim, J. Inorg. Nucl. Chem., 32, 2443 (1970).
64. H. W. Whitlock, Jr., R. Hanauer, M. Y. Oester, and B. K. Bower, J. Amer. Chem. Soc., 91, 7485 (1969).
65. J. Fajer, D. C. Brune, M. S. Davis, A. Forman, and L. D. Spaulding, Proc. Nat. Acad. Sci., USA, 71, 994 (1974).
66. L. Spaulding, private communication.
67. A. J. McCaffery, P. J. Stephens, and P. N. Schatz, Inorganic Chemistry, 6, 1614 (1967).
68. J. C. Sutherland, L. E. Vickery, and M. P. Klein, Rev. Sci. Instrum., 45, 1089 (1974).
69. R. H. Breeze and B. Ke. Anal. Biochem., 50, 281 (1972).
70. M. Gouterman, J. Chem. Phys., 30, 1139 (1959).
71. M. Gouterman, J. Mol. Spect., 6, 138 (1961).
72. V. G. Maslov, Opt. Spectrosc., 40, 275 (1976).
73. M. H. Perrin, J. Chem. Phys., 59, 2090 (1973).
74. P. J. Stephens, J. Chem. Phys., 52, 3489 (1970).
75. M. Gouterman, G. Wagniere, and L. C. Snyder, J. Mole. Spect., 11, 108 (1963).

76. A. Kaito, T. Nozawa, T. Yamamoto, M. Hatano, and Yorii, Chem. Phys. Letters, 52, 154 (1977).
77. G. Barth, R. E. Linder, E. Bunnenberg, C. Djerassi, L. Seamans, and A. Moscowitz, J. Chem. Soc. Perkin Trans. II, 1706 (1974).
78. R. Pariser, J. Chem. Phys., 24, 250 (1956).
79. R. E. Koning, H. Zandvoort, and P. J. Zandstra, Chem. Phys., 28, 343 (1978).
80. J. A. Pople, D. P. Santry, and G. A. Segal, J. Chem. Phys., 43, S129 (1965).
81. V. G. Maslov, Teor. Eksp. Khim., 9, 650 (1973).
82. V. G. Maslov, Opt. Spektrosk., 34, 876 (1973).
83. G. Closs and L. E. Closs, J. Am. Chem. Soc., 85, 81 (1963).
84. P. J. Davis and P. Rabinowitz, "Methods of Numerical Integration," (1975), Academic Press, New York, N. Y.
85. G. Barth, R. E. Linder, N. Waespe-Sarcevic, E. Bunnenberg, C. Djerassi, Y. J. Aronowitz, and M. Gouterman, J. Chem. Soc. Perkin Trans. II, 337 (1977).
86. J. Badoz, M. Billardon, A. C. Boccara, and B. Briat, Symposia of the Faraday Society, 3, 27 (1969).

## VITA

Gilbert F. Kuipers, son of Mr. and Mrs. Carl J. Kuipers, was born in Hawkinsville, Georgia on March 13, 1948.

He graduated from Castle Heights Military Academy, Lebanon, Tennessee in 1966. He then attended North Georgia College, where he obtained a Bachelor of Science degree in Chemistry in June, 1970. He immediately began graduate work in the School of Chemistry at the Georgia Institute of Technology. In 1977, he began teaching at Georgia Military College, where he is presently employed.